Bragg scattering of surface-gravity waves by an ice shelf with rolling surface morphology

Supplemental material

Yuri V. Konovalov

ORCID: 0000-0002-8469-9706

Department of Mathematics, MIREA - Russian Technological University, Vernadsky avenue 78, Moscow, Russian Federation, 119454

Content

Numerical experiments

Numerical experiments were carried out using three models with different combinations of parameters α_1 and α_2 in equation (10). The results presented below were obtained using **Model 1** for (i) $\alpha_1 = 1;\ \alpha_2 = 0$ and (ii) $\alpha_1 = 0.2;\ \alpha_2 = 0.8$; using **Model 2** for $\alpha_1 = 0;\ \alpha_2 = 1$ (the results obtained for $\alpha_1 = 1;\ \alpha_2 = 0$ are presented in the main manuscript); and using **Model 3** for $\alpha_1 = 1;\ \alpha_2 = 0$.

1. Results obtained by Model 1 (case of $\boldsymbol{\alpha_1 = 1.0, \alpha_2 = 0.0}$)

Experiments with ice shelves that having a rolling surface morphology have revealed the following. There is a threshold value of the amplitude of ice thickness oscillations (A_H), at which band gaps appear in the dispersion spectra (Figure 1) (Konovalov, 2023a). Essentially, the amplitude of ice thickness oscillations (A_H) determines the depth of the ice shelf cavities that result from the "rolling" morphology. These cavities are the analogous to crevasses in the base of an ice shelf (Freed-Brown et al., 2012).

In the considered experiments this threshold value depends on the value of the *Bragg wavenumber*. In particular, the first band gap, corresponding to the first *Bragg wavenumber* $k_b^{(1)} \approx 6.28\ km^{-1}$, appears in the spectrum at $A_H > 16\ m$ (Fig. 1a), i.e. the first threshold value $(A_H)_{th}^{(1)} \approx 16m$. Curves 4 and 5 in Figure 1 show that the typical dependence of wavenumber vs periodicity/frequency, similar to that observed in curves 1, 2 and 3, is absent for $A_H \geq 16\ m$. The algorithm used to determine the wavenumber (Konovalov, 2021b) in the general case provides the value of the wavenumber. However, the absence of a typical wavenumber dependence (as in curves 1, 2, 3 in Fig. 1a) should essentially be treated as the absence of a wavenumber. Essentially in the range (of periodicity of the forcing) 2..190 s the superposition of band gaps for two Bragg's wavenumbers ($\mathrm{k_b^{(1)}} \approx 6.28\,\mathrm{km^{-1}}$, $\mathrm{k_b^{(2)}} \approx 12.57\,\mathrm{km^{-1}}$) is observed in Curves 4 and 5 in Figure 1. Respectively, in the range of 5..190 s there are no resonances in the amplitude spectrum (Curve 3 in Fig. 4a).

The second band gap (Fig. 1b), which, accordingly, corresponds to the second *Bragg wavenumber* $k_b^{(2)} \approx 12.57\ km^{-1}$, appears in the spectrum at $A_H \geq 1\ m$, i.e. the second threshold value $(A_H)_{th}^{(2)} \leq 1m$. Similarly, the third and fourth band gaps (Fig. 1c) which respectively correspond to the *Bragg wavenumbers* $k_b^{(3)} \approx 19.04\,km^{-1}$ *and* $k_b^{(4)} \approx 25.13\ km^{-1}$, also appear in the spectrum at $A_H \geq 1\ m$, so that $(A_H)_{th}^{(3)} \leq 1m$ and $(A_H)_{th}^{(4)} \leq 1m$.

If the amplitude of ice thickness oscillations (A_H) is less than the threshold value, then the dominant effect in the model is resonance (Figure 2, Curves 1 and 2) and the dispersion spectra reveal areas of the expected appearance of band gaps (Curves 1, 2 and 3 in Figure 1a). These areas are located in the vicinity of the Bragg value (for the considered periodicity of the rolls the first Bragg wavenumber is equal to 6.28 km^{-1}).

When the amplitude of ice thickness oscillations (A_H) exceeds the threshold value, the band gaps become the dominant effect and abate the resonances in the amplitude spectra (Figure 2, Curve 3).

Thus, we can say that the abatement of the incident wave by the ice shelf with a "rolling" surface/base morphology protects the ice shelf on the resonant impact.

Figure 3 shows superpositions of the dispersion spectrum and the amplitude spectrum in the periodicity range containing the region of the expected first band gap. These superpositions reveal that in the region of the expected band gap, the resonance peak coincides with the part of the dispersion spectrum, where the wavenumbers are close to the first *Bragg wavenumber* $k_b^{(1)} \approx 6.28\,km^{-1}$. In particular, with the amplitude of ice thickness fluctuations $\boldsymbol{A_H = 5\ m}$, the resonance peak is observed at the periodicity $T_n \approx 32.68\ s$ (i.e. $T_n \approx 32.68\ s$ is one of the eigenvalues), at which the wavenumber in the dispersion spectrum is about $5.86\ km^{-1}$ (i.e. $k_n \approx 5.86\ km^{-1}$) (Fig. 3a). Similarly, with the amplitude of ice thickness fluctuations $\boldsymbol{A_H = 10\ m}$, the wavenumber k_n is about $6.23\ km^{-1}$ (Fig. 3b) and, with the amplitude of ice thickness fluctuation is $\boldsymbol{A_H = 12\ m}$, the wavenumber k_n is about $6.43\ km^{-1}$ (Fig. 3c). Thus, the relative deviation of k_n from the first *Bragg wavenumber* $k_b^{(1)}$ does not exceed 7%.

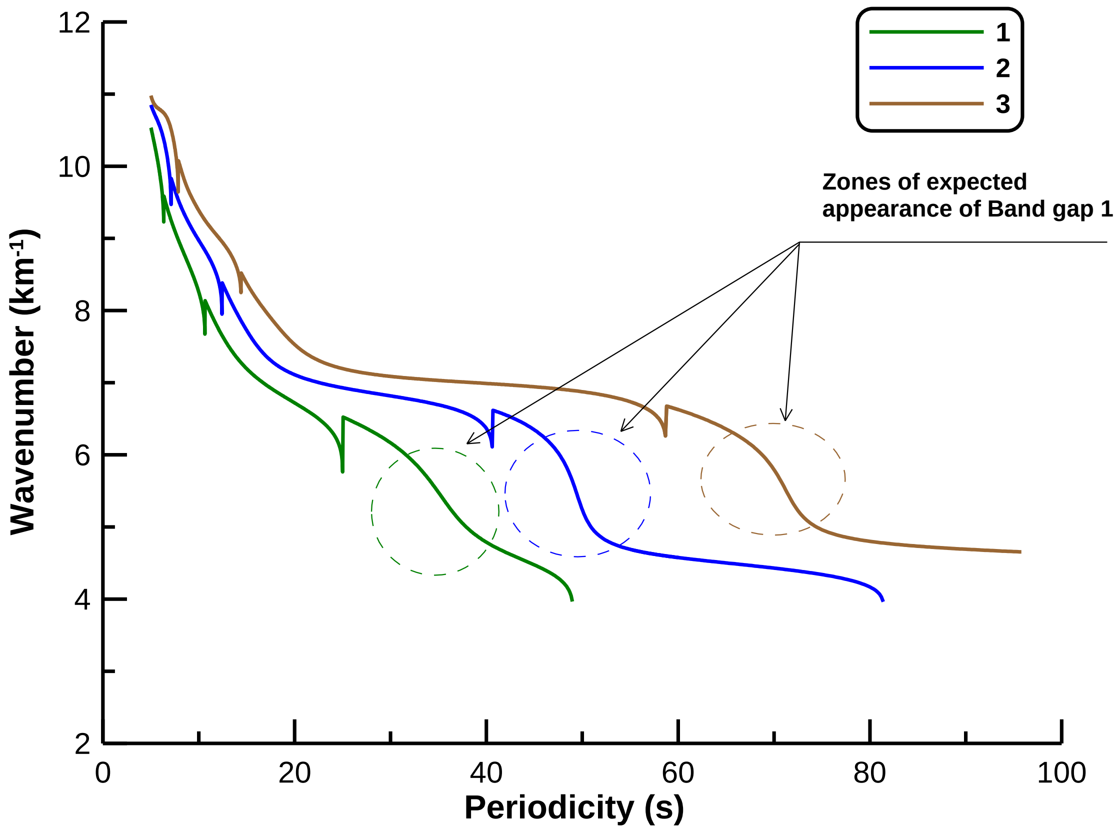
1
2
3
Zones of expected
appearance of Band gap 1
Wavenumber (km-1)
Periodicity (s)
12
10
8
6
4
2
0
20
40
60
80
100

Fig. 1a

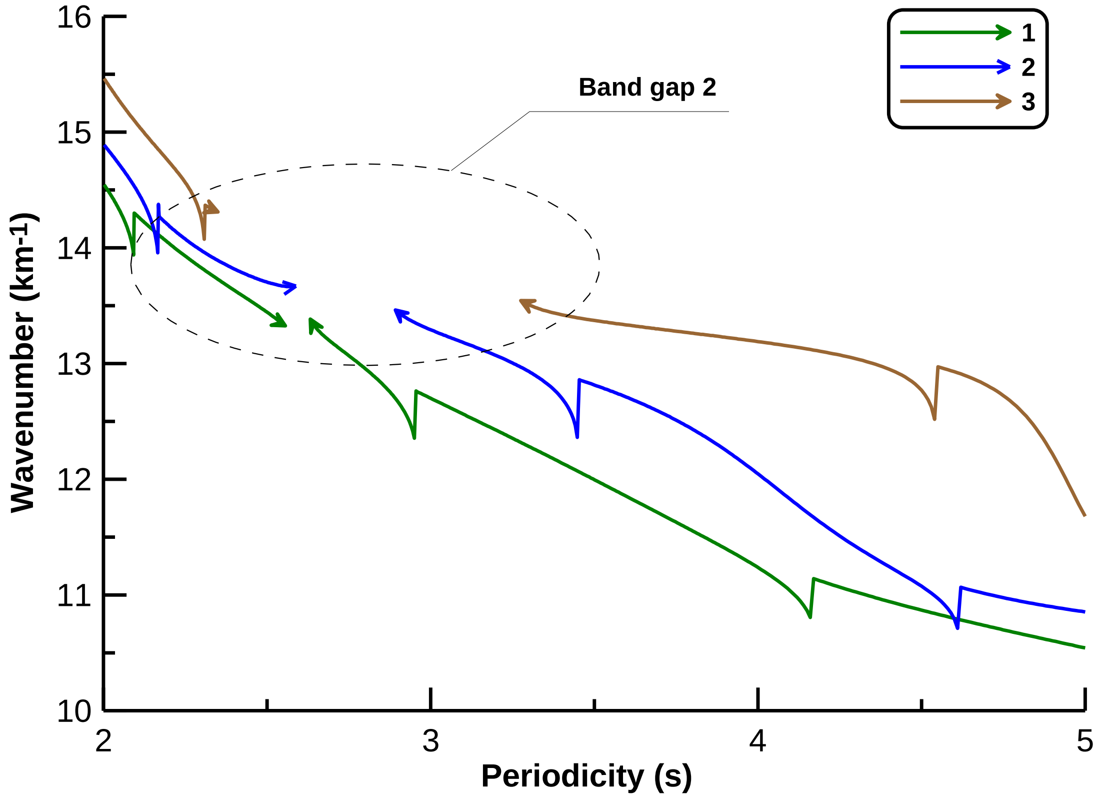
1
2
3
Band gap 2
Wavenumber (km-1)
Periodicity (s)
16
15
14
13
12
11
10
2
3
4
5

Fig. 1b

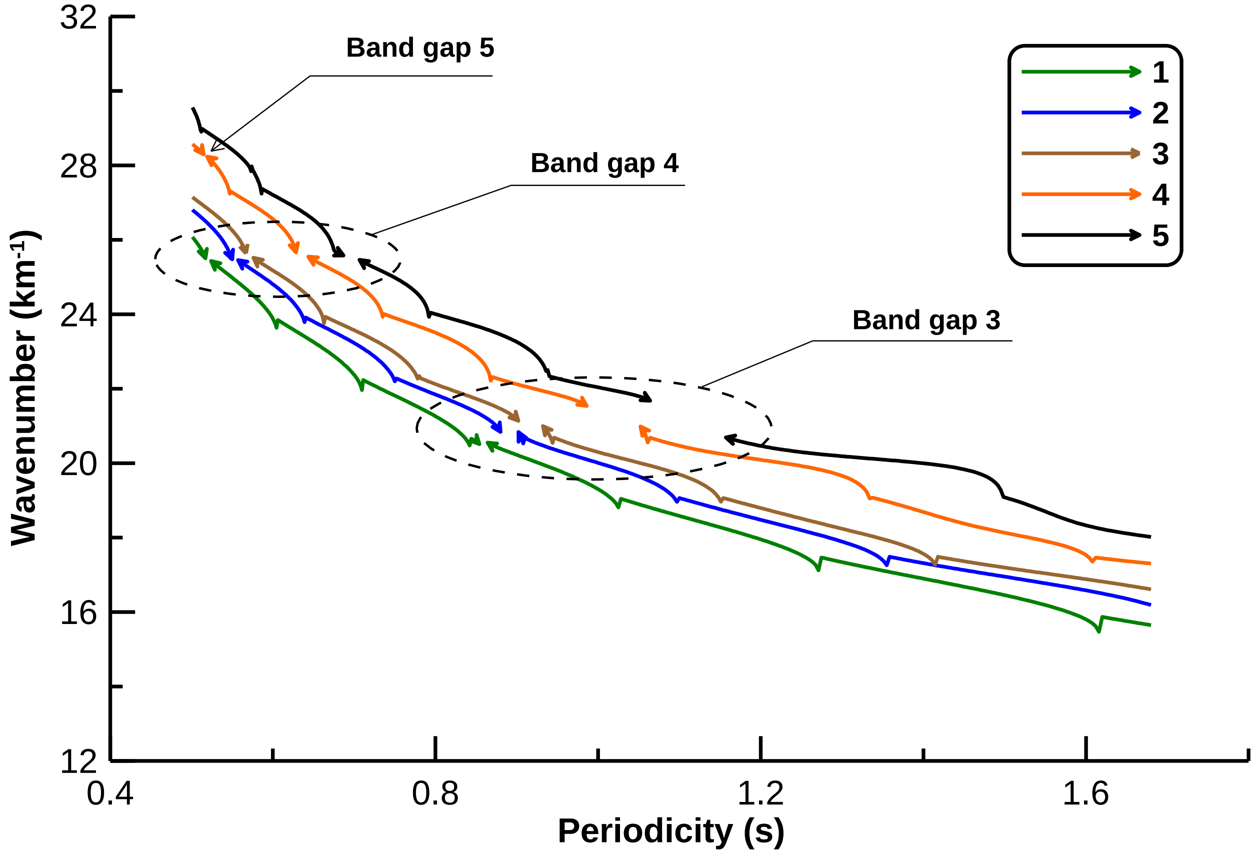

Fig. 1c

Figure 1. Dispersion spectra obtained using **Model 1** with $\boldsymbol{\alpha_1} = \mathbf{1}, \boldsymbol{\alpha_2} = \mathbf{0}$ for ice shelf geometries differing in the amplitude of ice thickness oscillations A_H: **1** $-A_H = 5\ m$; **2** $- A_H = 10\ m$; **3** $-A_H = 12\ m$; **4** $-A_H = 16\ m$; **5** $-A_H = 18\ m$. **(a)** area of the expected first band gap; **(b)** area of the expected second band gap; **(c)** area of expected third and fourth band gaps.

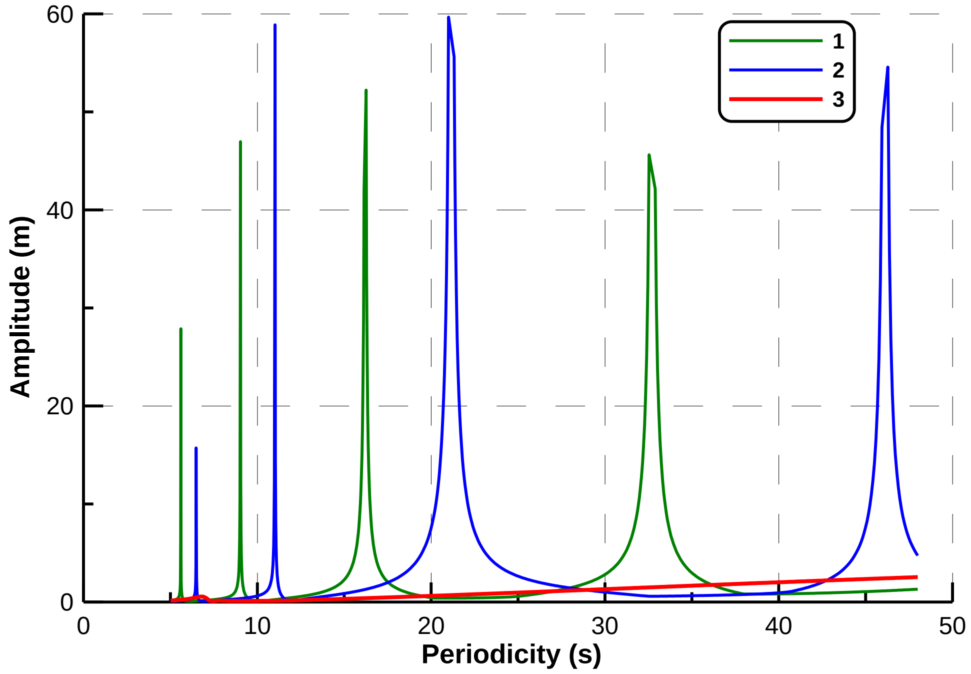

Fig. 2a

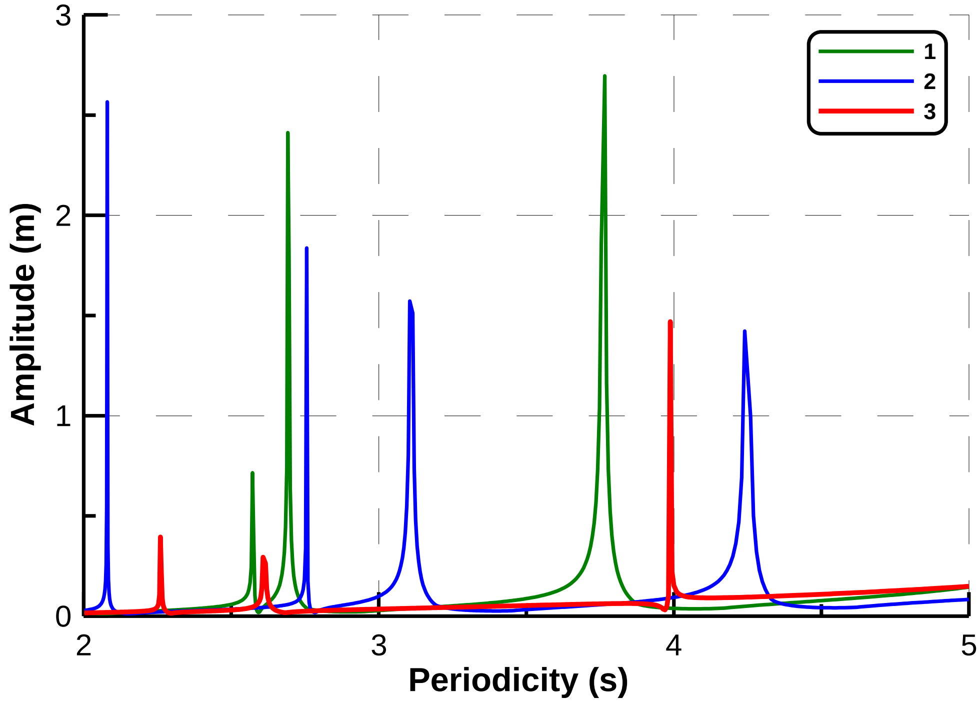

Fig. 2b

Figure 2. Amplitude spectra obtained using **Model 1** with $\boldsymbol{\alpha_1 = 1}, \boldsymbol{\alpha_2 = 0}$ for ice shelf geometries differing in the amplitude of ice thickness oscillations A_H: **1** – $A_H = 5\ m$; **2** – $A_H = 10\ m$; **3** – $A_H = 18\ m$. **(a)** area of the expected first band gap (Fig 1a); **(b)** area of the expected second band gap (Fig. 1b).

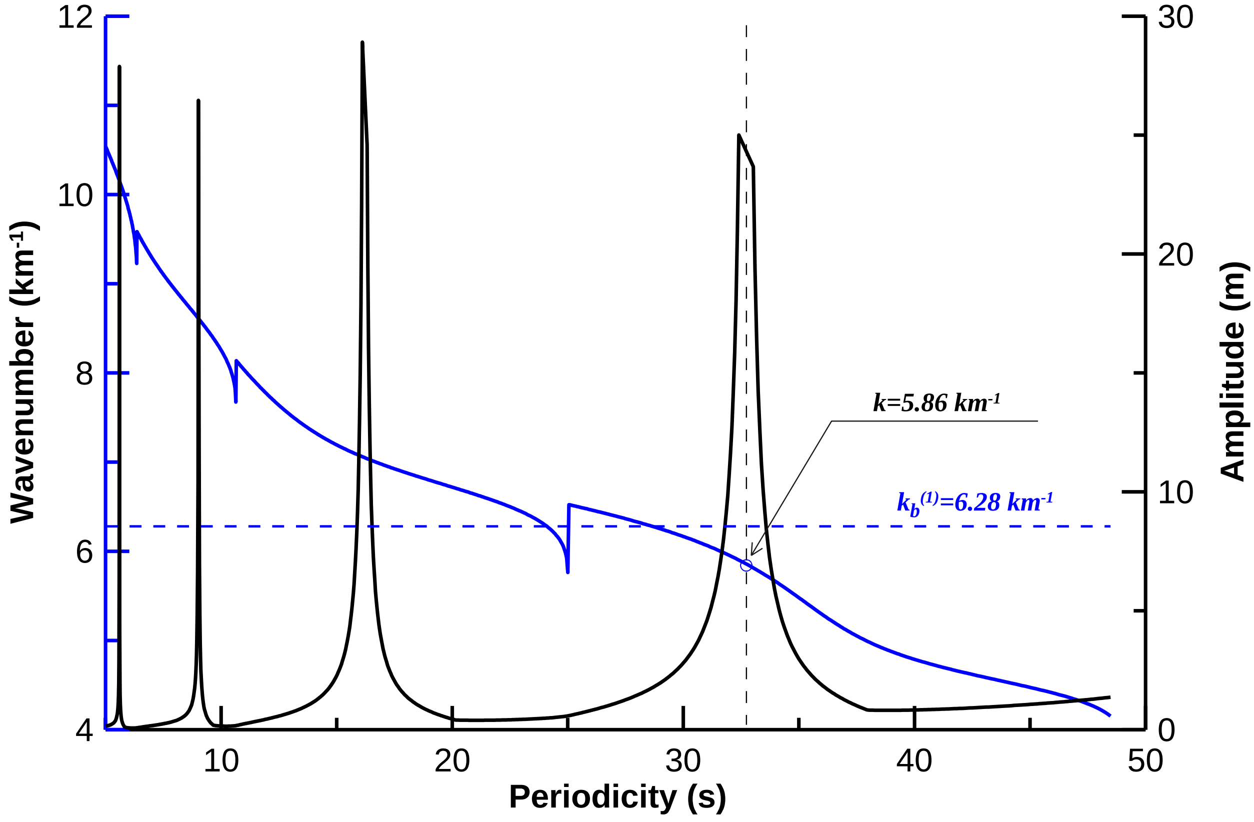
Wavenumber (km-1)
Amplitude (m)
Periodicity (s)
k=5.86 km-1
kb(1)=6.28 km-1
12
10
8
6
4
30
20
10
0
10
20
30
40
50

Fig. 3a

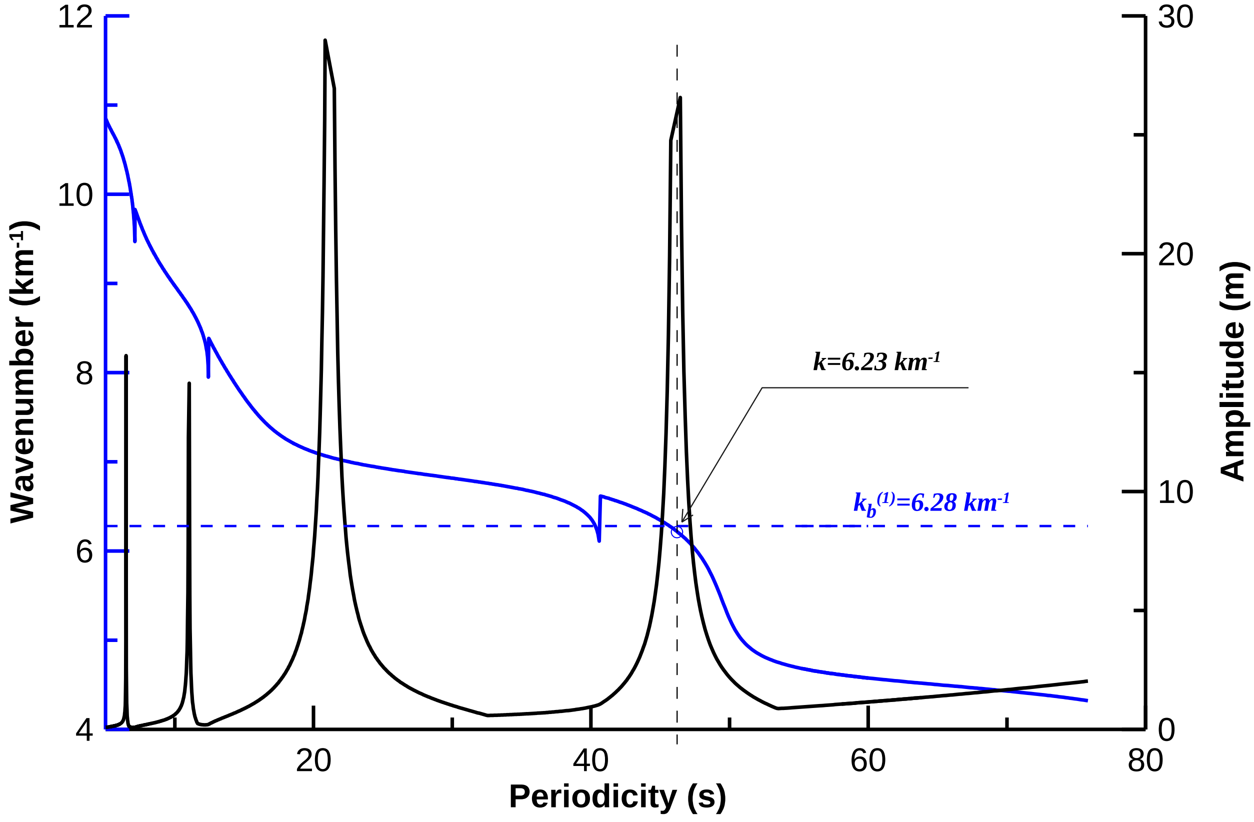
Wavenumber (km-1)
Amplitude (m)
Periodicity (s)
k=6.23 km-1
kb(1)=6.28 km-1
12
10
8
6
4
30
20
10
0
20
40
60
80

Fig. 3b

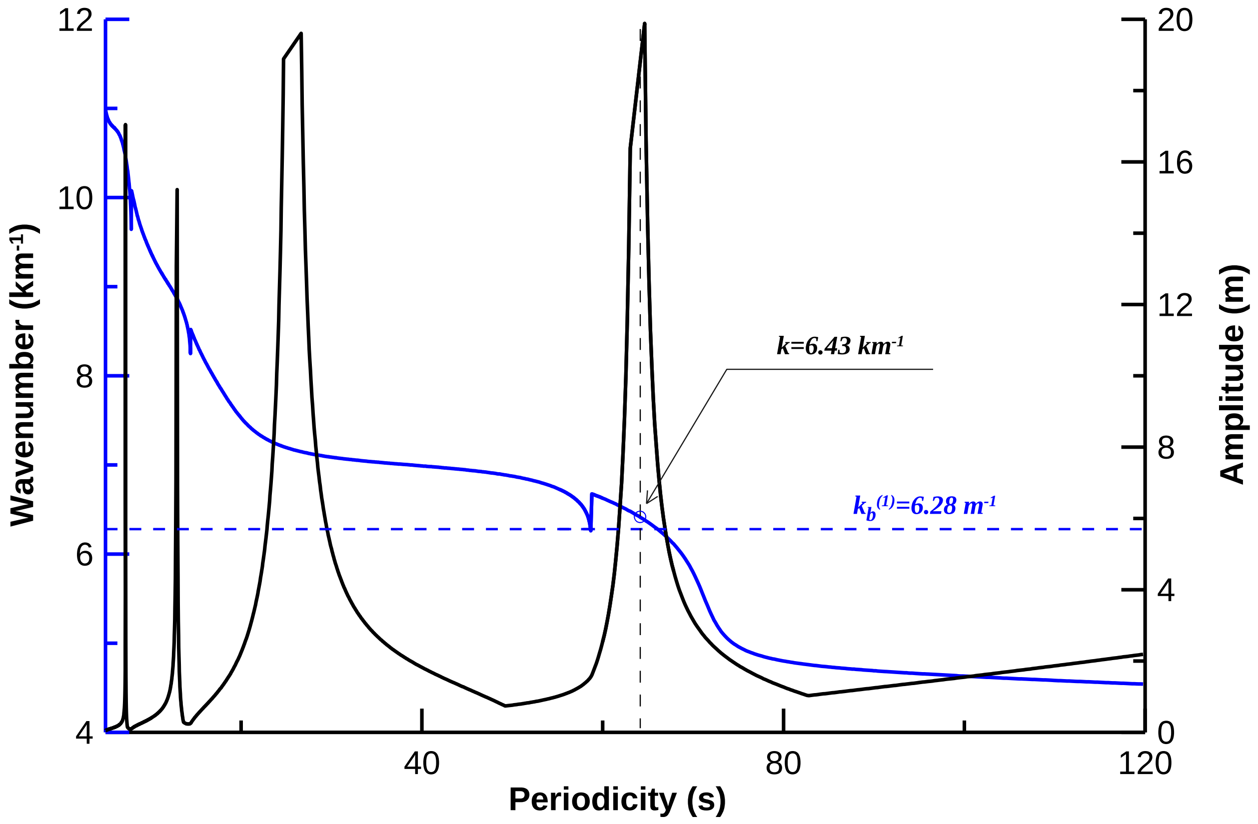

Fig. 3b

Figure 3. Dispersion spectrum and amplitude spectrum, including the area of the expected first band gap, obtained using **Model 1** with $\boldsymbol{\alpha_1 = 1, \alpha_2 = 0}$ for ice shelf geometries differing in the amplitude of ice thickness fluctuations A_H: **(a)** $A_H = 5\ m$; **(b)** $A_H = 10\ m$; **(c)** $A_H = 12\ m$.

2. Results obtained by Model 1 (case of $\alpha_1 = 0.2, \alpha_2 = 0.8$)

In Konovalov (2023) it was found that the dominance of the second type of boundary conditions in equation (10) (i.e. $\alpha_2 > \alpha_1$ in equation (10)) provides higher sensitivity in the appearance of band gaps. Similar results are observed for an ice shelf with a rolling surface morphology (Figure 4). The transition from a typical dispersion spectrum with intermode spaces to a dispersion spectrum, containing bad gaps, occurs at $A_H = 1\ m$, i.e. the threshold value $(A_H)_{th} \approx 1\ m$ (Fig. 4a).

In this case, in contrast to the case of $\alpha_1 = 1, \alpha_2 = 0$ in Model 1, the widths of the third and fourth bad gaps increase relatively quickly in the range of A_H from 1 m to 2 m (Fig 4a). Essentially, at $A_H > 2\ m$, two band gaps merge into a ban gap located in a wide part of the dispersion spectrum (for example, curve 2 in Fig. 4b).

Nevertheless, more significant degradation of the amplitude spectrum is observed at higher values of A_H, than considered in Figure 4(as in Figure 2 at $A_H \approx 18\ m$). That is, the amplitude spectra obtained at $A_H = 2..3\ m$ reveal approximately the same resonance peaks as the spectrum obtained at $A_H = 1\ m$ (Figure 5), although we observe a thinning of the resonance peaks obtained at $A_H = 3\ m$, compared the peaks obtained at $A_H = 1\ m$ (Fig. 5a).

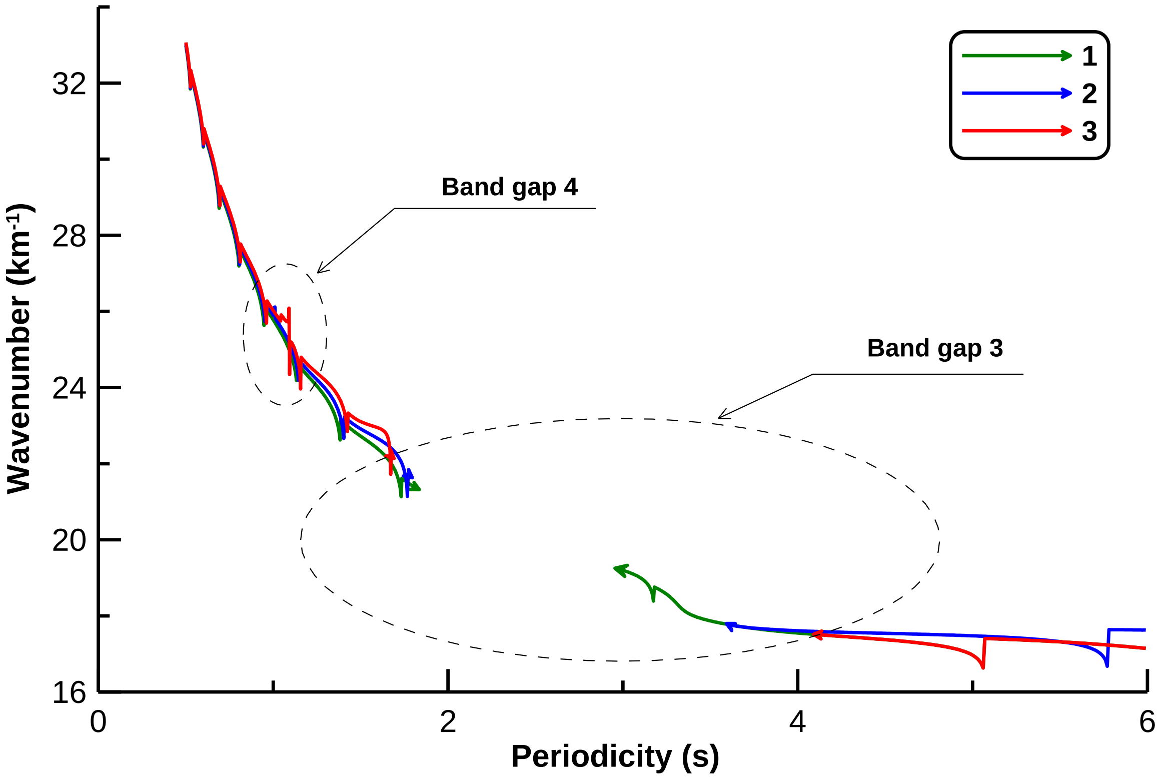

Fig. 4a

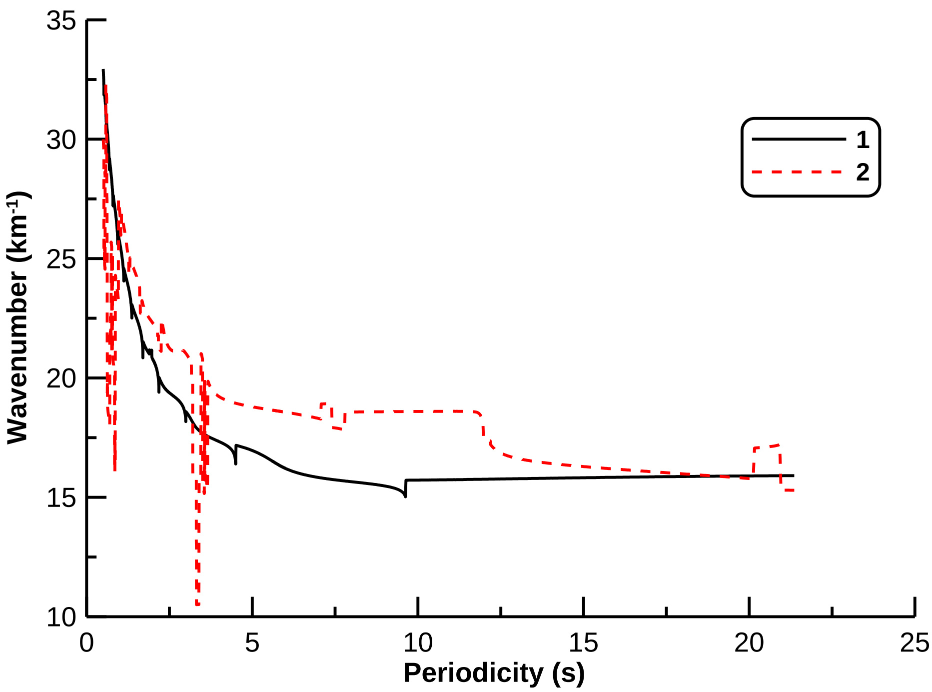

Fig. 4b

Figure 4. Dispersion spectra obtained using **Model 1** with $\boldsymbol{\alpha_1 = 0.2, \alpha_2 = 0.8}$ for ice shelf geometries differing in the amplitude of ice thickness oscillations A_H: **(a)** **1** –$A_H = 1.2\ m$; **2** – $A_H = 1.3\ m$; **3** –$A_H = 1.4\ m$; **(b)** **1** –$A_H = 1.1\ m$; **2** – $A_H = 3\ m$.

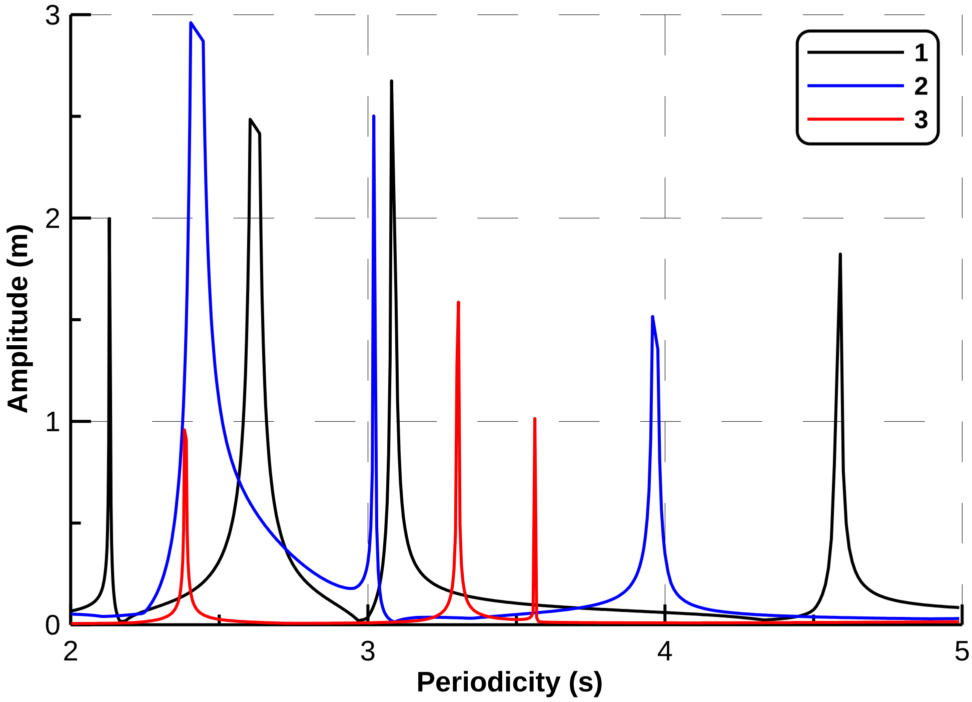

Fig. 5a

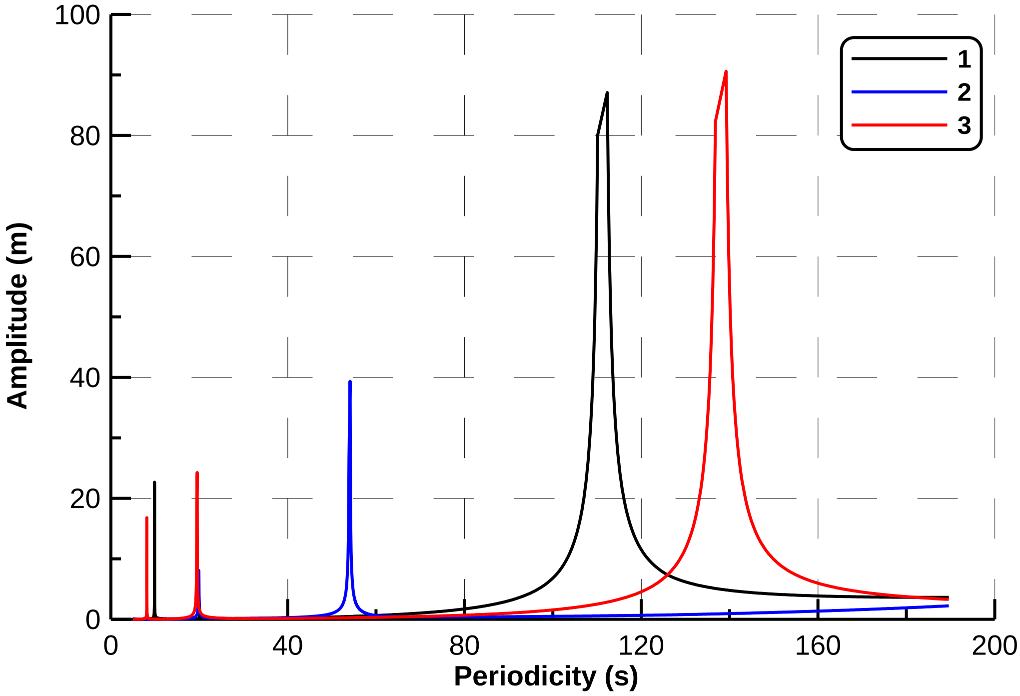

Fig. 5b

Figure 5. Amplitude spectra obtained using **Model 1** with $\boldsymbol{\alpha_1 = 0.2, \alpha_2 = 0.8}$ for ice shelf geometries differing in the amplitude of ice thickness oscillations A_H: **1** $-A_H = 1\ m$; **2** $-A_H = 2\ m$; **3** $- A_H = 3\ m$.

3. Results obtained by Model 2 (case of $\boldsymbol{\alpha_1 = 0, \alpha_2 = 1}$)

In the case of $\alpha_1 = 0, \alpha_2 = 1$ in Model 2 the first band gap ($k_b^{(1)} \approx 6.28\ km^{-1}$) appears in the spectrum at $A_H > 15\ m$ (Fig. 6a), i.e. the first threshold value is about the same as in the case of $\alpha_1 = 1, \alpha_2 = 0$: $(A_H)_{th}^{(1)} \approx 15m$.

Second band gap ($k_b^{(2)} \approx 12.57\ km^{-1}$, Fig. 6b) appears in the spectrum at $A_H > 2\ m$, i.e. corresponding threshold value $(A_H)_{th}^{(2)} \approx 2m$.

Third band gap ($k_b^{(3)} \approx 19.04\ km^{-1}$, Fig. 6c) appears in the spectrum at $A_H > 1\ m$, i.e. corresponding threshold value $(A_H)_{th}^{(3)} \leq 1m$.

Fourth band gap ($k_b^{(4)} \approx 25.13\ km^{-1}$, Fig. 6c) is observed in the spectrum at $A_H > 2\ m$, i.e. corresponding threshold values are also $(A_H)_{th}^{(4)} \approx 2m$.

Comparing Fig.2a or Fig. 5a from the main manuscript with Fig. 7a, in the case of $\alpha_1 = 0, \alpha_2 = 1$ we also observe a decline of the amplitude spectrum at the highest values of A_H from the considered range.

Similarly Figure 6 from the main manuscript, Figure 8 shows the combination of two spectra: dispersion spectrum and amplitude spectrum in the area where the first band gap is expected to appear ($k_b^{(1)} \approx 6.28\ km^{-1}$).

In particular,

(a) when the amplitude of ice thickness fluctuations A_H is equal to $\mathbf{5\ m}$ (Fig. 8a), the resonance peak is observed at the periodicity $T_n \approx 29.28\ s$ (i.e. $T_n \approx 29.28\ s$ is one of the eigenvalues), at which the wavenumber in the dispersion spectrum is about $5.77\ km^{-1}$ (i.e. $k_n \approx 5.77\ km^{-1}$);

(b) when the amplitude of ice thickness fluctuations A_H is equal to $\mathbf{10}\ \boldsymbol{m}$ (Fig. 8b), the resonance peak is observed at the periodicity $T_n \approx 32.68\ s$, at which the wavenumber in the dispersion spectrum is about $5.74\ km^{-1}$ (i.e. $k_n \approx 5.74\ km^{-1}$);

and

(c) when the amplitude of ice thickness fluctuations A_H is equal to $\mathbf{12}\ \boldsymbol{m}$ (Fig. 8c), the resonance peak is observed at the periodicity $T_n \approx 36.18\ s$, at which the wavenumber in the dispersion spectrum is about $5.1\ km^{-1}$ (i.e. $k_n \approx 5.1\ km^{-1}$).

Respectively, the relative deviation of k_n from the first *Bragg wavenumber* $k_b^{(1)}$ doesn't exceed 20%.

The main difference of the case $\alpha_1 = 0, \alpha_2 = 1$ and the previous one ($\alpha_1 = 0, \alpha_2 = 1$) is the presence of a torsional component of deformations in the deformations of the ice shelf (Konovalov, 2023c). The presence of a torsional component of deformation (Figure 2b) from the main manuscript) yields the appearance of additional inter-mode spaces in the dispersion spectra, accompanying the transitions between torsional components of deformation (torsion eigenmodes). These inter-mode spaces appear most significantly in Model 3 (see next paragraph).

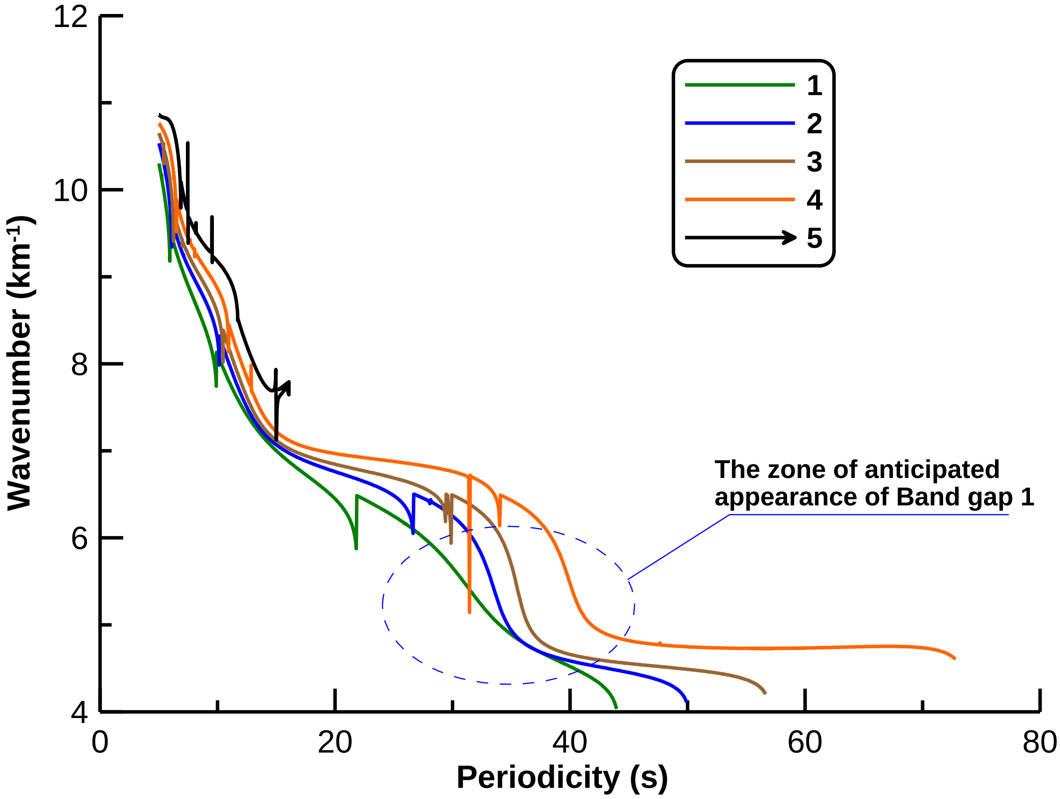

Wavenumber (km-1)
12
10
8
6
4
0
20
40
60
80
Periodicity (s)
1
2
3
4
5
The zone of anticipated appearance of Band gap 1

Fig. 6a

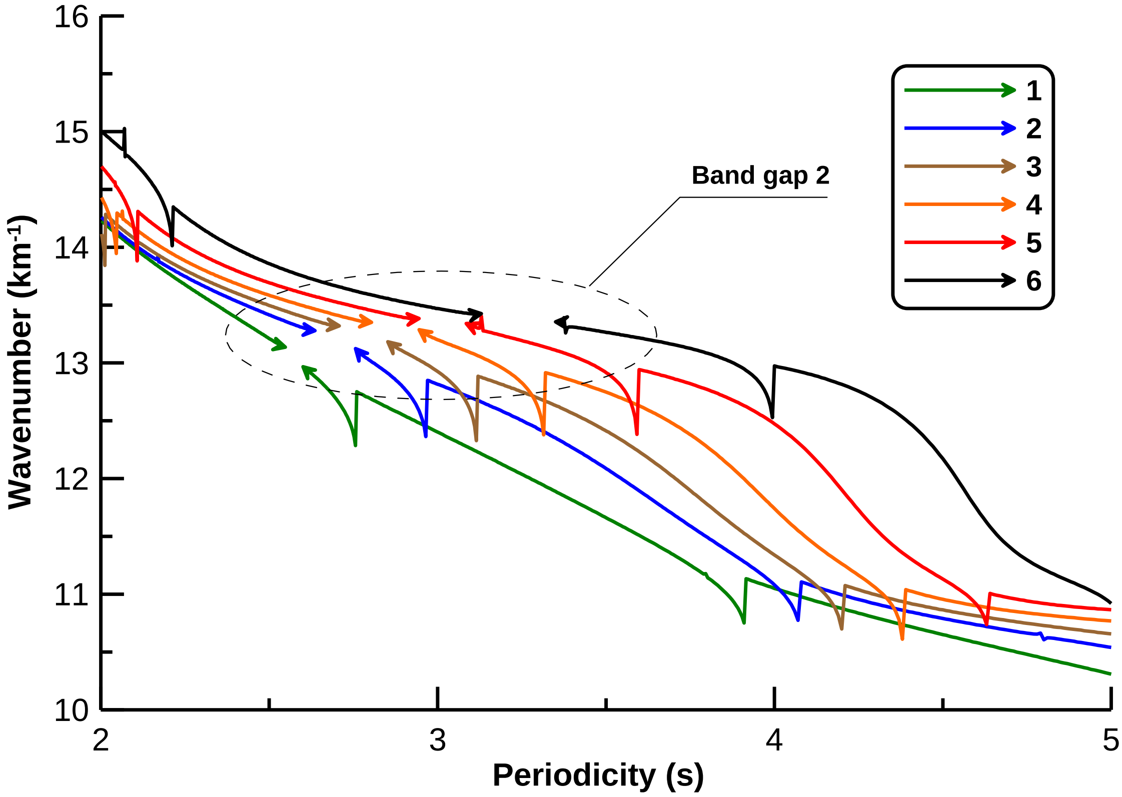

Wavenumber (km-1)
16
15
14
13
12
11
10
2
3
4
5
Periodicity (s)
Band gap 2
1
2
3
4
5
6

Fig. 6b

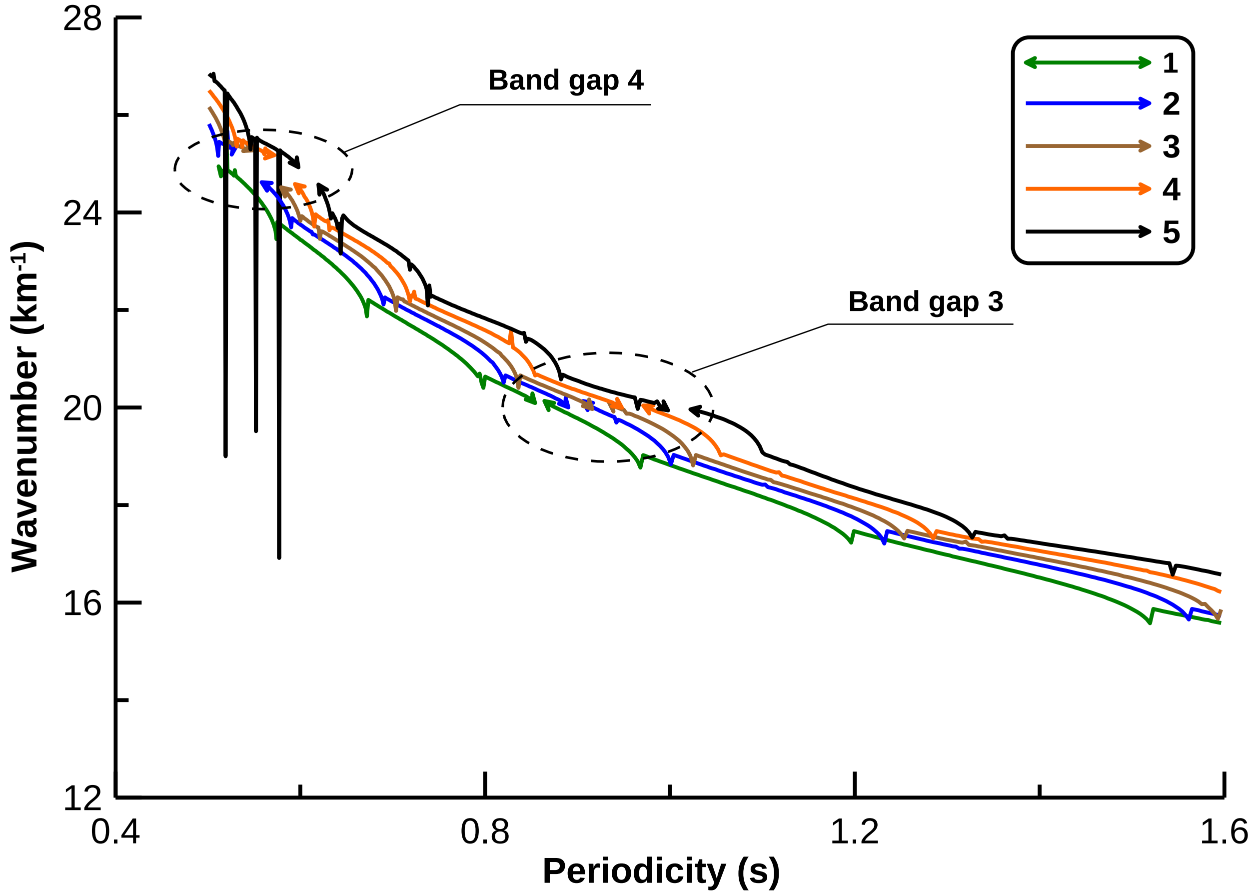

Fig. 6c

Figure 6. Dispersion spectra obtained using **Model 2** with $\boldsymbol{\alpha_1 = 0}, \boldsymbol{\alpha_2 = 1}$ for ice shelf geometries differing in the amplitude of ice thickness oscillations A_H.

(a) area of the expected first band gap; **1** $-A_H = 5\ m$; **2** $-\ A_H = 10\ m$; **3** $-A_H = 12\ m$; **4** $-A_H = 14\ m$; **5** $-A_H = 16\ m$;

(b) area of the expected second band gap; **1** $-A_H = 5\ m$; **2** $-\ A_H = 10\ m$; **3** $-A_H = 12\ m$; **4** $-A_H = 14\ m$; **5** $-A_H = 16\ m$; **6** $-A_H = 18\ m$;

(c) area of expected third and fourth band gaps; **1** $-A_H = 5\ m$; **2** $-\ A_H = 10\ m$; **3** $-A_H = 12\ m$; **4** $-A_H = 14\ m$; **5** $-A_H = 16\ m$.

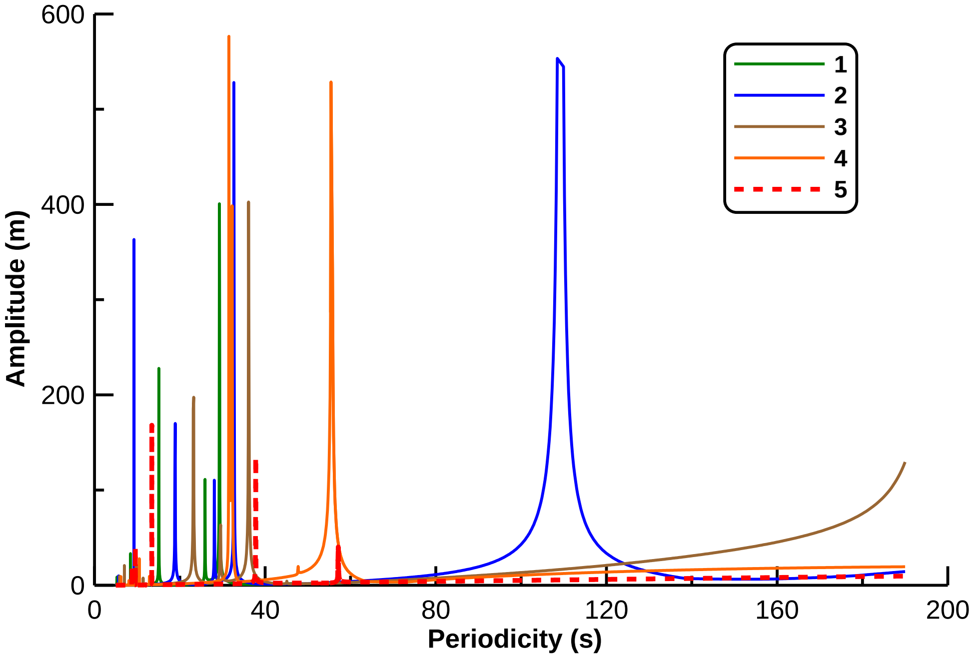

Fig. 7a

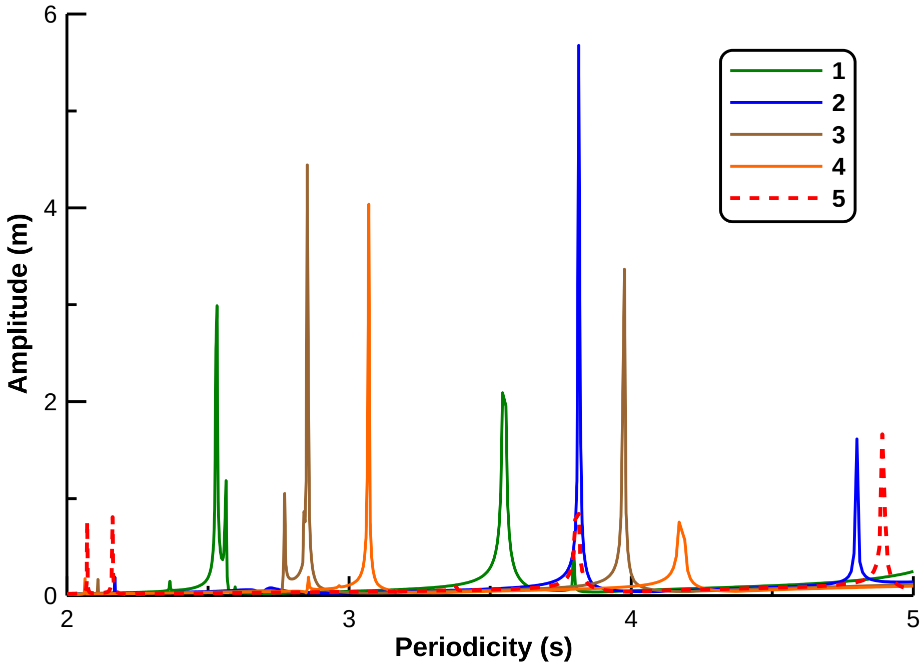

Fig. 7b

Figure 7. Amplitude spectra obtained using **Model 2** with $\boldsymbol{\alpha_1 = 0}, \boldsymbol{\alpha_2 = 1}$ for ice shelf geometries differing in the amplitude of ice thickness oscillations A_H: **1** $-A_H = 5\ m$; **2** $- A_H = 10\ m$; **3** $-A_H = 12\ m$; **4** $-A_H = 14\ m$; **5** $-A_H = 18\ m$;

(a) area of the expected first band gap (Fig 6a); **(b)** area of the expected second band gap (Fig. 6b)

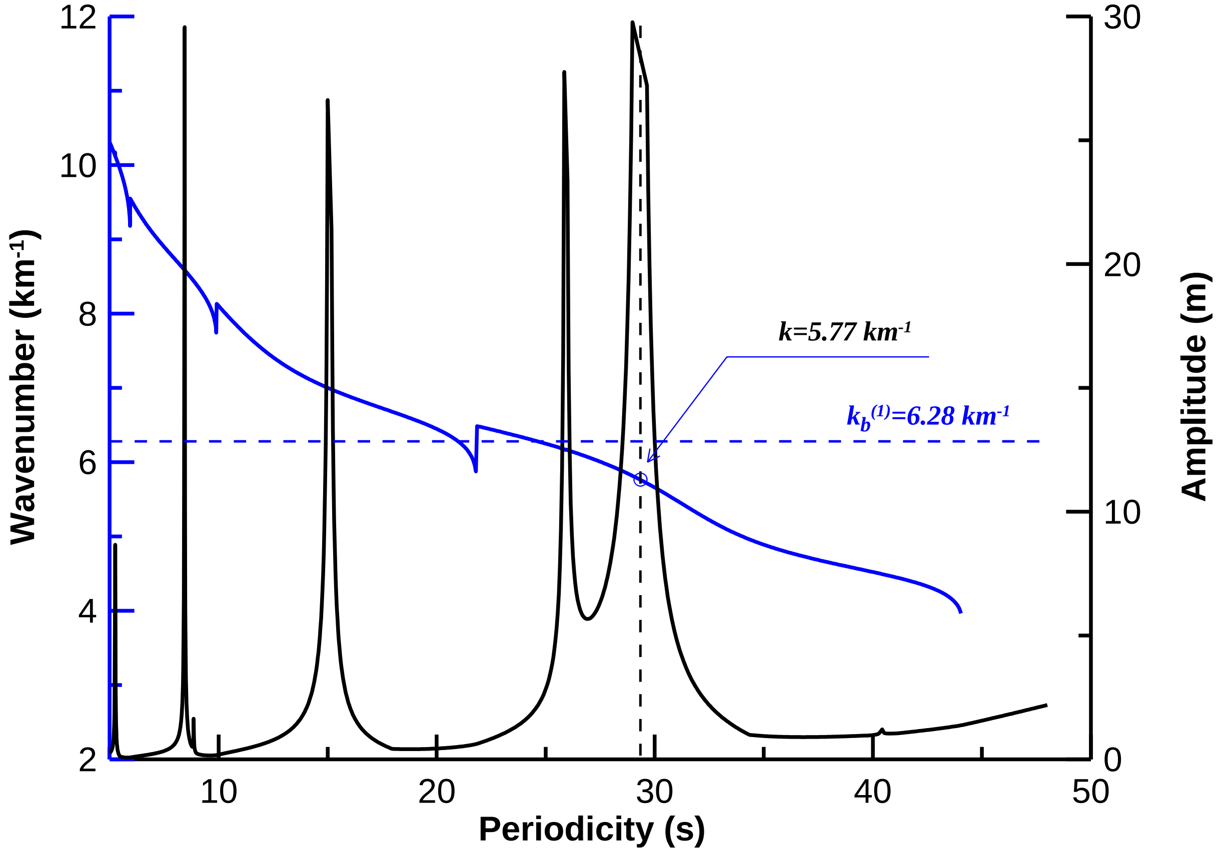
Wavenumber (km-1)
Amplitude (m)
Periodicity (s)
k=5.77 km-1
$k_b^{(1)}$=6.28 km-1

Fig. 8a

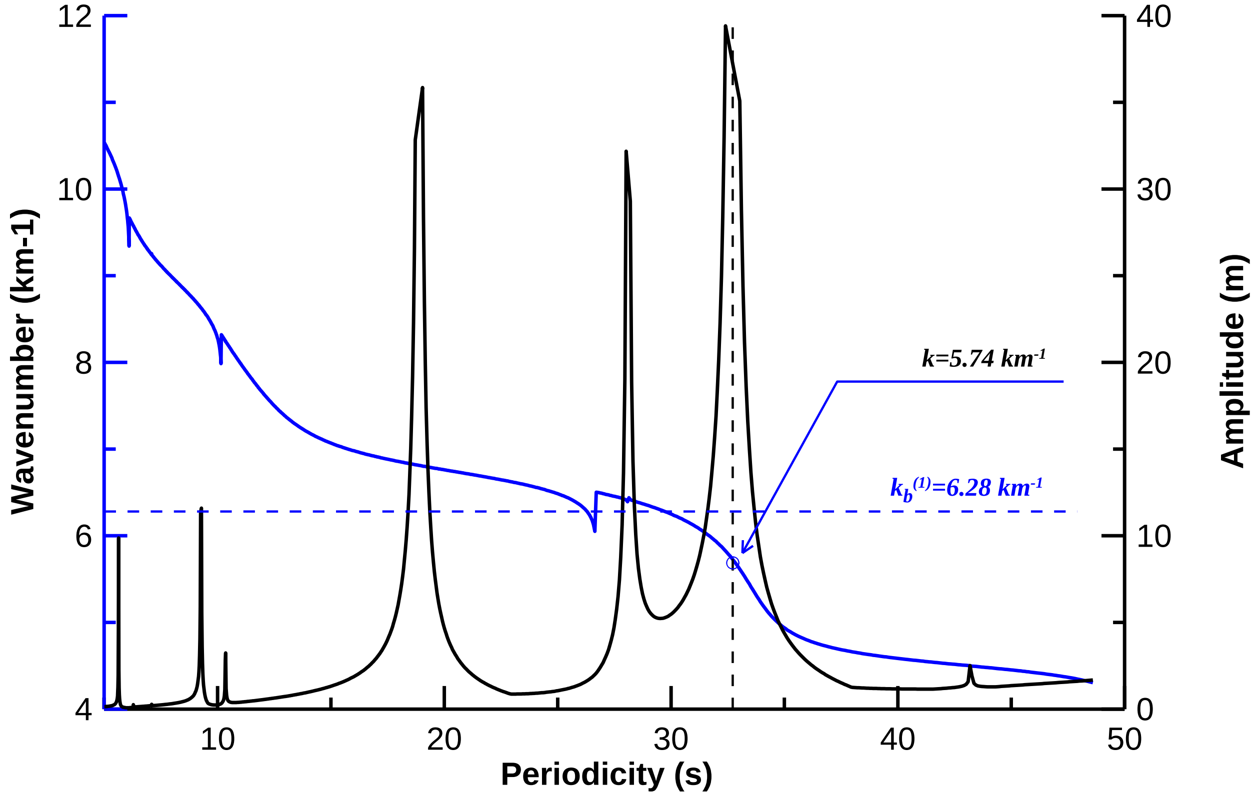
Wavenumber (km-1)
Amplitude (m)
Periodicity (s)
k=5.74 km-1
$k_b^{(1)}$=6.28 km-1

Fig. 8b

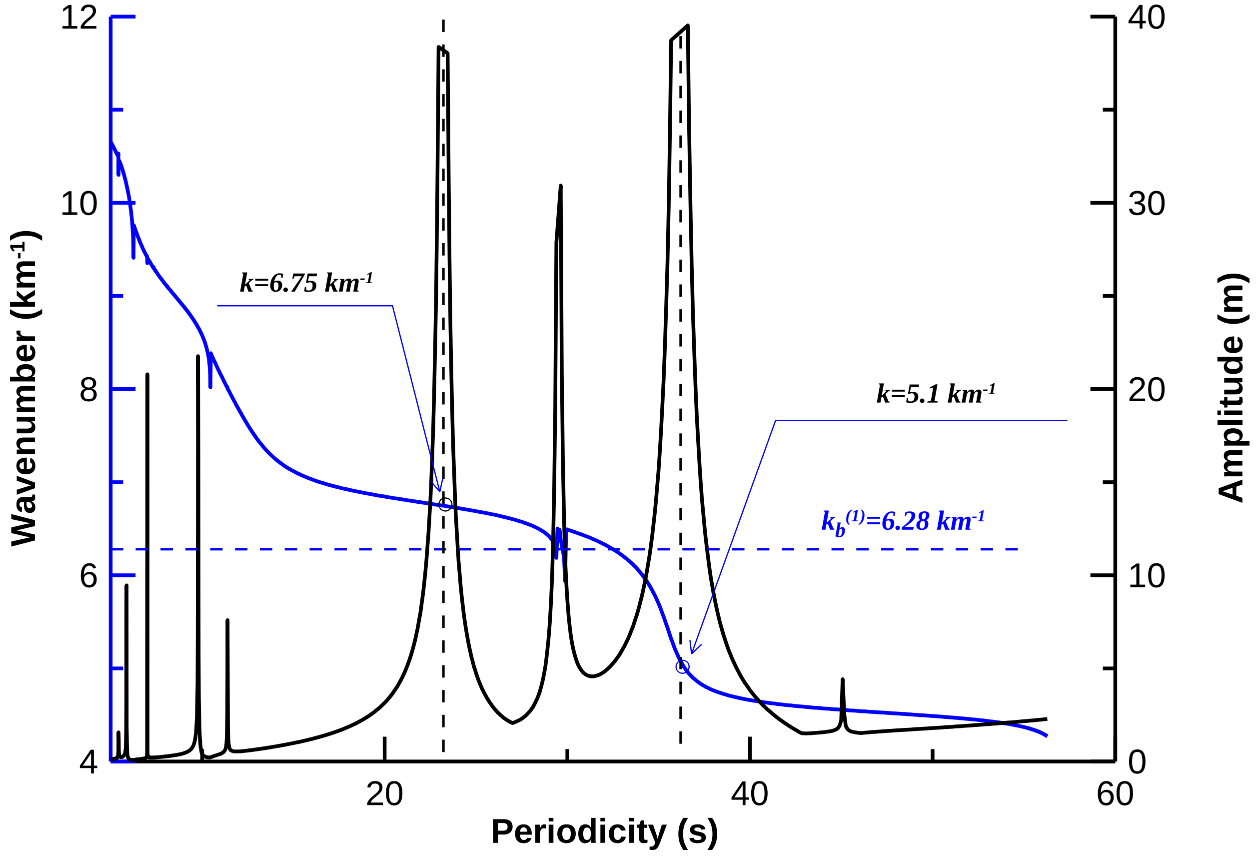

Fig. 8c

Figure 8. Dispersion spectrum and amplitude spectrum, including the area of the expected first band gap, obtained using **Model 2** with $\boldsymbol{\alpha_1 = 0, \alpha_2 = 1}$ for ice shelf geometries differing in the amplitude of ice thickness fluctuations A_H: **(a)** $A_H = 5\ m$; **(b)** $A_H = 10\ m$; **(c)** $A_H = 12\ m$.

4. Results obtained by Model 3 (case of $\alpha_1 = 1, \alpha_2 = 0$)

Dispersion spectra obtained using Model 3 reveal many areas of discontinuity in the curves (Figure 9). Firstly, there are discontinuities in the dispersion spectra, which as was previously established (e.g. Konovalov, 2021a), represent inter-mode spaces accompanying changes in the flexural component of ice shelf deformations (transitions between bending eigenmodes) (Fig. 9b; Fig. 9c). Secondly, discontinuities are observed in the dispersion spectra, which look like band gaps corresponding to Bragg scattering of the incident wave. However, not all of these discontinuity regions coincide with the values of the Bragg wavenumbers, which are determined by the equation (13), and they cannot be associated with the band gaps corresponding to the Bragg scattering of the incident wave.

The combination of the dispersion spectrum with the amplitude spectrum (Figure 10 and Figure 11) allows us to establish the following. The discontinuities in the dispersion spectra, which have the form of band gaps, but do not correspond to the Bragg scattering of the incident wave, coincide with resonance peaks in the amplitude spectra (Figure 10 and Figure 11). In other words, these discontinuities are accompanied by a transition through resonances, while the band gaps corresponding to Bragg scattering are not accompanied by the same transition. Moreover, investigations of these resonances reveal that they accompany changes in the torsional component of ice shelf deformations (transitions between torsion eigenmodes) (Figure 12 and Figure 13). Thus, changes in the torsional component of ice shelf deformations (transitions between torsion eigenmodes) are accompanied by resonances in the amplitude spectra and are reflected in the dispersion spectra in the form of discontinuities. While changes in the flexural component of ice shelf deformations (transitions between bending Lamb-type eigenmodes) are not accompanied by resonances in the amplitude spectra but, on the contrary, coincide with the amplitude minima in the spectrum (Figure 10 and Figure 11, and, also, Figure 3, Figure 6 from the main manuscript).

Therefore, the combination of the dispersion and amplitude spectra allows us to establish the type of observed discontinuity in the dispersion spectra in Model 3 (Figure 10 and Figure 11).

In the case of $\alpha_1 = 1, \alpha_2 = 0$ in Model 3 the first band gap ($k_b^{(1)} \approx 6.28\ km^{-1}$), appears in the spectrum at $A_H > 3\ m$ (Figure 9a), i.e. the first threshold value $(A_H)_{th}^{(1)} \approx 3m$. However, in particular, at $A_H = 8\ m$ the first band gap in the dispersion spectrum disappears due to the alignment of the areas of the expected band gap with the resonance peak in the corresponding regions of the dispersion spectrum. Then, at $A_H \geq 10\ m$ the first band gap appears again in the dispersion spectrum.

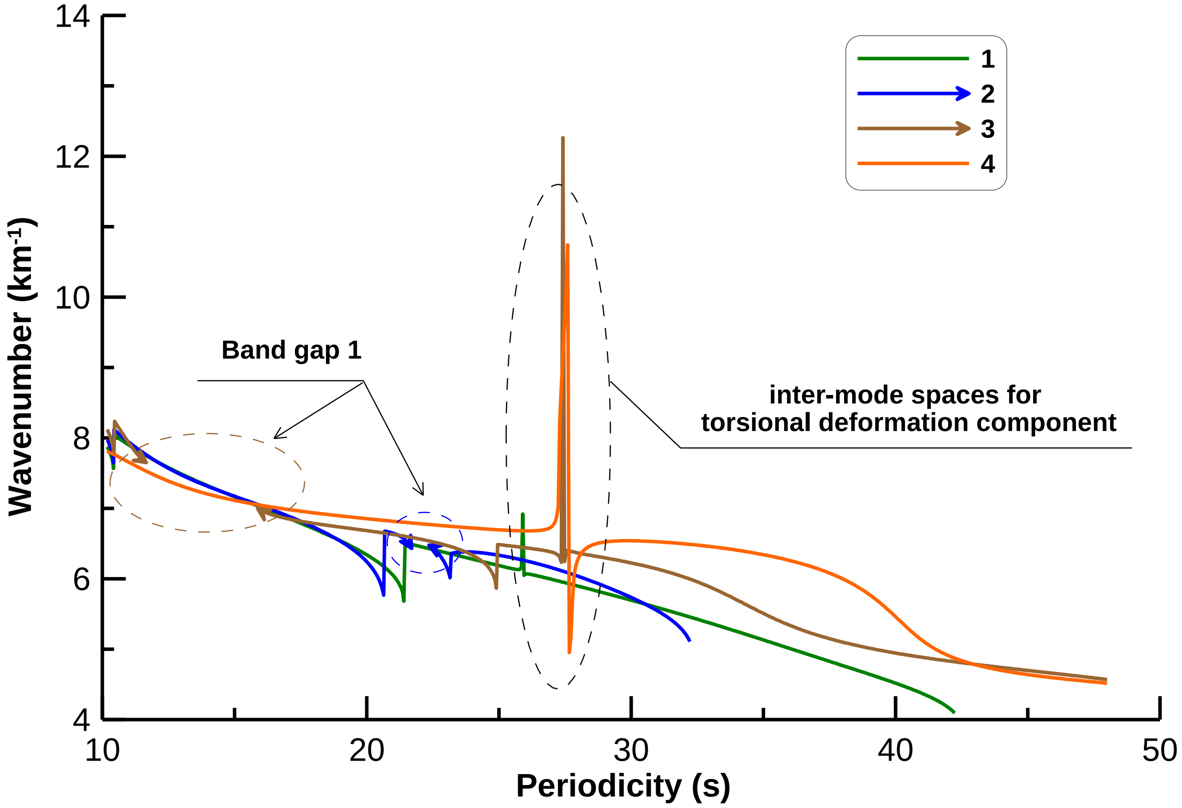
Wavenumber (km-1)
Periodicity (s)
Band gap 1
inter-mode spaces for
torsional deformation component
1
2
3
4
14
12
10
8
6
4
10
20
30
40
50

Fig. 9a

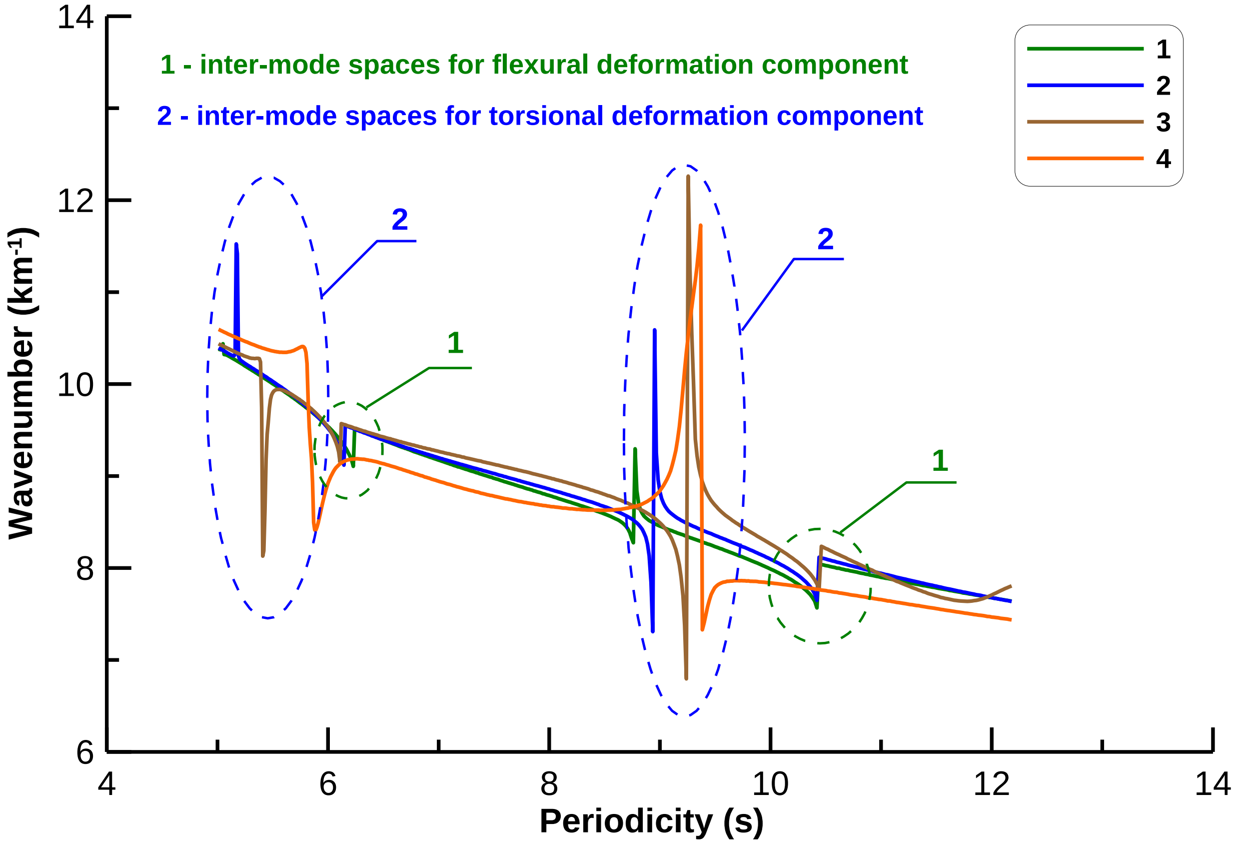
1 - inter-mode spaces for flexural deformation component
2 - inter-mode spaces for torsional deformation component
Wavenumber (km-1)
Periodicity (s)
1
2
3
4
2
2
1
1
14
12
10
8
6
4
6
8
10
12
14

Fig. 9b

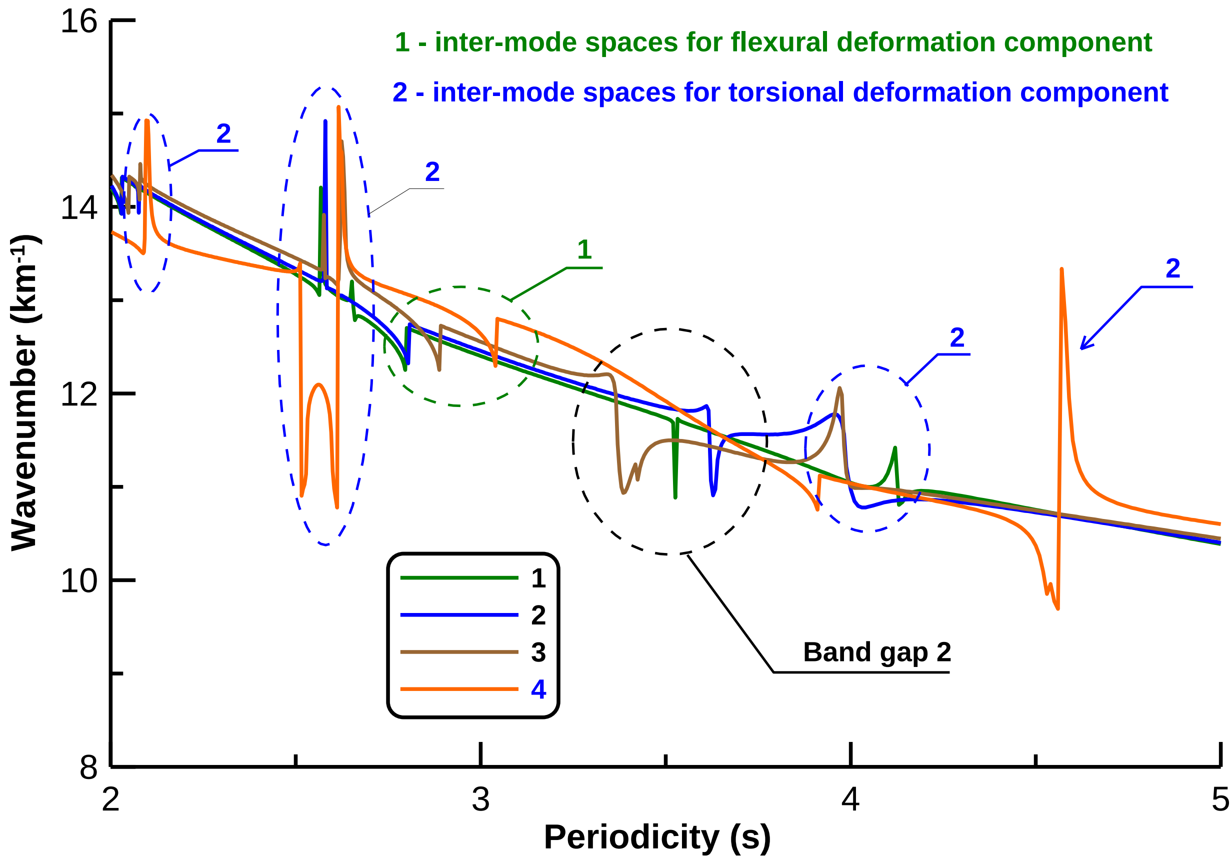

Fig. 9c

Figure 9. Dispersion spectra obtained using **Model 3** with $\boldsymbol{\alpha_1 = 1}, \boldsymbol{\alpha_2 = 0}$ for ice shelf geometries differing in the amplitude of ice thickness oscillations A_H.

(a) area of the expected first band gap; **1** $-A_H = 1\ m$; **2** $- A_H = 3\ m$; **3** $-A_H = 5\ m$; **4** $-A_H = 8\ m$;

(b) and (c) areas of the expected second band gap; **1** $-A_H = 1\ m$; **2** $- A_H = 3\ m$; **3** $-A_H = 5\ m$; **4** $-A_H = 8\ m$;

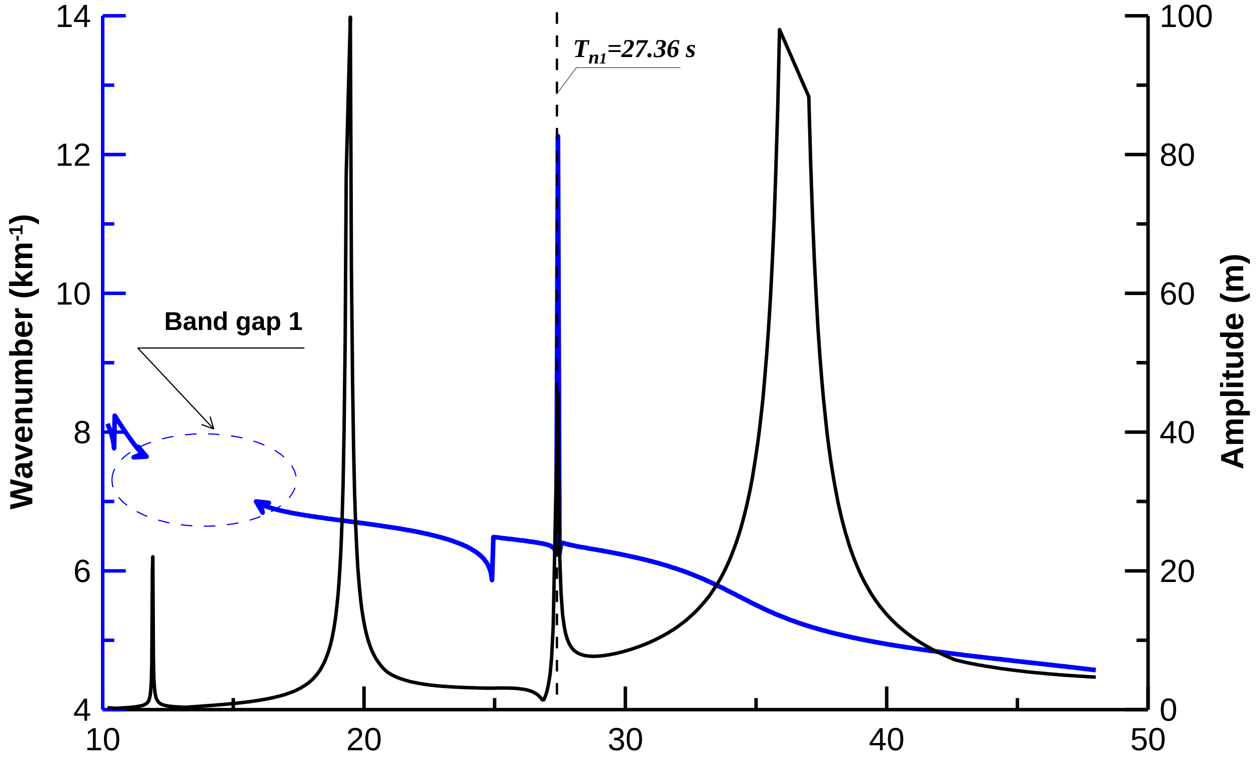

Fig. 10a

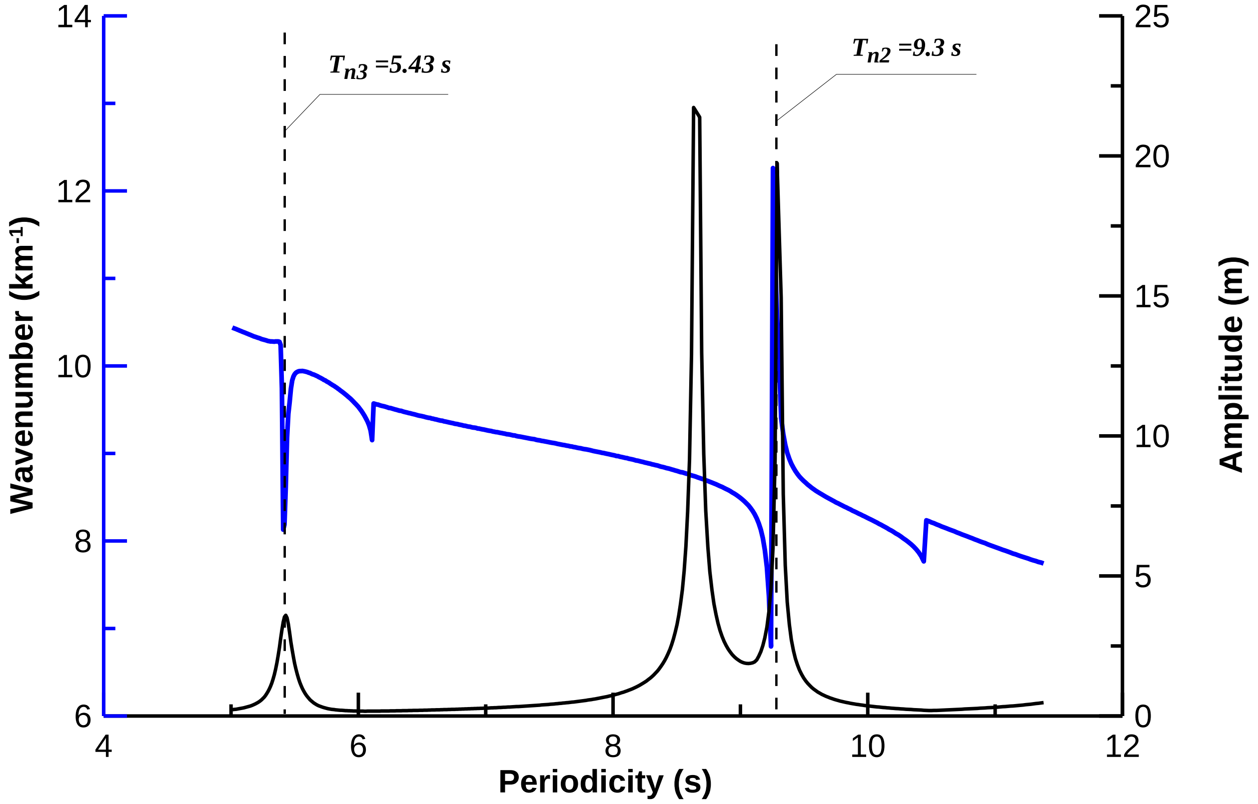

Fig. 10b

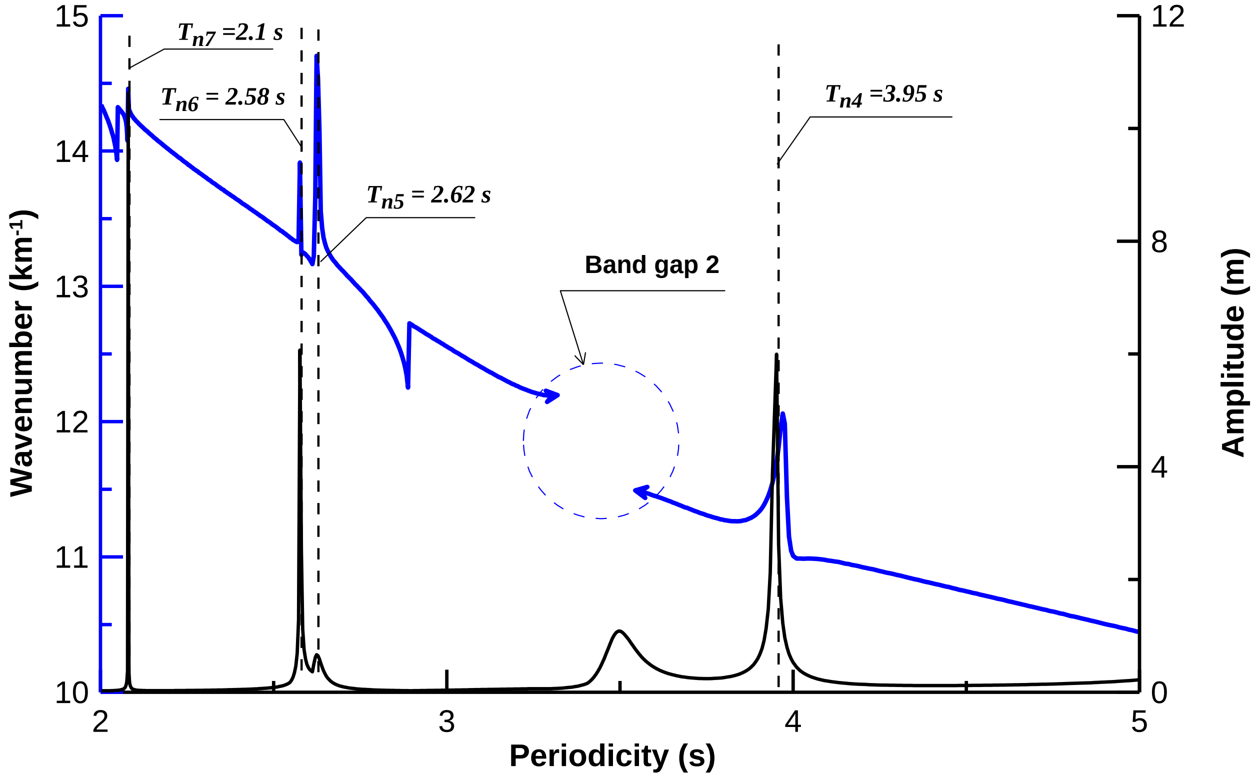

Fig. 10c

Figure 10. Dispersion spectrum and amplitude spectrum, including **(a)** and **(b)** the area of the expected first band gap, **(c)** the area of the expected second band gap, obtained using **Model 3** with $\boldsymbol{\alpha_1 = 1, \alpha_2 = 0}$ for the amplitude of ice thickness fluctuations $\boldsymbol{A_H = 5\ m}$.

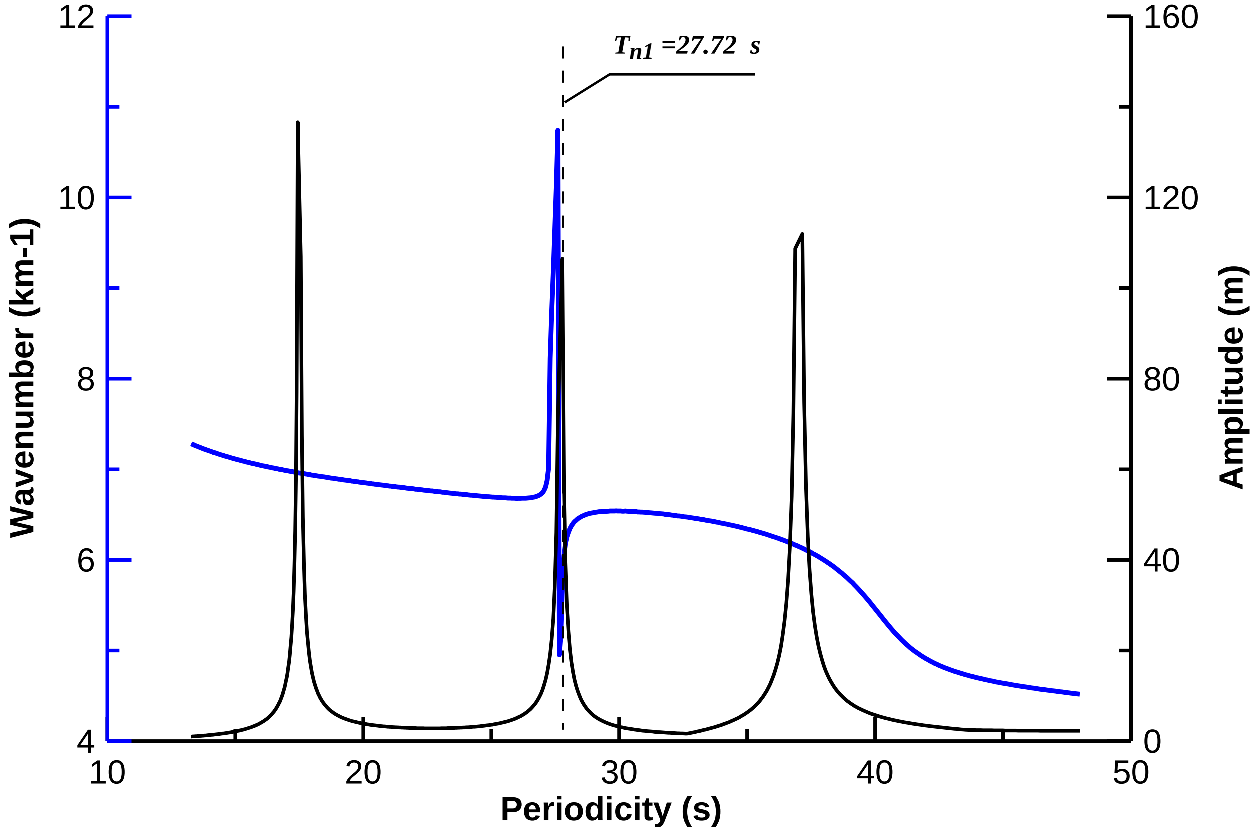

Fig. 11a

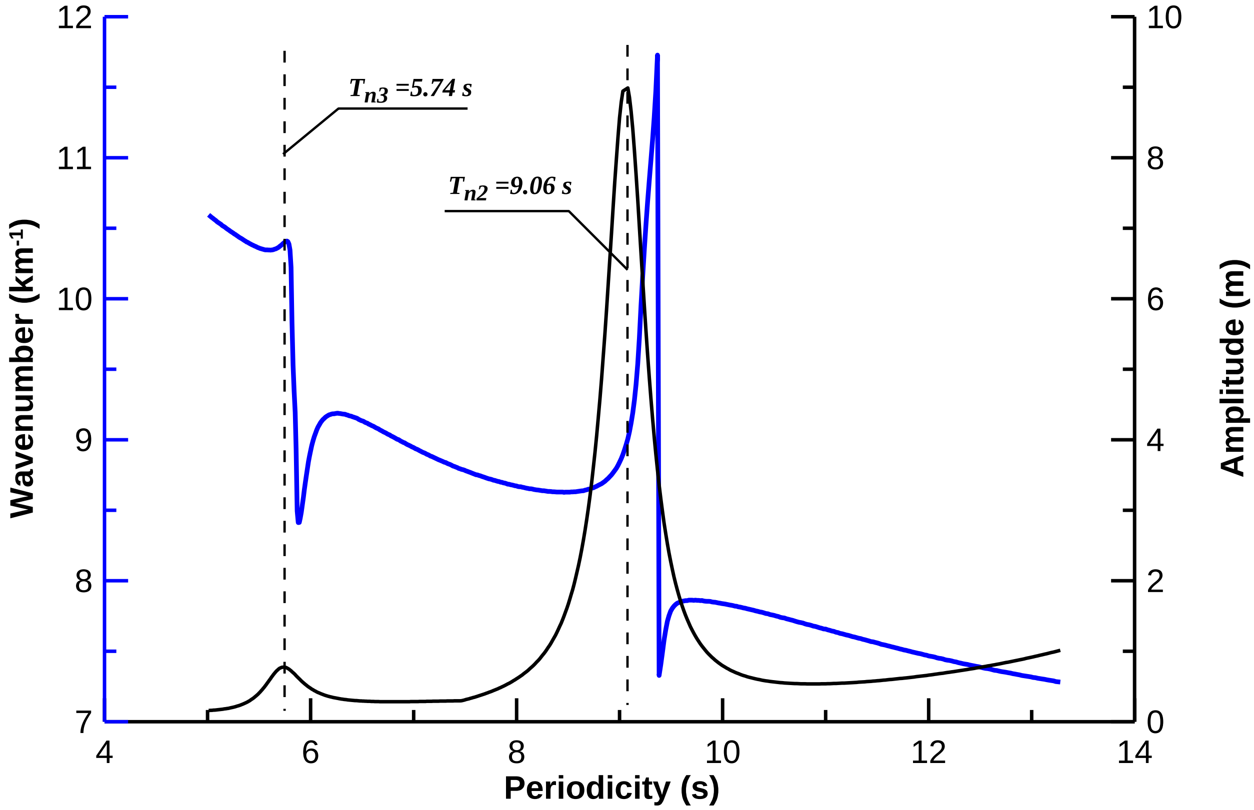

Fig. 11b

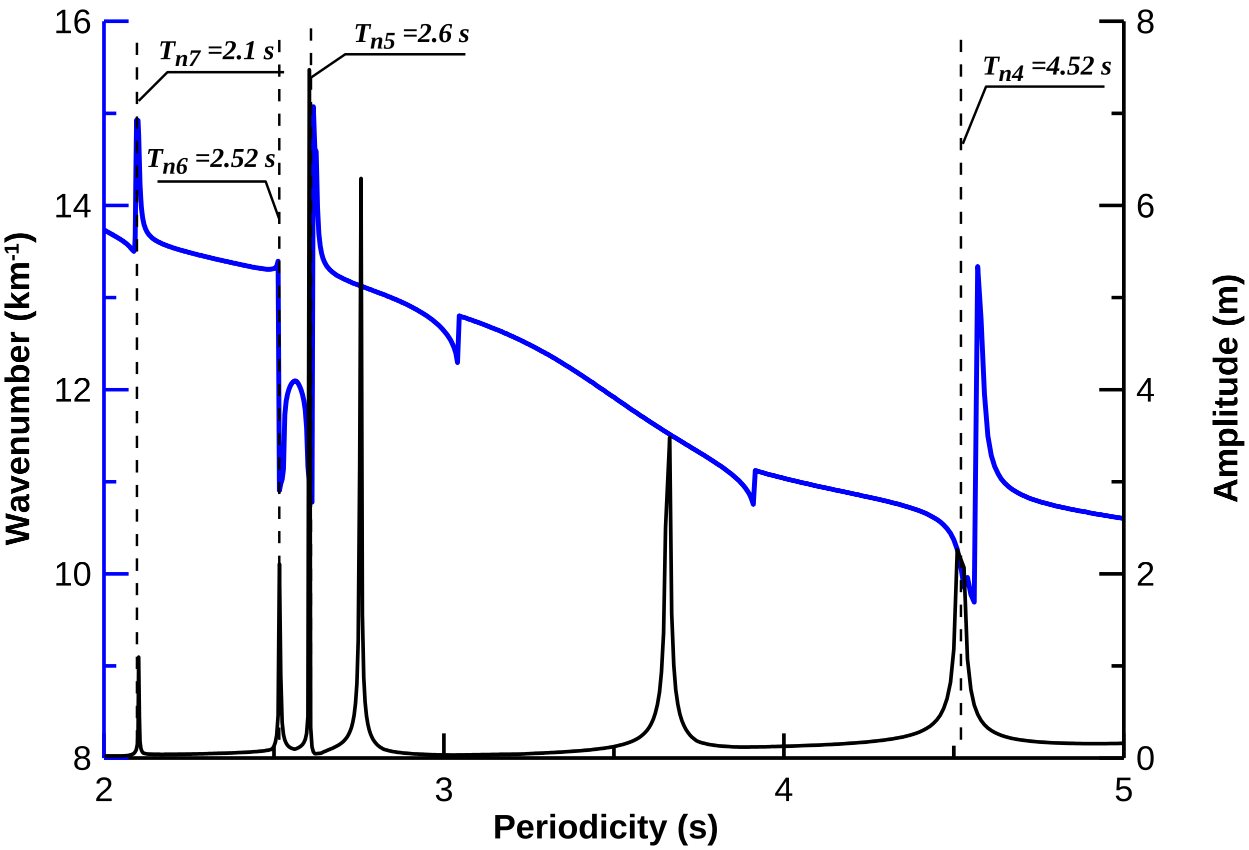

Fig. 11c

Figure 11. Dispersion spectrum and amplitude spectrum, including **(a)** and **(b)** the area of the expected first band gap, **(c)** the area of the expected second band gap, obtained using **Model 3** with $\boldsymbol{\alpha_1 = 1}, \boldsymbol{\alpha_2 = 0}$ for the amplitude of ice thickness fluctuations $\boldsymbol{A_H = 8\ m}$.

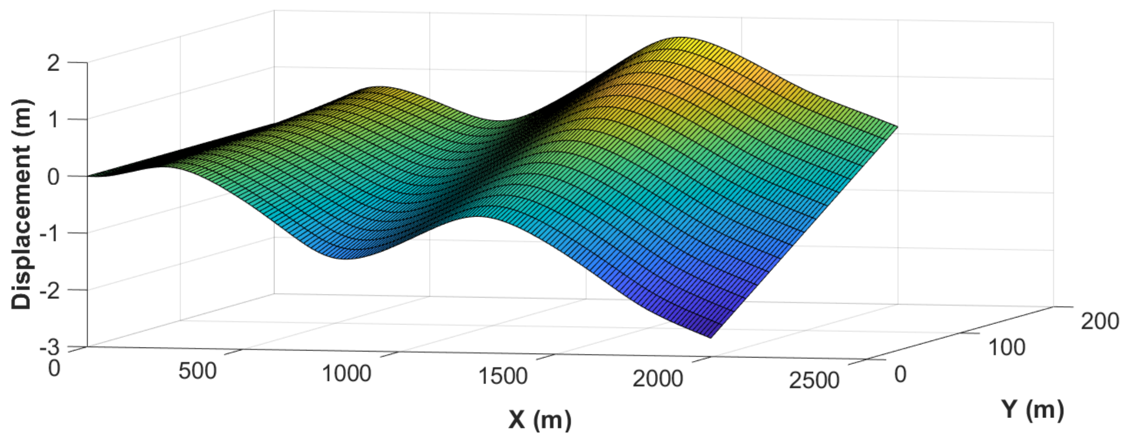

Fig. 12.1a

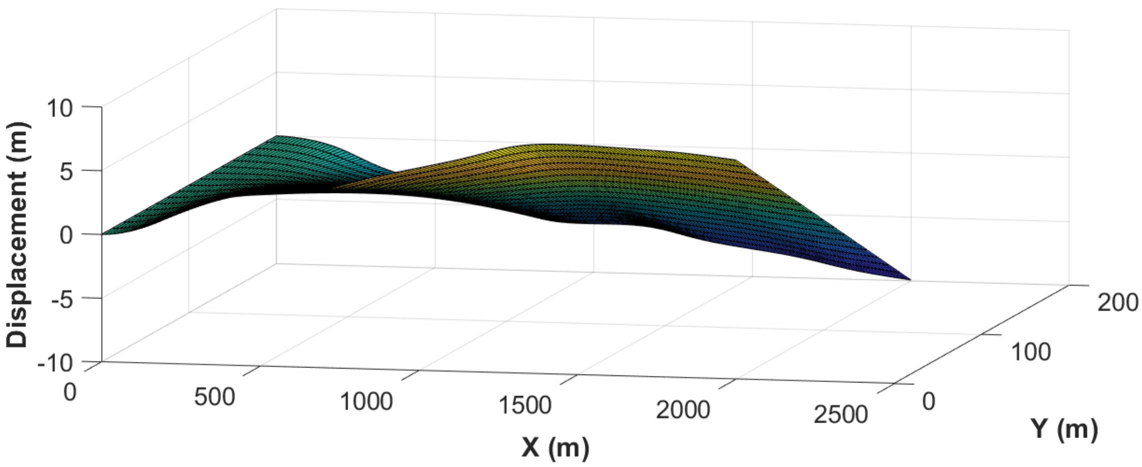

Fig. 12.1b

Figure 12.1. The vertical deflections of the ice shelf surface resulting from the impact of the frontal incident wave were obtained from **Model 3** with the forcing periodicity of **(a)** $\boldsymbol{T = 27.0\, s}$ and **(b)** $\boldsymbol{T = 27.8\, s}$. These periodicities are located, respectively, to the left and to the right of the resonance peak observed at $\boldsymbol{T_{n_1} = 27.36\, s}$ (in **Fig. 10a**). The amplitude of ice thickness fluctuations $\boldsymbol{A_H = 5\, m}$.

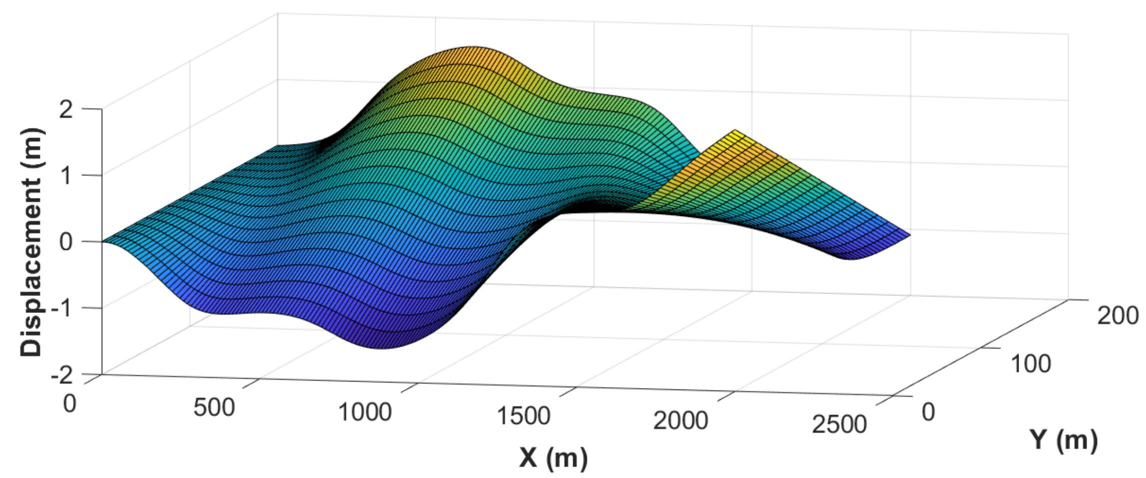

Fig. 12.2a

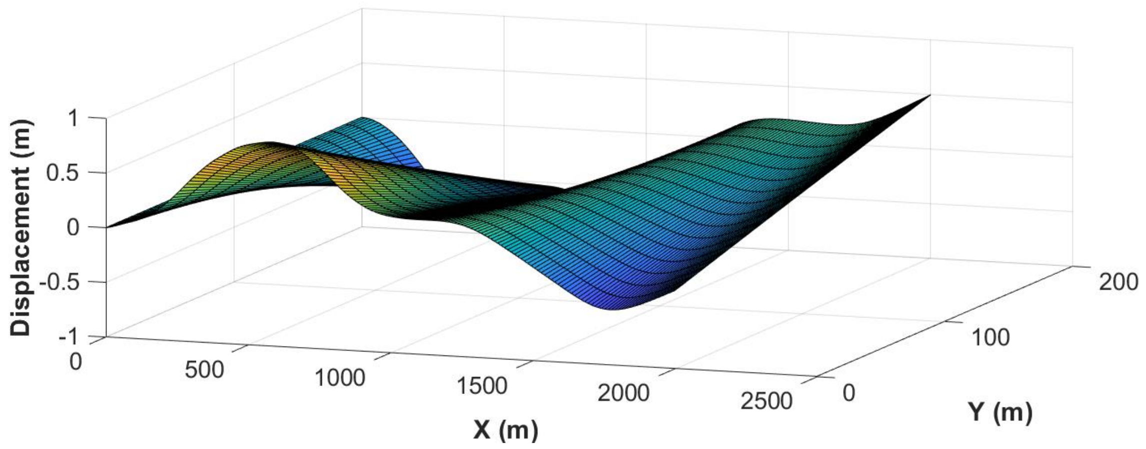

Fig. 12.2b

Figure 12.2. The vertical deflections of the ice shelf surface resulting from the impact of the frontal incident wave were obtained from **Model 3** with the forcing periodicity of **(a)** $\boldsymbol{T = 9.0\ s}$ and **(b)** $\boldsymbol{T = 9.6\ s}$. These periodicities are located, respectively, to the left and to the right of the resonance peak observed at $\boldsymbol{T_{n_2} = 9.3\ s}$ (in **Fig. 10b**). The amplitude of ice thickness fluctuations $\boldsymbol{A_H = 5\ m}$.

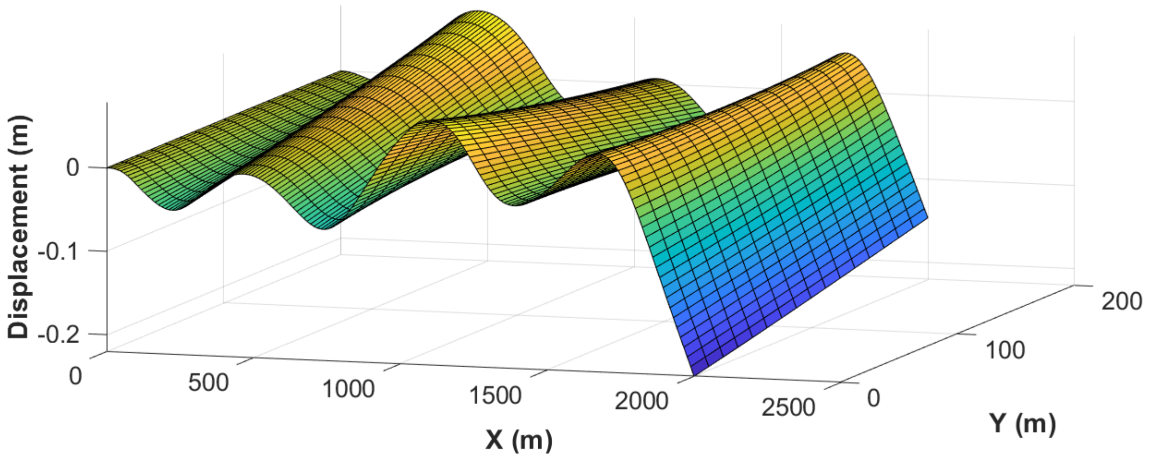

Fig. 12.3a

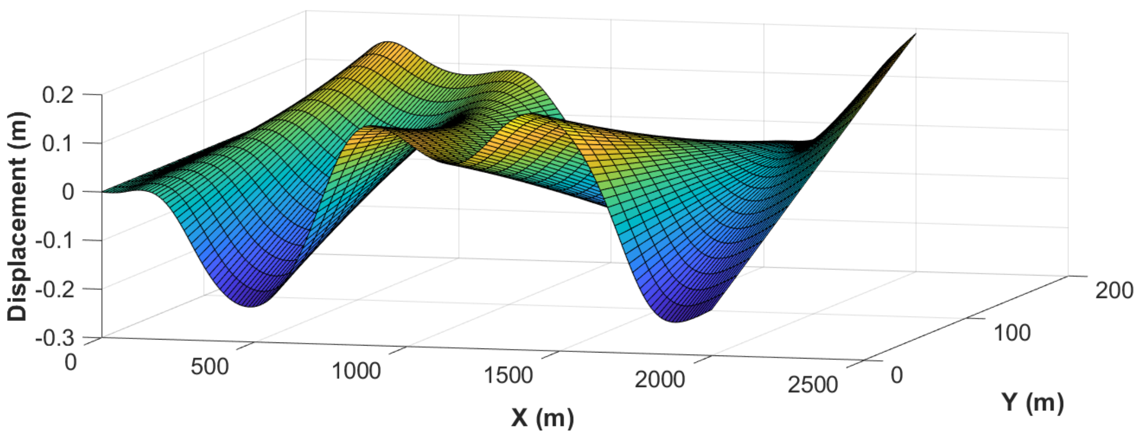

Fig. 12.3b

Figure 12.3. The vertical deflections of the ice shelf surface resulting from the impact of the frontal incident wave were obtained from **Model 3** with the forcing periodicity of **(a)** $\boldsymbol{T = 5.0\ s}$ and **(b)** $\boldsymbol{T = 5.8\ s}$. These periodicities are located, respectively, to the left and to the right of the resonance peak observed at $\boldsymbol{T_{n_3} = 5.43\ s}$ (in **Fig. 10b**). The amplitude of ice thickness fluctuations $\boldsymbol{A_H = 5\ m}$.

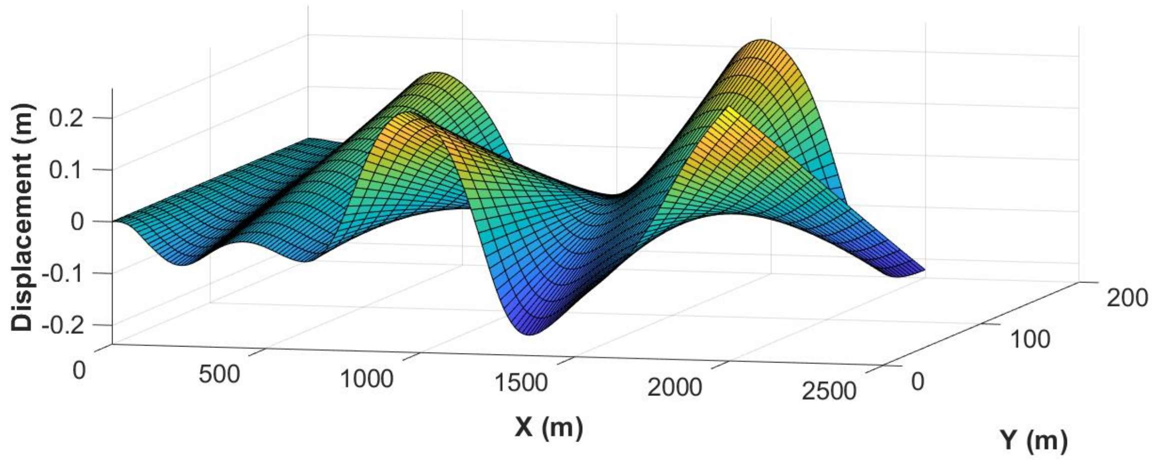

Fig. 12.4a

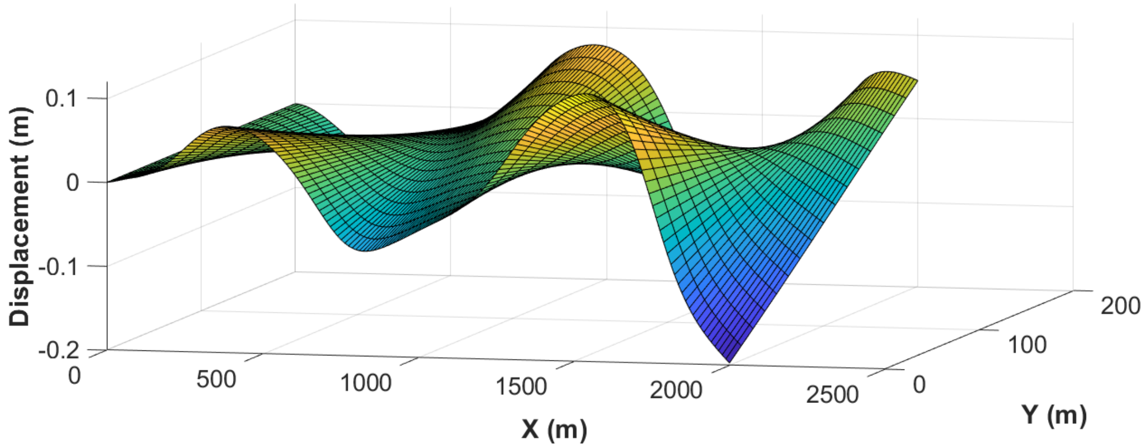

Fig. 12.4b

Figure 12.4. The vertical deflections of the ice shelf surface resulting from the impact of the frontal incident wave were obtained from **Model 3** with the forcing periodicity of **(a)** $\boldsymbol{T = 3.7\ s}$ and **(b)** $\boldsymbol{T = 4.1\ s}$. These periodicities are located, respectively, to the left and to the right of the resonance peak observed at $\boldsymbol{T_{n_4} = 3.95\ s}$ (in **Fig. 10c**). The amplitude of ice thickness fluctuations $\boldsymbol{A_H = 5\ m}$.

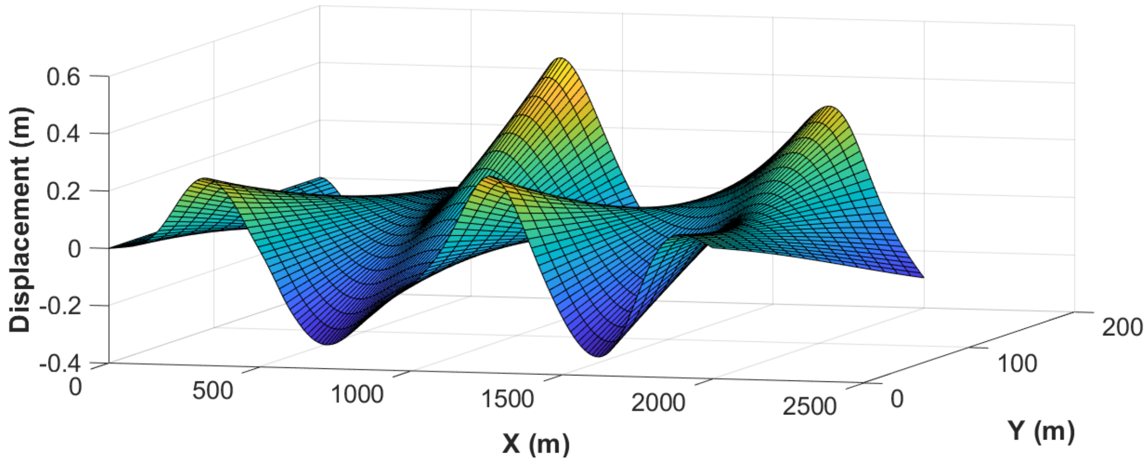

Fig. 12.5a

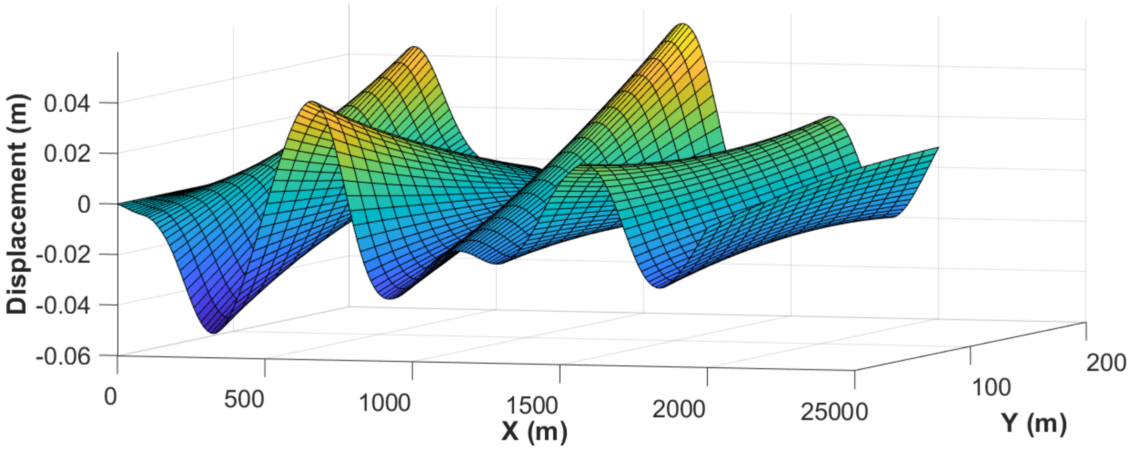

Fig. 12.5b

Figure 12.5. The vertical deflections of the ice shelf surface resulting from the impact of the frontal incident wave were obtained from **Model 3** with the forcing periodicity of **(a)** $\boldsymbol{T = 2.6\ s}$ and **(b)** $\boldsymbol{T = 2.75\ s}$. These periodicities are located, respectively, to the left and to the right of the resonance peak observed at $\boldsymbol{T_{n_5} = 2.62\ s}$ (in **Fig. 10c**). The amplitude of ice thickness fluctuations $\boldsymbol{A_H = 5\ m}$**.**

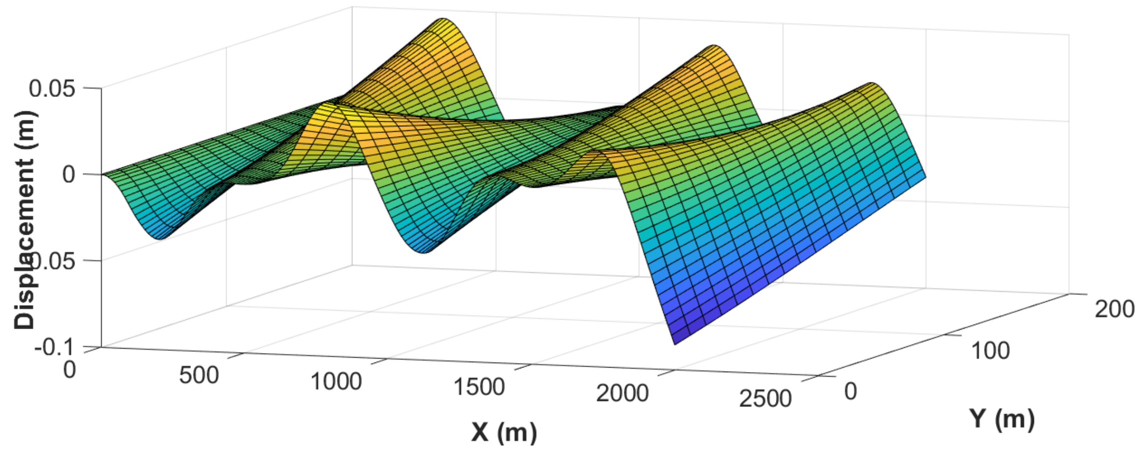

Fig. 12.6a

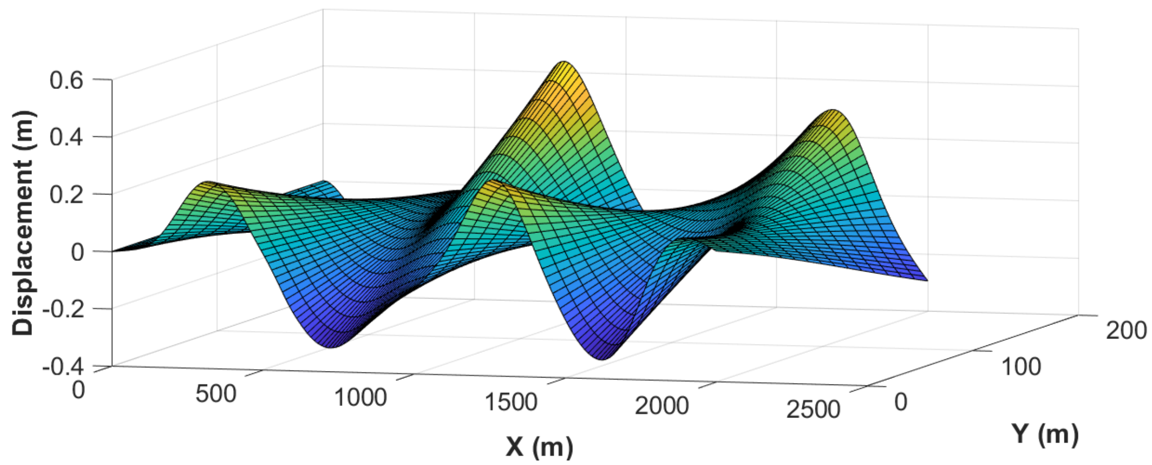

Fig. 12.6b

Figure 12.6. The vertical deflections of the ice shelf surface resulting from the impact of the frontal incident wave were obtained from **Model 3** with the forcing periodicity of **(a)** $\boldsymbol{T = 2.5\ s}$ and **(b)** $\boldsymbol{T = 2.6\ s}$. These periodicities are located, respectively, to the left and to the right of the resonance peak observed at $\boldsymbol{T_{n_6} = 2.58\ s}$ (in **Fig. 10c**). The amplitude of ice thickness fluctuations $\boldsymbol{A_H = 5\ m}$.

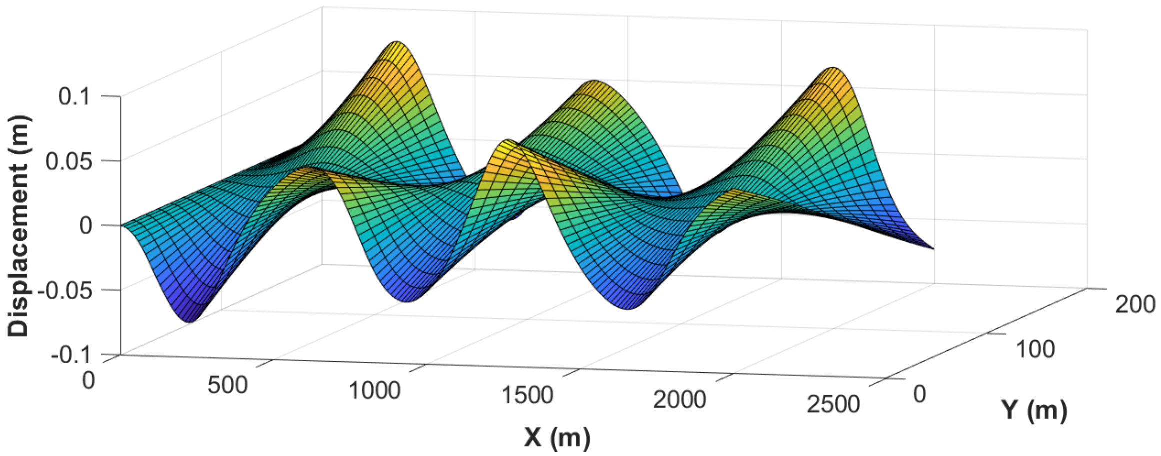

Fig. 12.7a

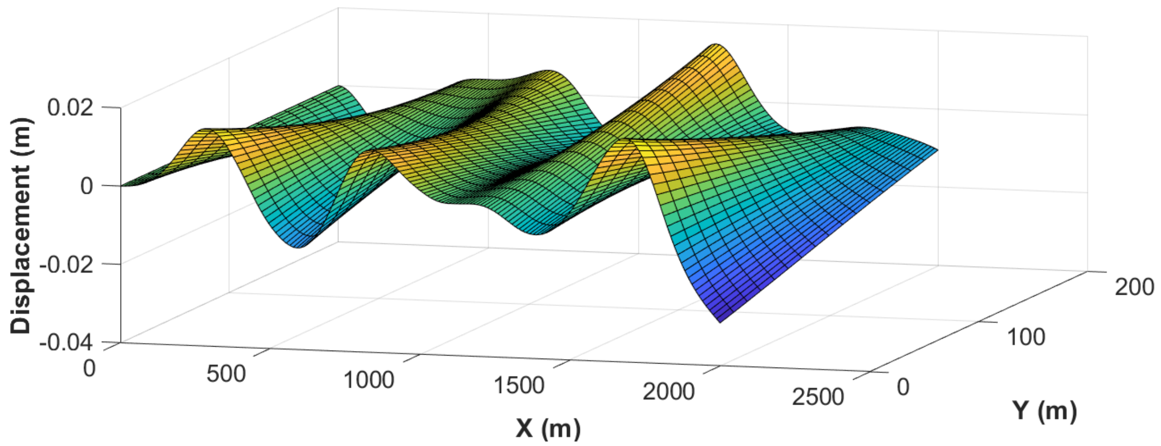

Fig. 12.7b

Figure 12.7. The vertical deflections of the ice shelf surface resulting from the impact of the frontal incident wave were obtained from **Model 3** with the forcing periodicity of **(a)** $\boldsymbol{T = 2.07\ s}$ and **(b)** $\boldsymbol{T = 2.13\ s}$. These periodicities are located, respectively, to the left and to the right of the resonance peak observed at $\boldsymbol{T_{n_7} = 2.1\ s}$ (in **Fig. 10c**). The amplitude of ice thickness fluctuations $\boldsymbol{A_H = 5\ m}$.

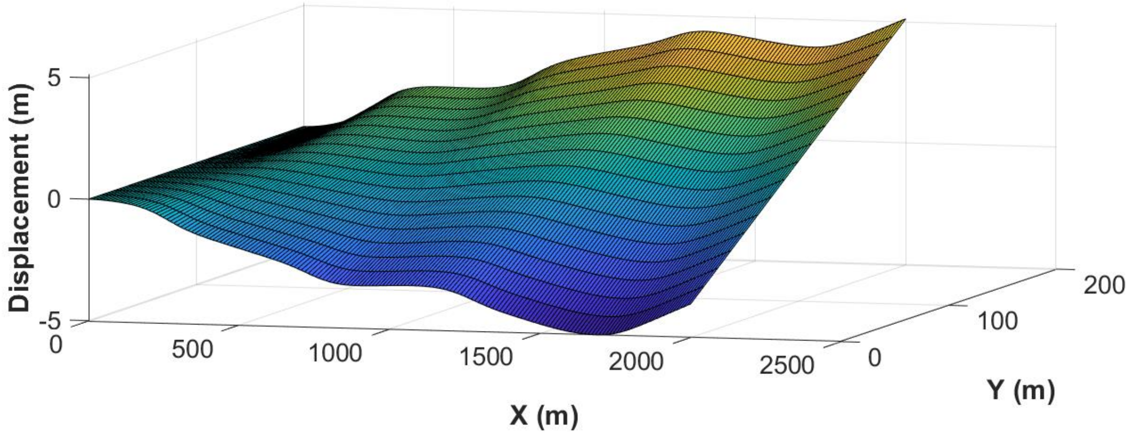

Fig. 13.1a

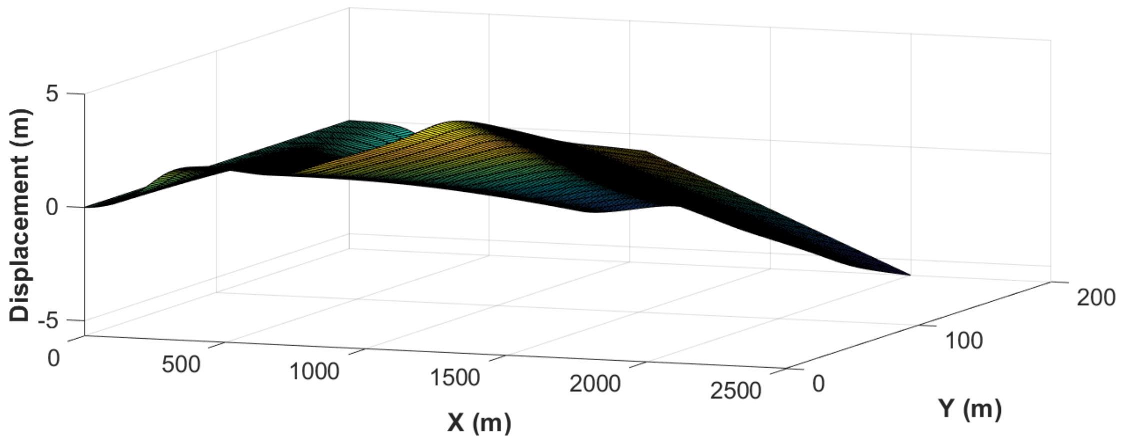

Fig. 13.1b

Figure 13.1. The vertical deflections of the ice shelf surface resulting from the impact of the frontal incident wave were obtained from **Model 3** with the forcing periodicity of **(a)** $\boldsymbol{T = 26.0\ s}$ and **(b)** $\boldsymbol{T = 29.0\ s}$. These periodicities are located, respectively, to the left and to the right of the resonance peak observed at $\boldsymbol{T_{n_1} = 27.72\ s}$ (in **Fig. 11a**). The amplitude of ice thickness fluctuations $\boldsymbol{A_H = 8\ m}$.

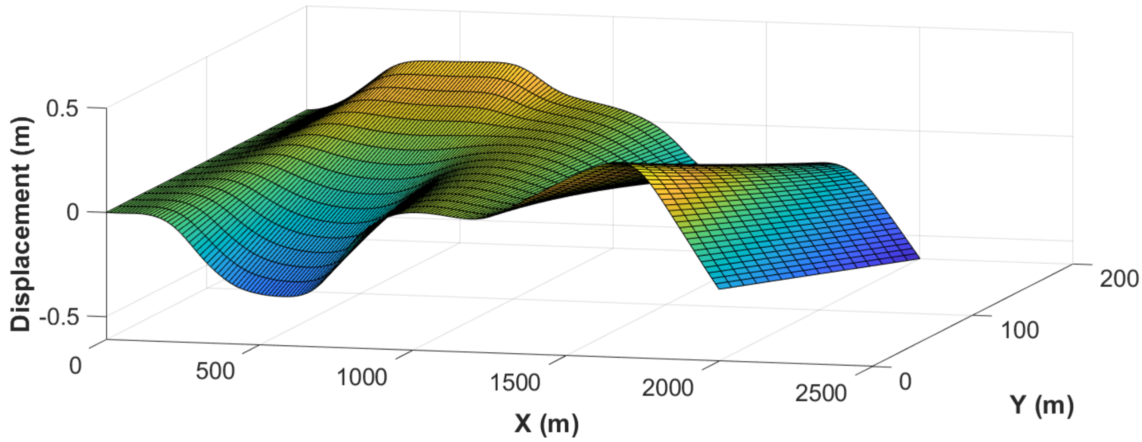

Fig. 13.2a

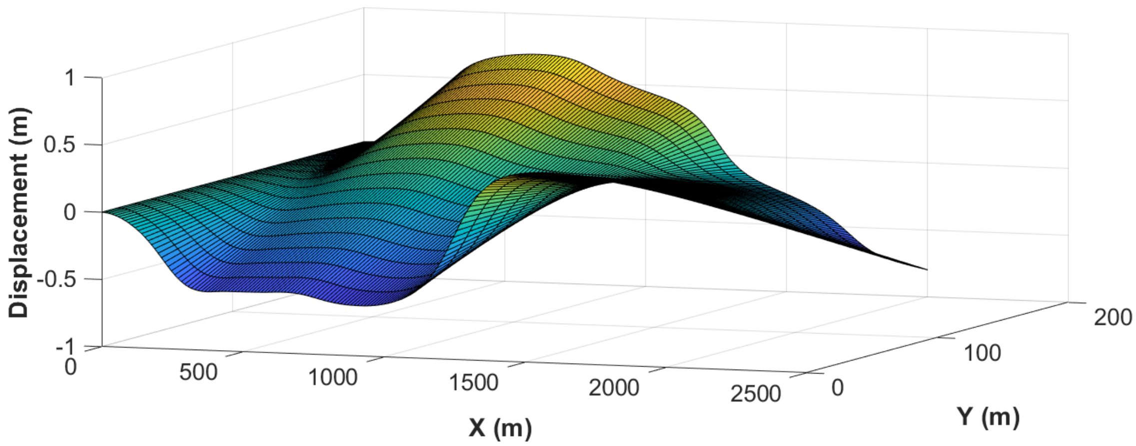

Fig. 13.2b

Figure 13.2. The vertical deflections of the ice shelf surface resulting from the impact of the frontal incident wave were obtained from **Model 3** with the forcing periodicity of **(a)** $\boldsymbol{T = 8.0\ s}$ and **(b)** $\boldsymbol{T = 10.0\ s}$. These periodicities are located, respectively, to the left and to the right of the resonance peak observed at $\boldsymbol{T_{n_2} = 9.06\ s}$ (in **Fig. 11b**). The amplitude of ice thickness fluctuations $\boldsymbol{A_H = 8\ m}$.

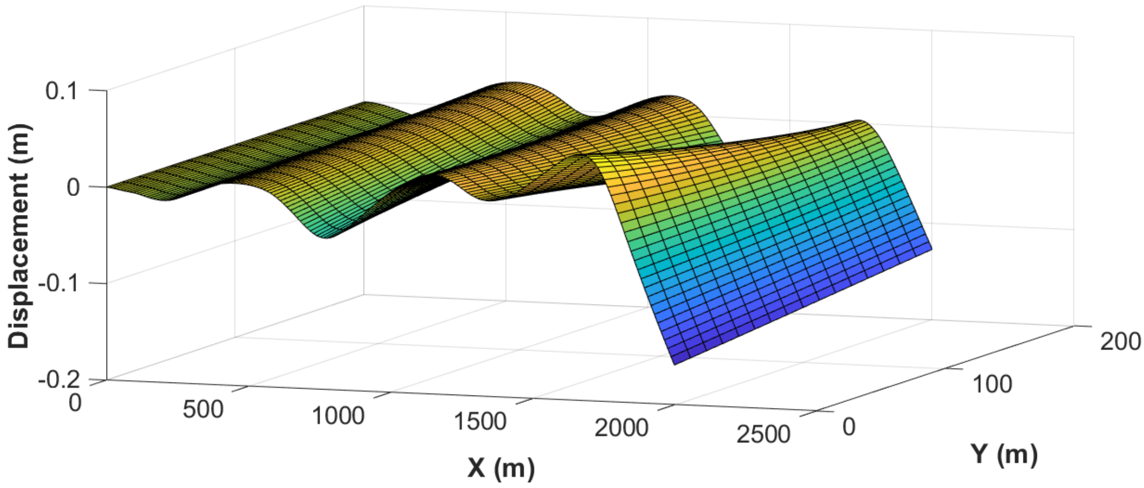

Fig. 13.3a

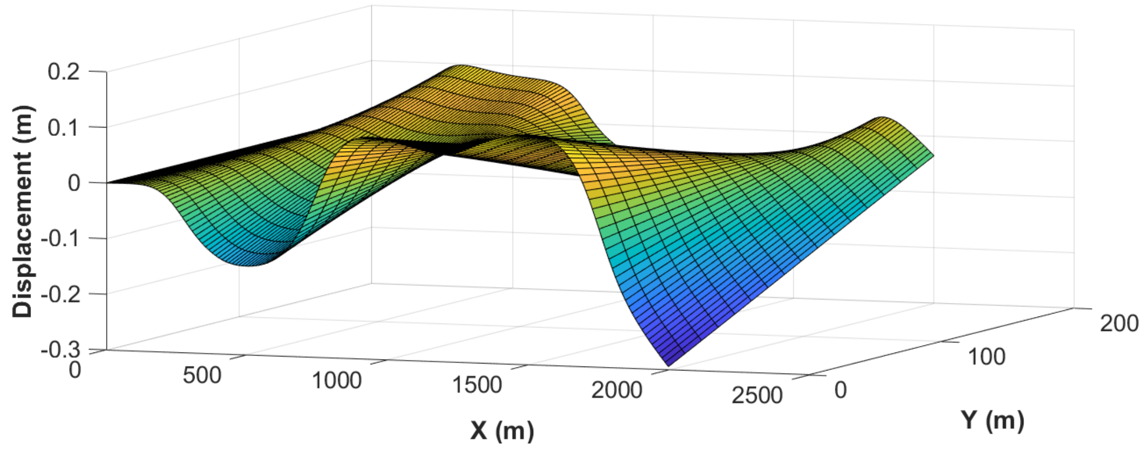

Fig. 13.3b

Figure 13.3. The vertical deflections of the ice shelf surface resulting from the impact of the frontal incident wave were obtained from **Model 3** with the forcing periodicity of **(a)** $\boldsymbol{T = 5.0\ s}$ and **(b)** $\boldsymbol{T = 6.5\ s}$. These periodicities are located, respectively, to the left and to the right of the resonance peak observed at $\boldsymbol{T_{n_3} = 5.74\ s}$ (in **Fig. 11b**). The amplitude of ice thickness fluctuations $\boldsymbol{A_H = 8\ m}$.

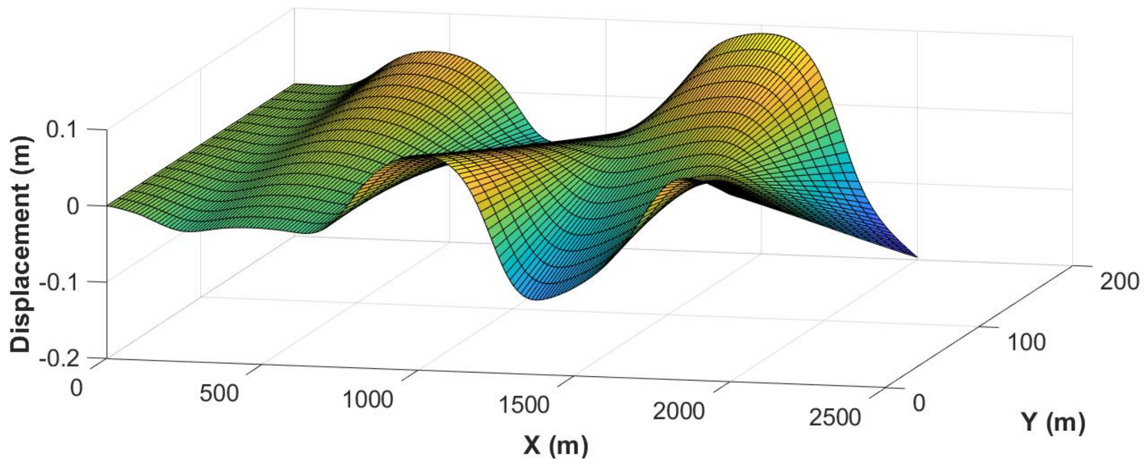

Fig. 13.4a

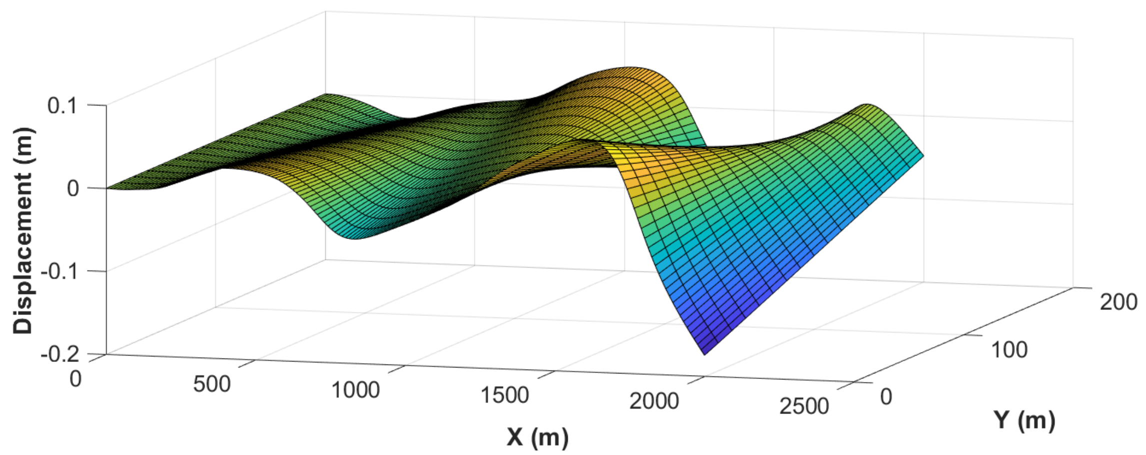

Fig. 13.4b

Figure 13.4. The vertical deflections of the ice shelf surface resulting from the impact of the frontal incident wave were obtained from **Model 3** with the forcing periodicity of **(a)** $\boldsymbol{T = 4.3\ s}$ and **(b)** $\boldsymbol{T = 4.75\ s}$. These periodicities are located, respectively, to the left and to the right of the resonance peak observed at $\boldsymbol{T_{n_4} = 4.52\ s}$ (in **Fig. 11c**). The amplitude of ice thickness fluctuations $\boldsymbol{A_H = 8\ m}$.

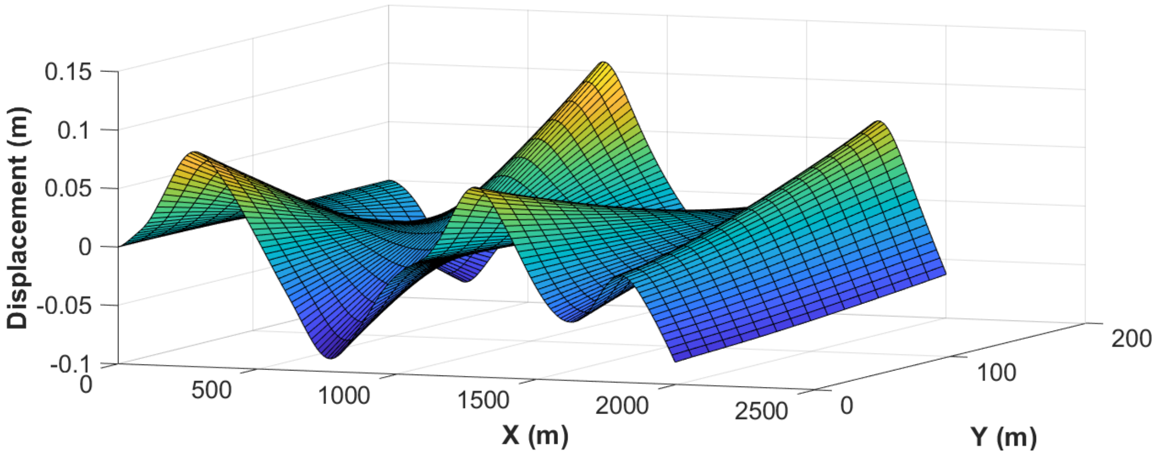

Fig. 13.5a

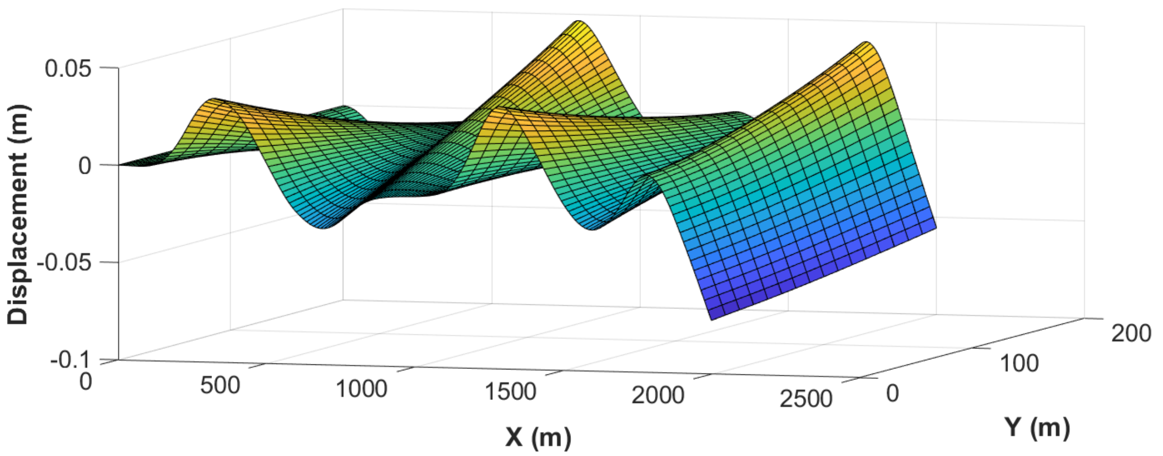

Fig. 13.5b

Figure 13.5. The vertical deflections of the ice shelf surface resulting from the impact of the frontal incident wave were obtained from **Model 3** with the forcing periodicity of **(a)** $\boldsymbol{T = 2.55\ s}$ and **(b)** $\boldsymbol{T = 2.65\ s}$. These periodicities are located, respectively, to the left and to the right of the resonance peak observed at $\boldsymbol{T_{n_5} = 2.6\ s}$ (in **Fig. 11c**). The amplitude of ice thickness fluctuations $\boldsymbol{A_H = 8\ m}$.

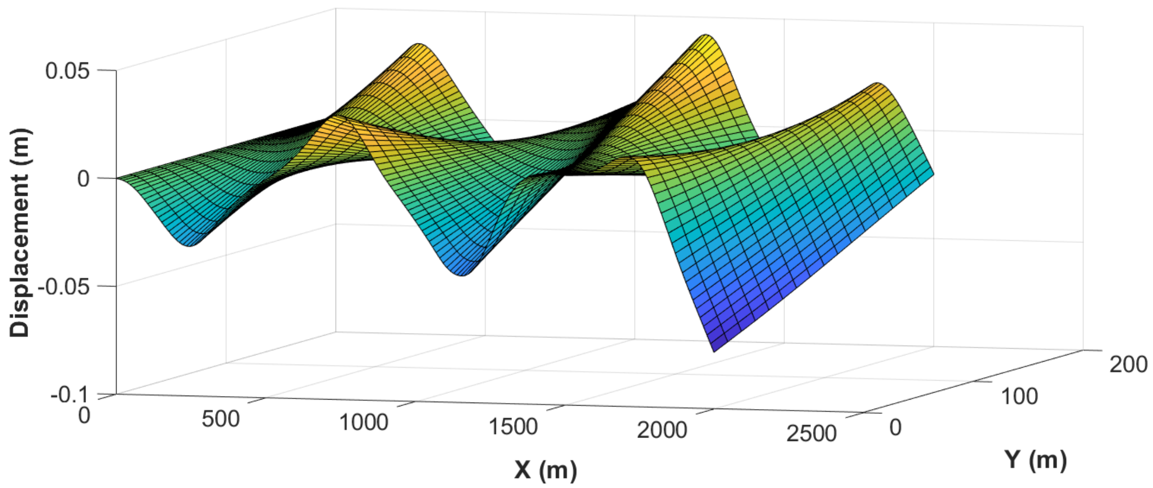

Fig. 13.6a

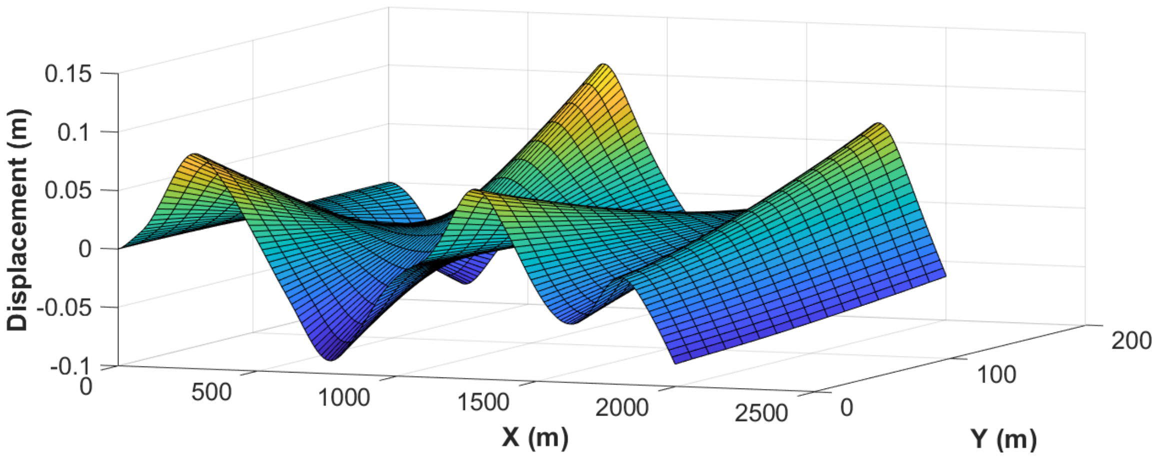

Fig. 13.6b

Figure 13.6. The vertical deflections of the ice shelf surface resulting from the impact of the frontal incident wave were obtained from **Model 3** with the forcing periodicity of **(a)** $\boldsymbol{T = 2.46\ s}$ and **(b)** $\boldsymbol{T = 2.55\ s}$. These periodicities are located, respectively, to the left and to the right of the resonance peak observed at $\boldsymbol{T_{n_6} = 2.52\ s}$ (in **Fig. 11c**). The amplitude of ice thickness fluctuations $\boldsymbol{A_H = 8\ m}$.

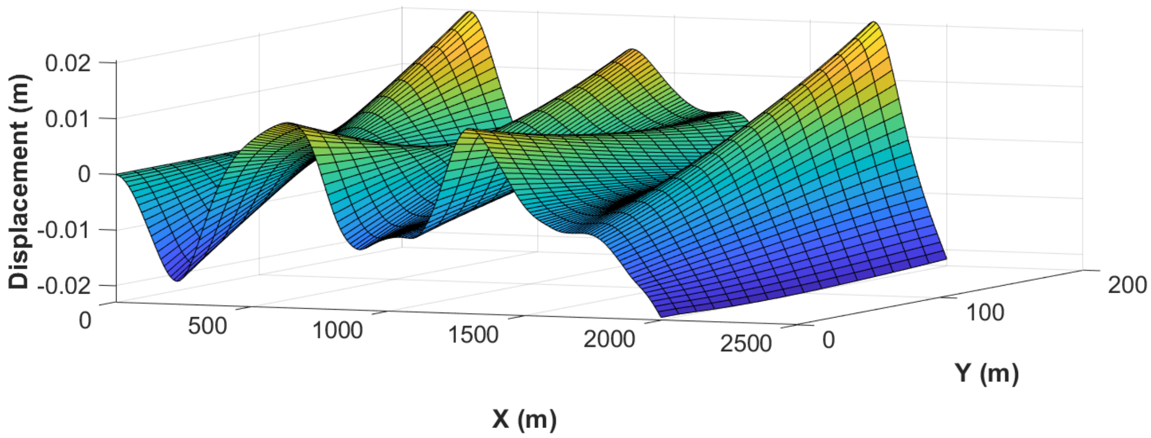

Fig. 13.7a

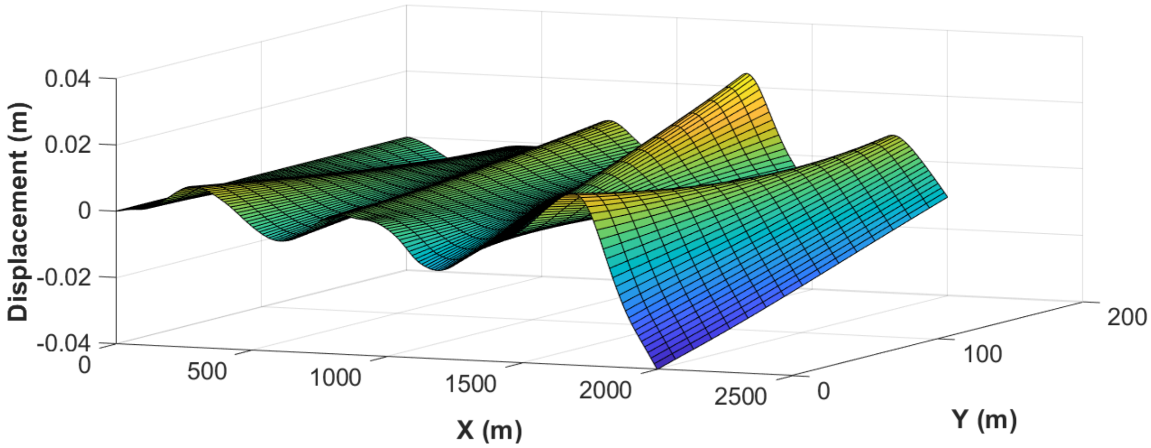

Fig. 13.7b

Figure 13.7. The vertical deflections of the ice shelf surface resulting from the impact of the frontal incident wave were obtained from **Model 3** with the forcing periodicity of **(a)** $\boldsymbol{T = 2.05\ s}$ and **(b)** $\boldsymbol{T = 2.15\ s}$. These periodicities are located, respectively, to the left and to the right of the resonance peak observed at $\boldsymbol{T_{n_7} = 2.1\ s}$ (in **Fig. 11c**). The amplitude of ice thickness fluctuations $\boldsymbol{A_H = 8\ m}$.

<u>Appendix A.</u> Ice stress distributions along the ice shelf center-line profile obtained by Model 1

1) The amplitude of ice thickness oscillations in Eq. (3) $A_H = 11\ m$

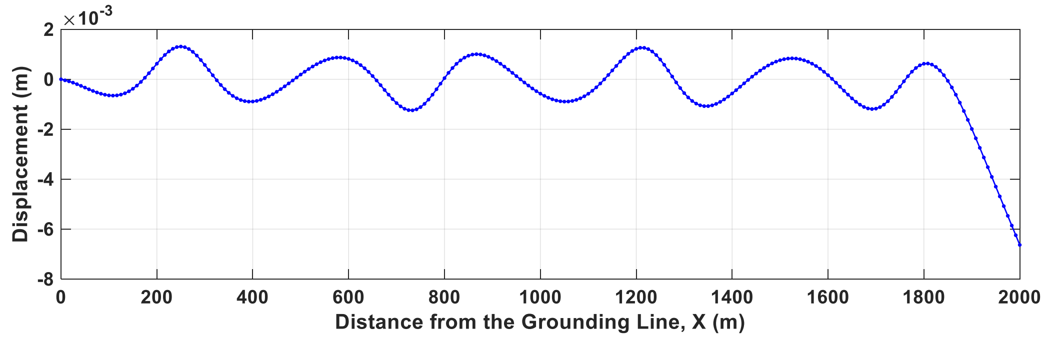

Fig. A1a

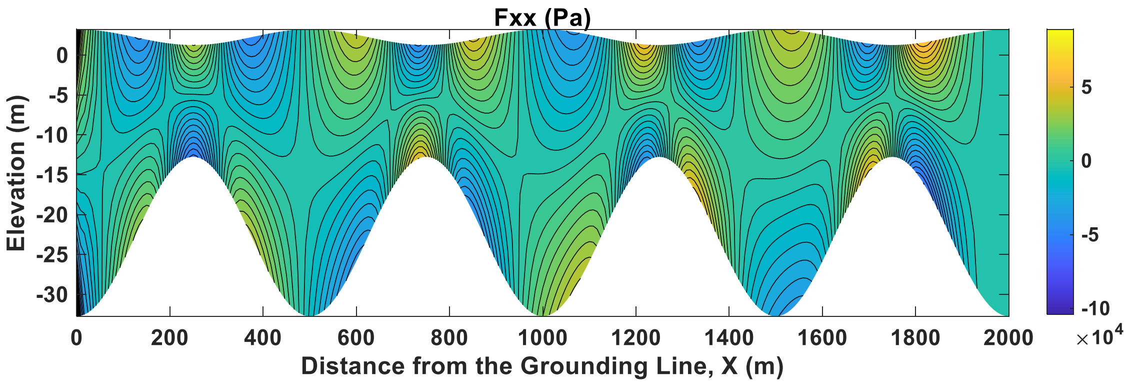

Fig. A1b

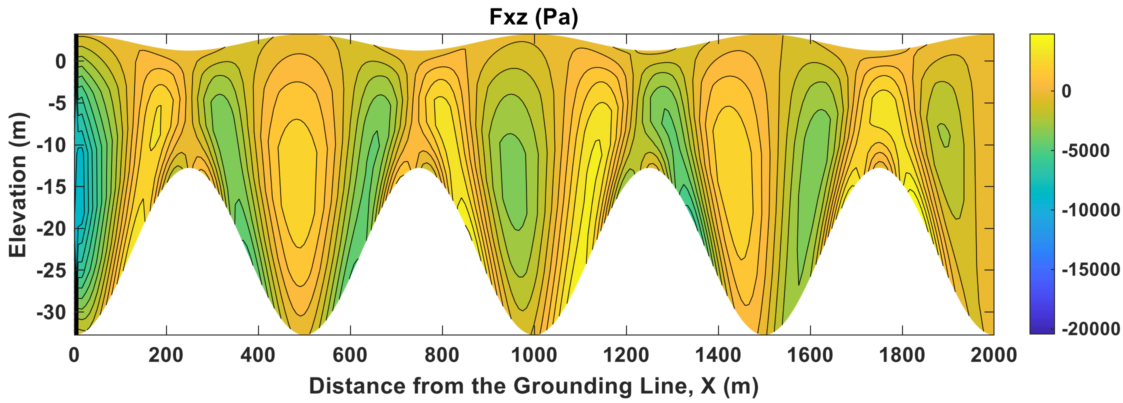

Fig. A1c

Figure A1. (a) Vertical displacement of ice W along the centerline due to the impact of the frontal incident wave. **(b)** Distribution of longitudinal stress (σ_{xx}) in a vertical cross-section of the ice shelf along the centerline. **(c)** Distribution of shear stress (σ_{xz}) in a vertical cross-section of the ice shelf along the centerline. The periodicity of the forcing $\boldsymbol{T = 1s}$. The amplitude of ice thickness oscillations $\boldsymbol{A_H = 11m}$.

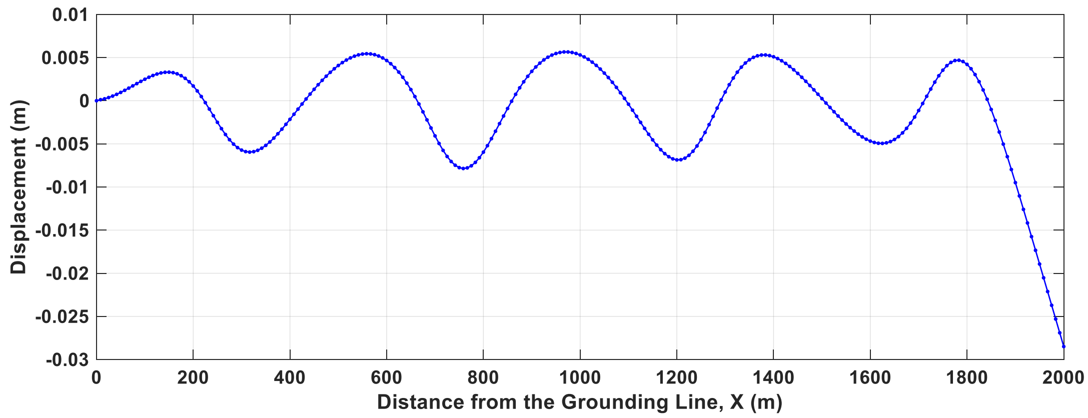

Fig. A2a

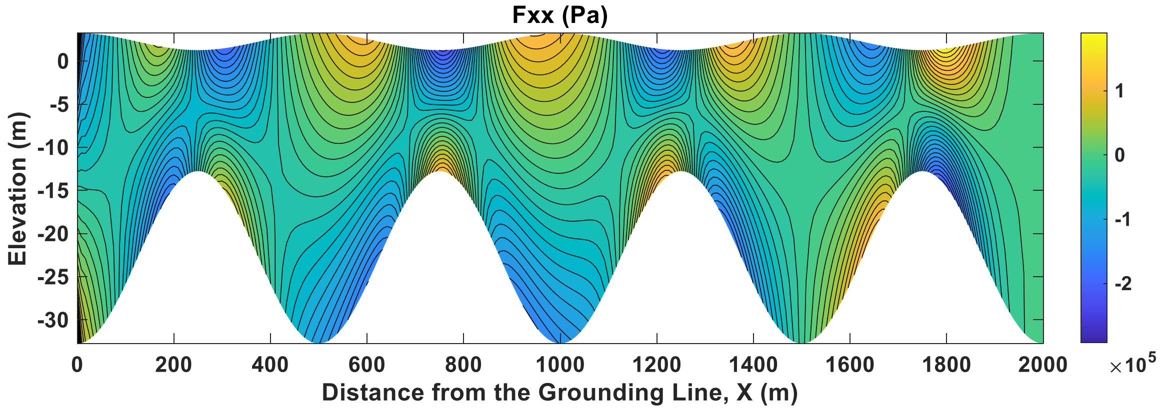

Fig. A2b

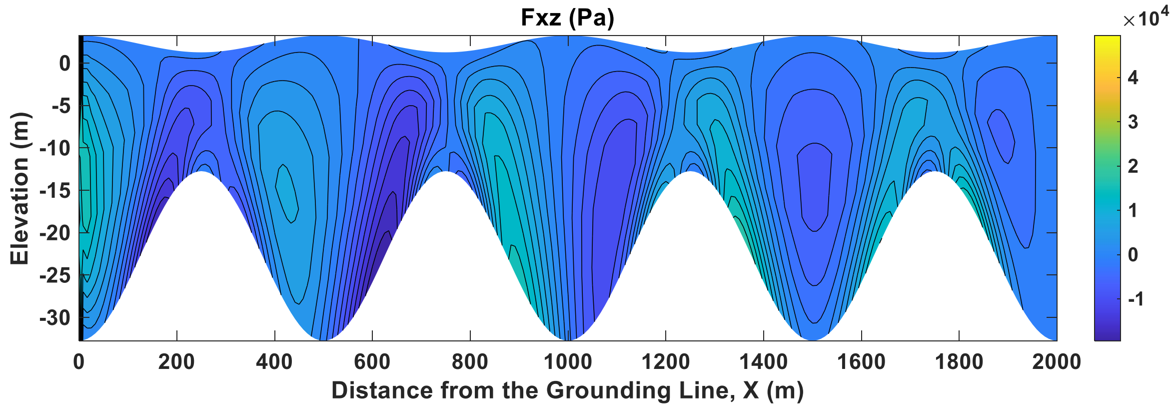

Fig. A2c

Figure A2. (a) Vertical displacement of ice W along the centerline due to the impact of the frontal incident wave. **(b)** Distribution of longitudinal stress (σ_{xx}) in a vertical cross-section of the ice shelf along the centerline. **(c)** Distribution of shear stress (σ_{xz}) in a vertical cross-section of the ice shelf along the centerline. The periodicity of the forcing $\boldsymbol{T = 2s}$. The amplitude of ice thickness oscillations $\boldsymbol{A_H = 11m.}$

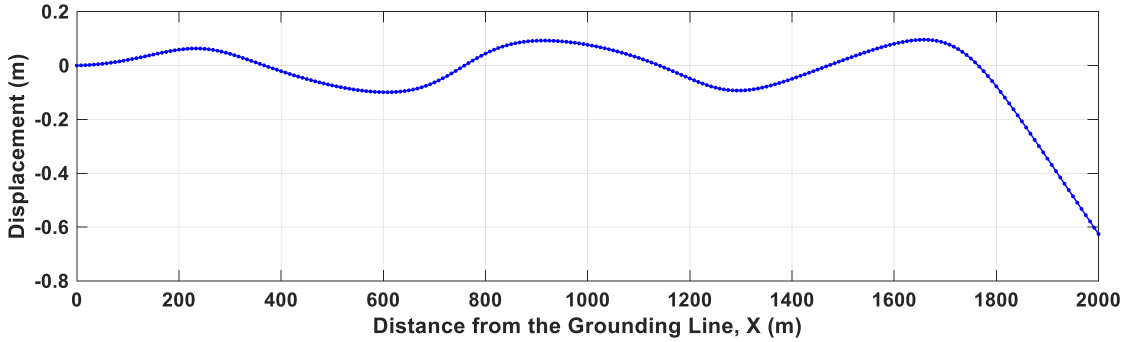

Fig. A3a

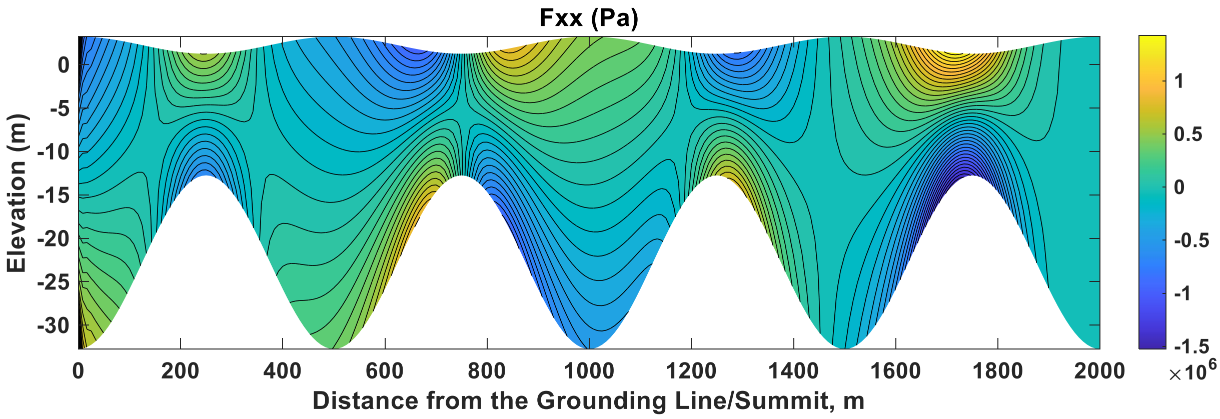

Fig. A3b

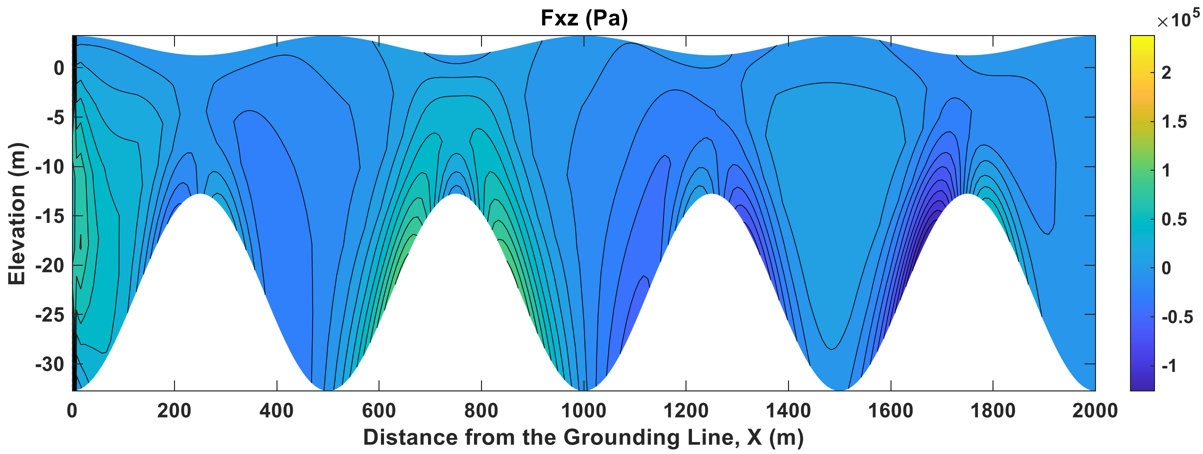

Fig. A3c

Figure A3. (a) Vertical displacement of ice W along the centerline due to the impact of the frontal incident wave. **(b)** Distribution of longitudinal stress (σ_{xx}) in a vertical cross-section of the ice shelf along the centerline. **(c)** Distribution of shear stress (σ_{xz}) in a vertical cross-section of the ice shelf along the centerline. The periodicity of the forcing $\boldsymbol{T = 10s}$. The amplitude of ice thickness oscillations $\boldsymbol{A_H = 11m}$.

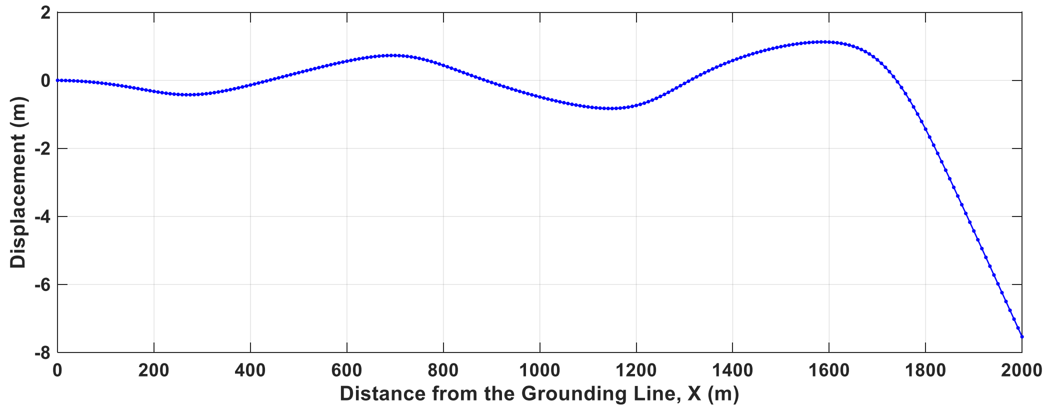

Fig. A4a

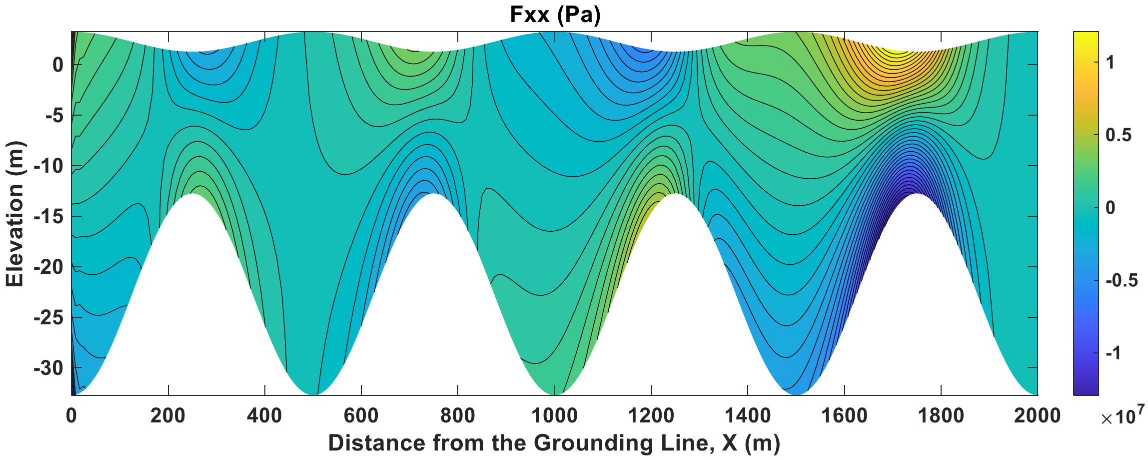

Fig. A4b

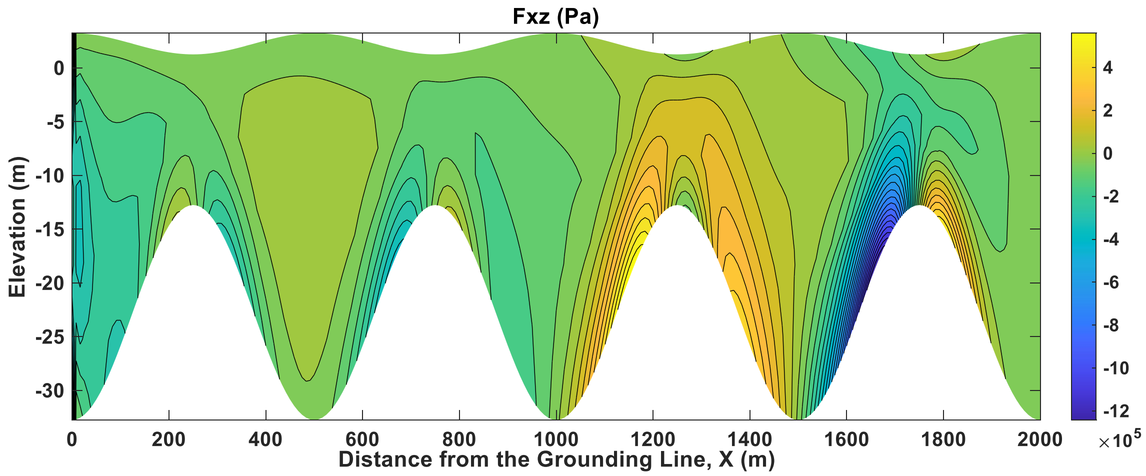

Fig. A4c

Figure A4. (a) Vertical displacement of ice W along the centerline due to the impact of the frontal incident wave. **(b)** Distribution of longitudinal stress (σ_{xx}) in a vertical cross-section of the ice shelf along the centerline. **(c)** Distribution of shear stress (σ_{xz}) in a vertical cross-section of the ice shelf along the centerline. The periodicity of the forcing $\boldsymbol{T = 20s}$. The amplitude of ice thickness oscillations $\boldsymbol{A_H = 11m}$.

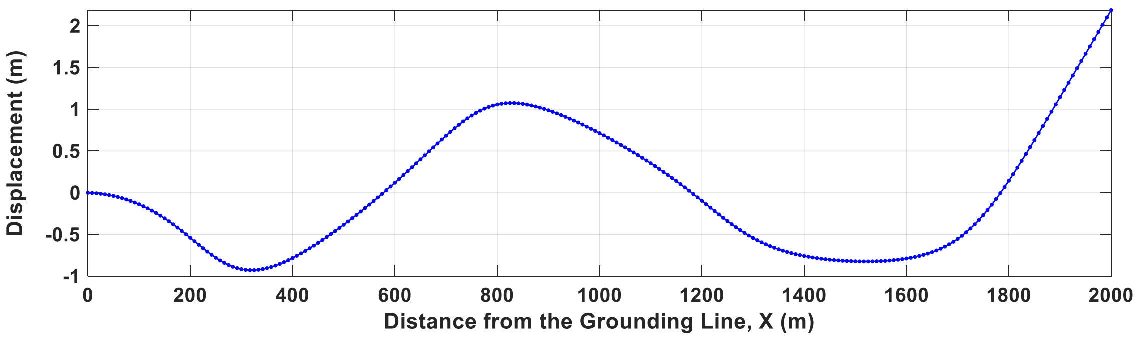

Fig. A5a

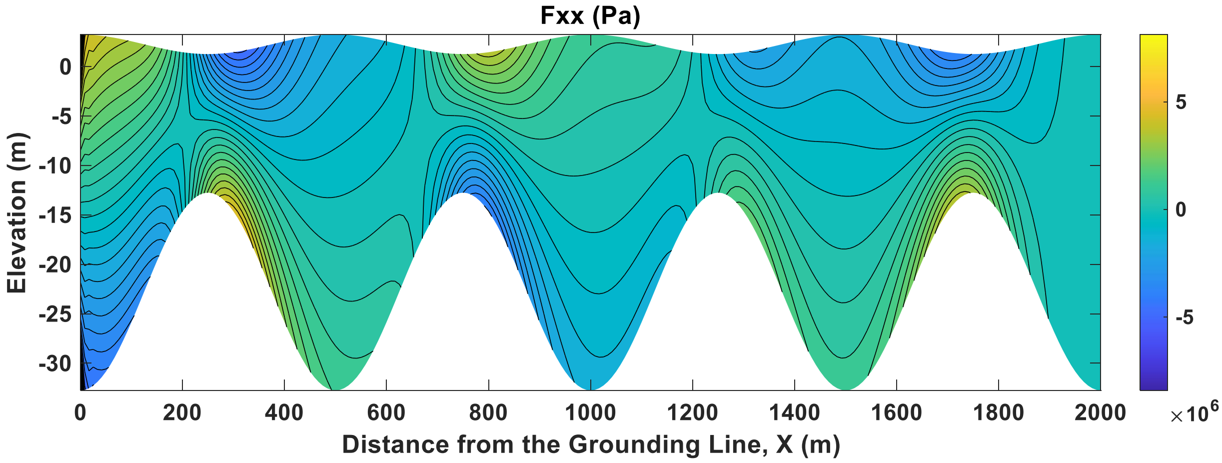

Fig. A5b

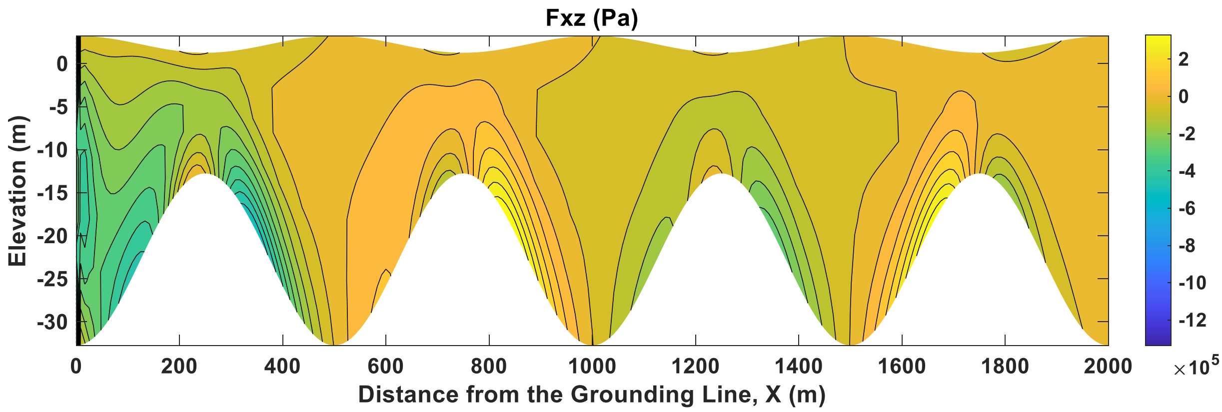

Fig. A5c

Figure A5. (a) Vertical displacement of ice W along the centerline due to the impact of the frontal incident wave. **(b)** Distribution of longitudinal stress (σ_{xx}) in a vertical cross-section of the ice shelf along the centerline. **(c)** Distribution of shear stress (σ_{xz}) in a vertical cross-section of the ice shelf along the centerline. The periodicity of the forcing $\boldsymbol{T = 50s}$. The amplitude of ice thickness oscillations $\boldsymbol{A_H = 11m.}$

2) The amplitude of ice thickness oscillations in Eq. (3) $A_H = 20\ m$

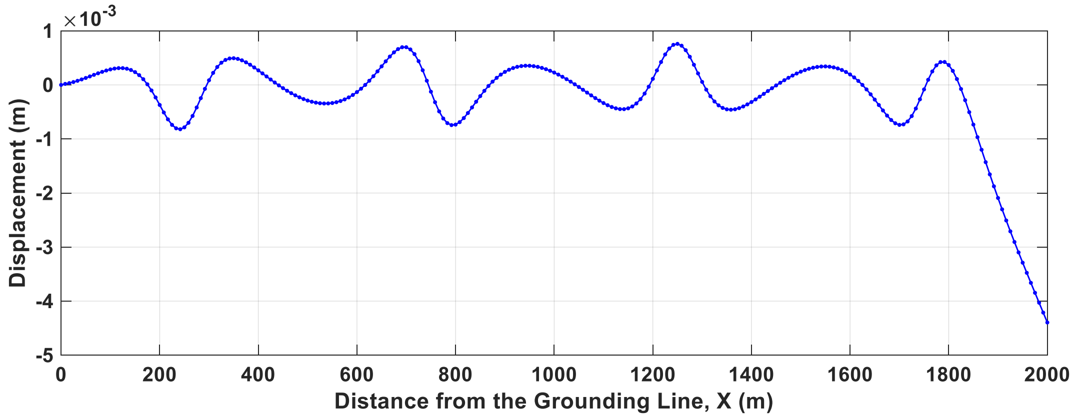

Fig. A6a

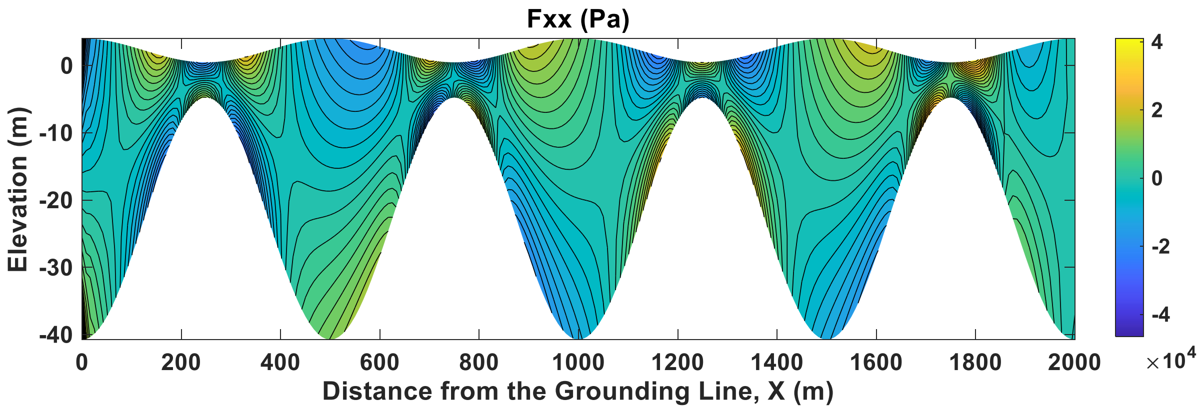

Fig. A6b

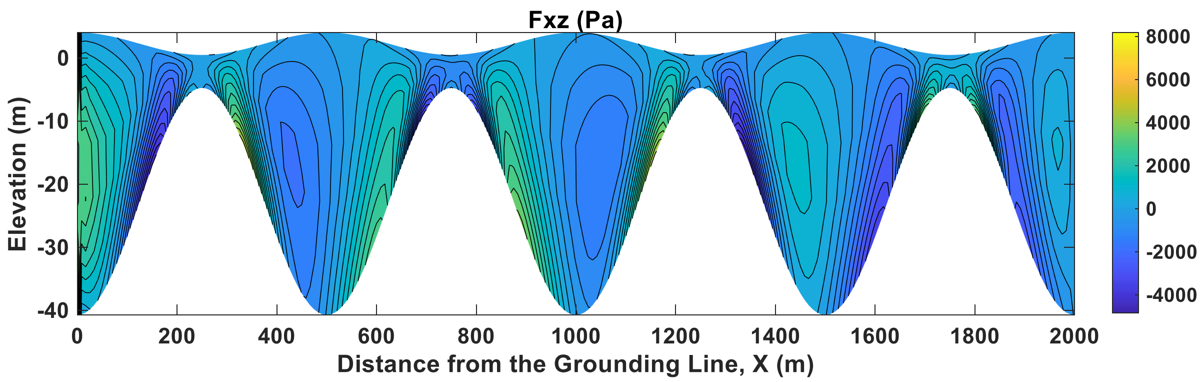

Fig. A6c

Figure A6. (a) Vertical displacement of ice W along the centerline due to the impact of the frontal incident wave. **(b)** Distribution of longitudinal stress (σ_{xx}) in a vertical cross-section of the ice shelf along the centerline. **(c)** Distribution of shear stress (σ_{xz}) in a vertical cross-section of the ice shelf along the centerline. The periodicity of the forcing $\boldsymbol{T = 1s}$. The amplitude of ice thickness oscillations $\boldsymbol{A_H = 20m}$.

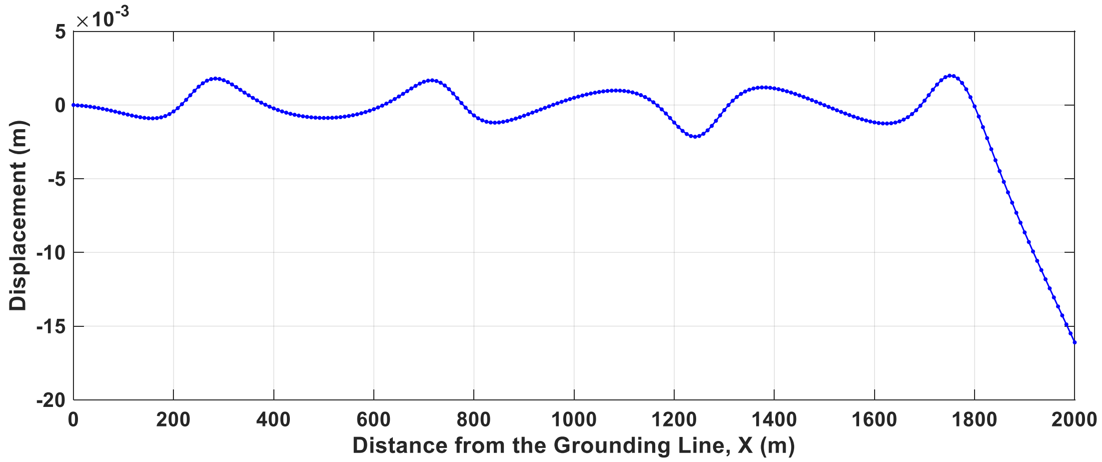

Fig. A7a

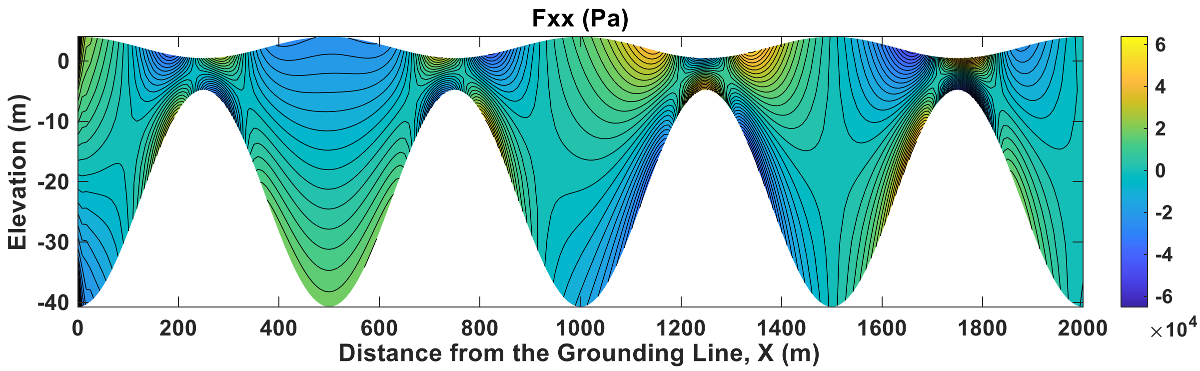

Fig. A7b

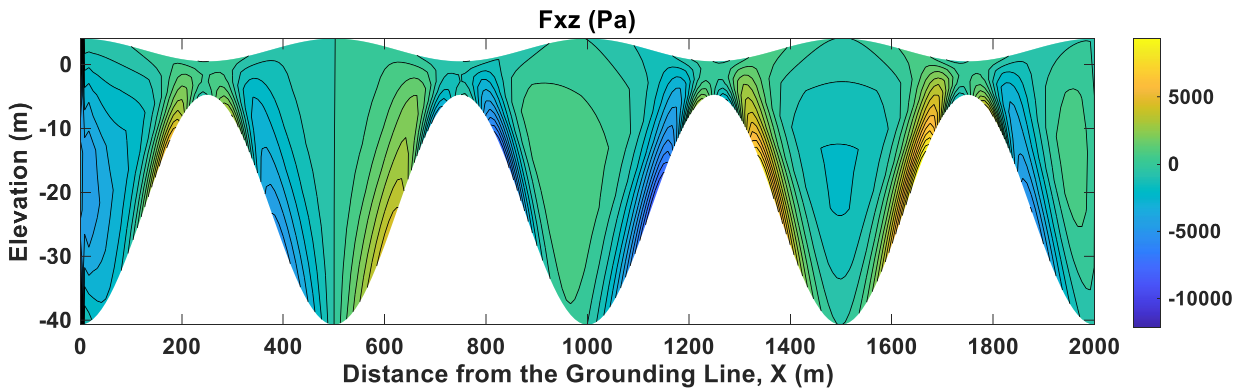

Fig. A7c

Figure A7. (a) Vertical displacement of ice W along the centerline due to the impact of the frontal incident wave. **(b)** Distribution of longitudinal stress (σ_{xx}) in a vertical cross-section of the ice shelf along the centerline. **(c)** Distribution of shear stress (σ_{xz}) in a vertical cross-section of the ice shelf along the centerline. The periodicity of the forcing $\boldsymbol{T = 2s}$. The amplitude of ice thickness oscillations $\boldsymbol{A_H = 20m.}$

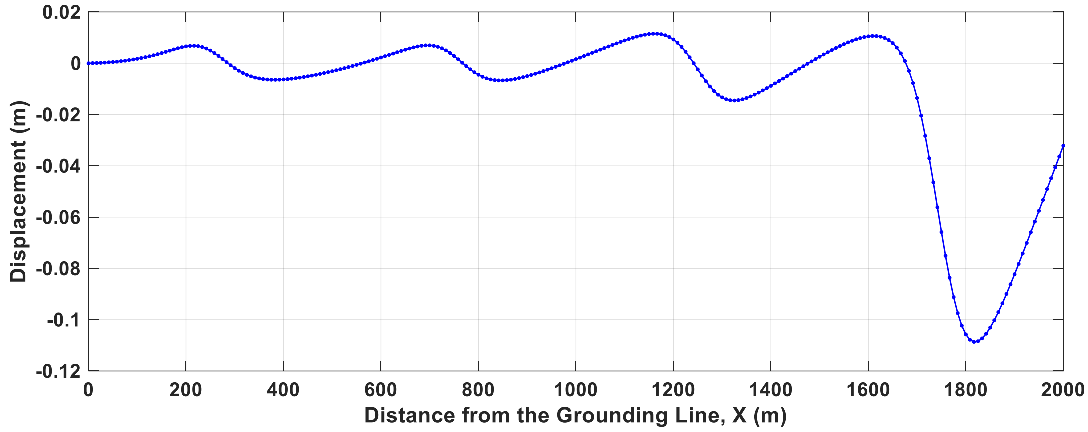

Fig. A8a

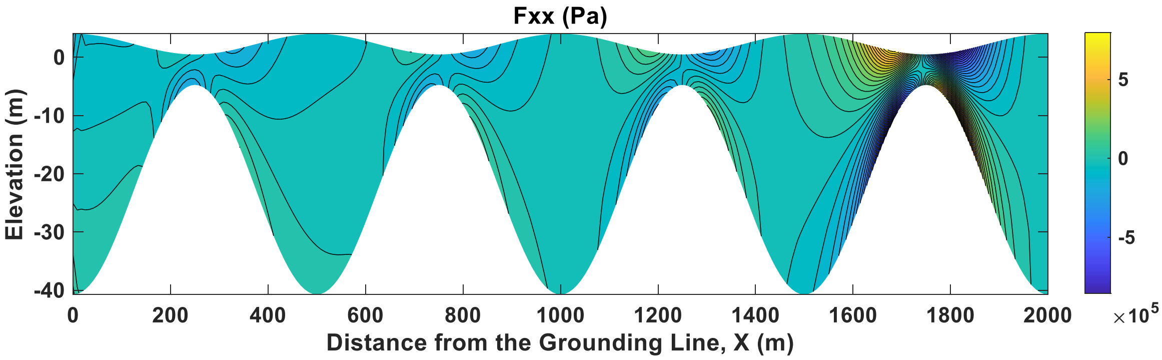

Fig. A8b

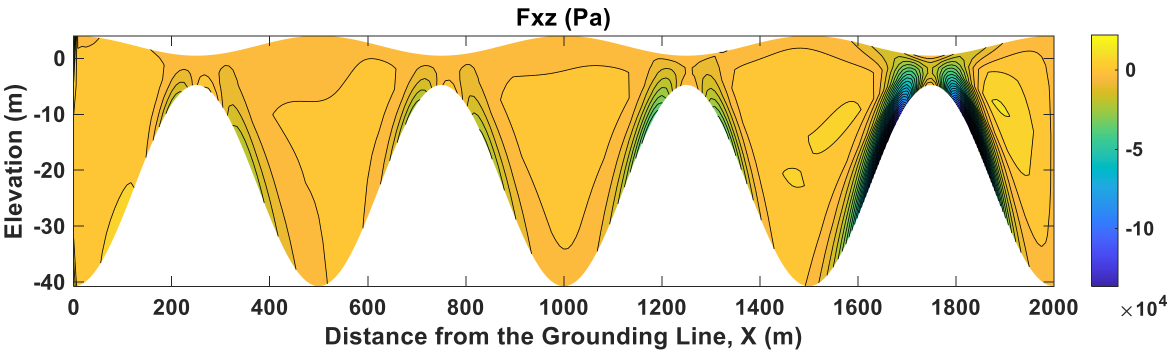

Fig. A8c

Figure A8. (a) Vertical displacement of ice W along the centerline due to the impact of the frontal incident wave. **(b)** Distribution of longitudinal stress (σ_{xx}) in a vertical cross-section of the ice shelf along the centerline. **(c)** Distribution of shear stress (σ_{xz}) in a vertical cross-section of the ice shelf along the centerline. The periodicity of the forcing $\boldsymbol{T = 10s}$. The amplitude of ice thickness oscillations $\boldsymbol{A_H = 20m}$.

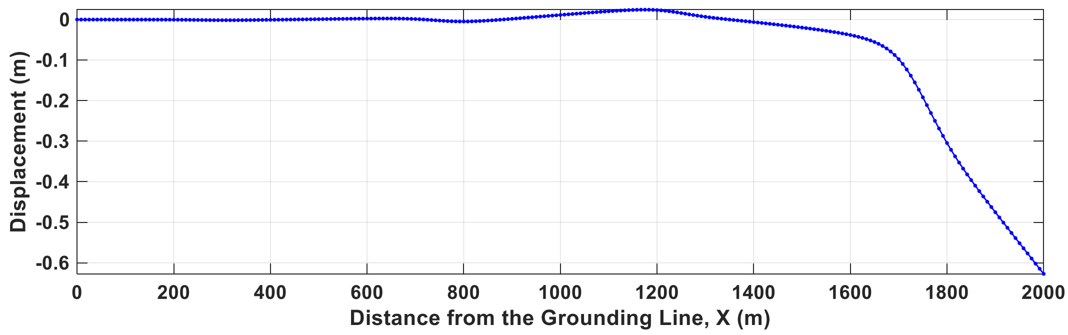

Fig. A9a

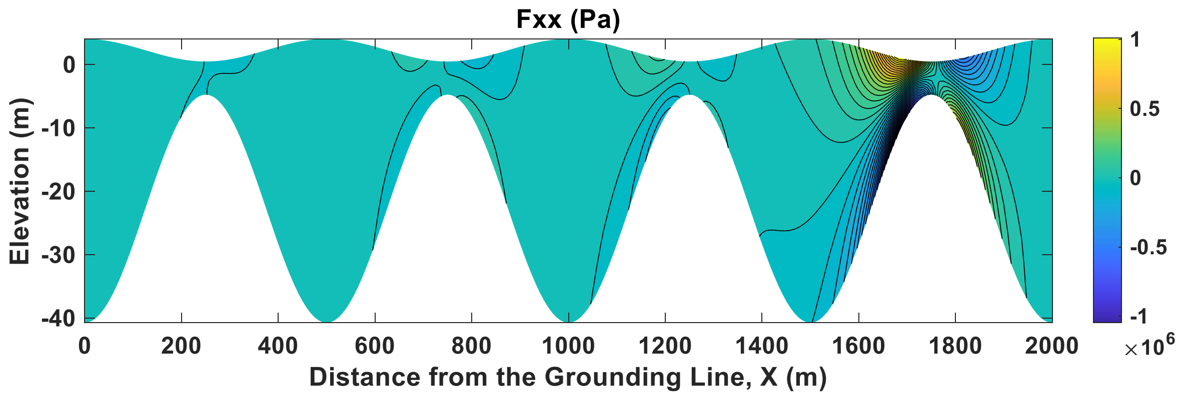

Fig. A9b

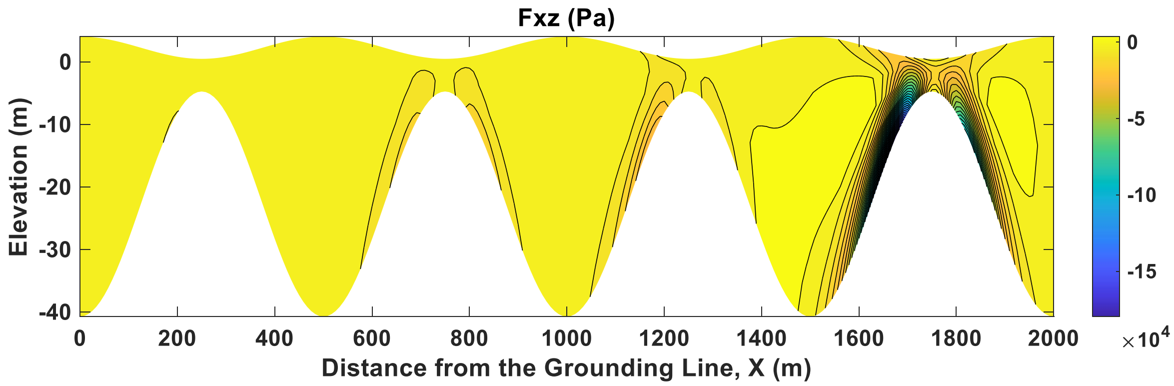

Fig. A9c

Figure A9(a) Vertical displacement of ice W along the centerline due to the impact of the frontal incident wave. **(b)** Distribution of longitudinal stress (σ_{xx}) in a vertical cross-section of the ice shelf along the centerline. **(c)** Distribution of shear stress (σ_{xz}) in a vertical cross-section of the ice shelf along the centerline. The periodicity of the forcing $\boldsymbol{T = 20s}$. The amplitude of ice thickness oscillations $\boldsymbol{A_H = 20m.}$

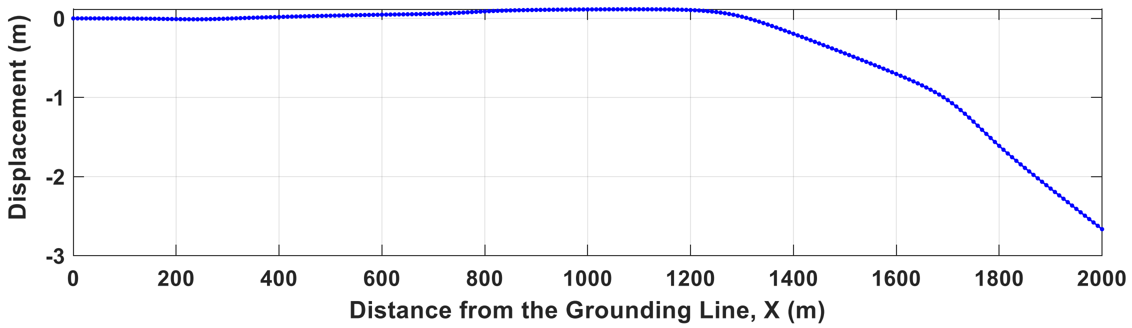

Fig. A10a

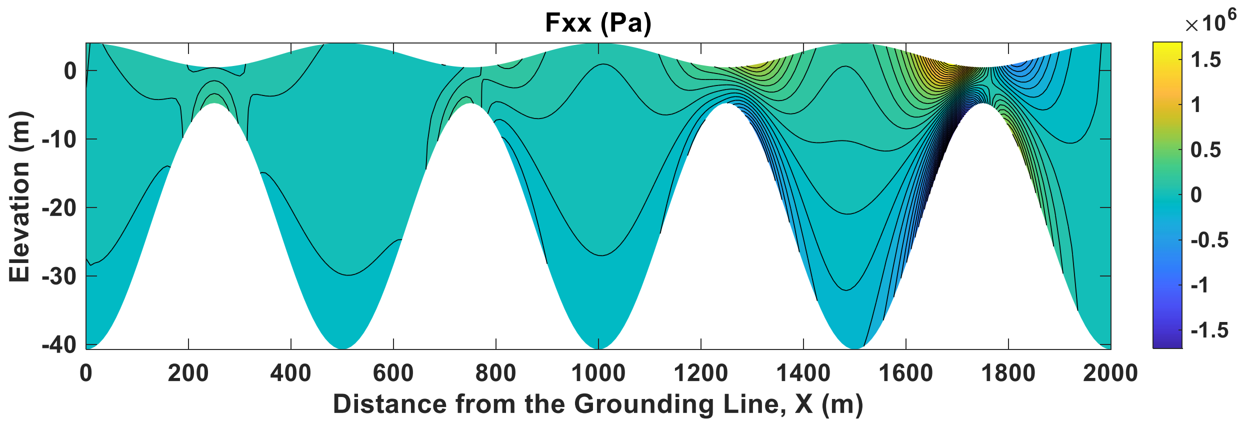

Fig. A10b

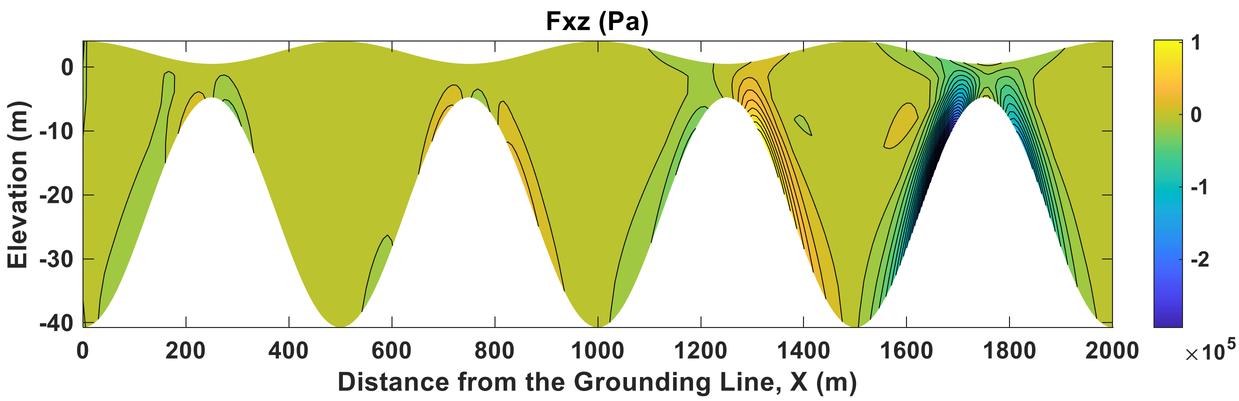

Fig. A10c

Figure A10. (a) Vertical displacement of ice W along the centerline due to the impact of the frontal incident wave. **(b)** Distribution of longitudinal stress (σ_{xx}) in a vertical cross-section of the ice shelf along the centerline. **(c)** Distribution of shear stress (σ_{xz}) in a vertical cross-section of the ice shelf along the centerline. The periodicity of the forcing $\boldsymbol{T = 50s}$. The amplitude of ice thickness oscillations $\boldsymbol{A_H = 20m}$.

Appendix B. Amplitude spectra and free energy spectra obtained using Model 1

The elastic free energy of the ice plate (the free energy of the elastic deformations of the ice plate) is expressed as (e.g. Landau & Lifshitz, 1986)

$$F_{full} = \frac{E}{2(1+\nu)} \int_V \left(u_{ik}^2 + \frac{\nu}{1-2\nu} u_{ii}^2 \right) dV, \qquad \text{(B1)}$$

where $\boldsymbol{u}$ is the strain tensor, E is Young's modulus, ν is Poisson's ratio, V is volume of undeformed ice plate.

Figures B1-B4 show the free energy spectra combined with amplitude spectra obtained using Model 1 for some values of the parameter A_H. In the experiments performed, no differences were revealed in the location of the resonance peaks in the two types of spectrum. This, in particularly, confirms that we can essentially use the amplitude spectra (as a simpler case) to analyze the vibrations (the possibility of resonant motion) of the ice shelf.

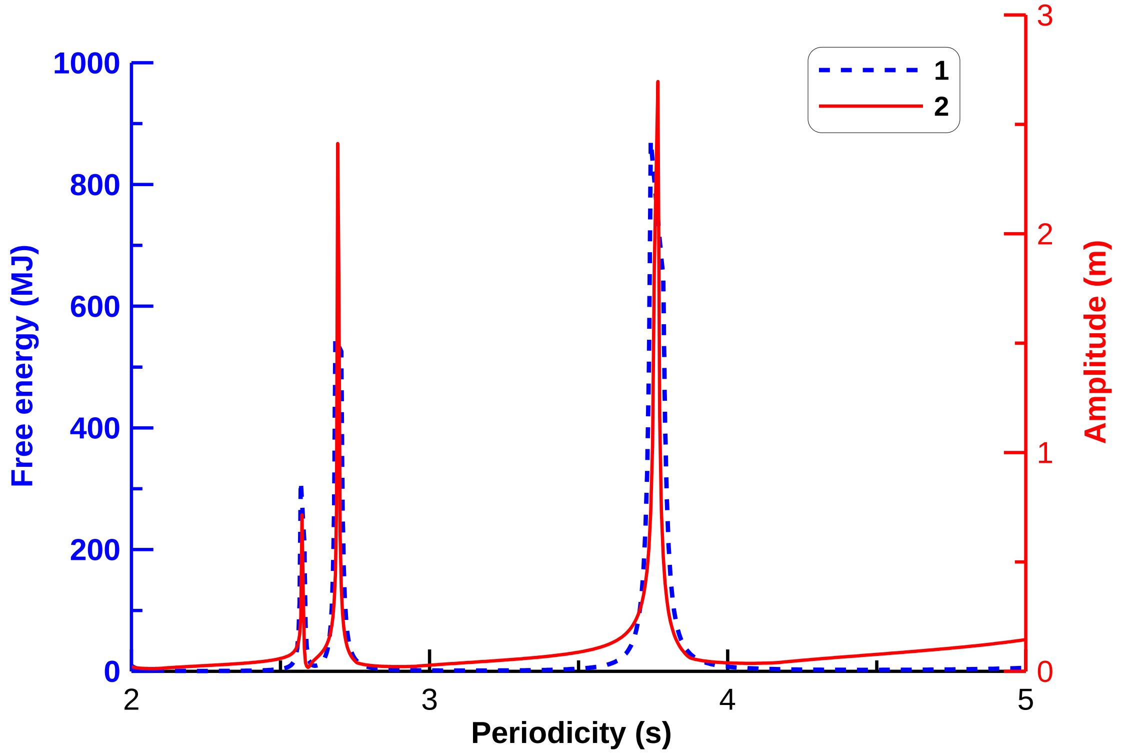

Figure B1. Free energy spectrum (**1**) and amplitude spectrum (**2**) obtained using **Model 1** for the ice thickness oscillation amplitude $\boldsymbol{A_H = 5\ m}$.

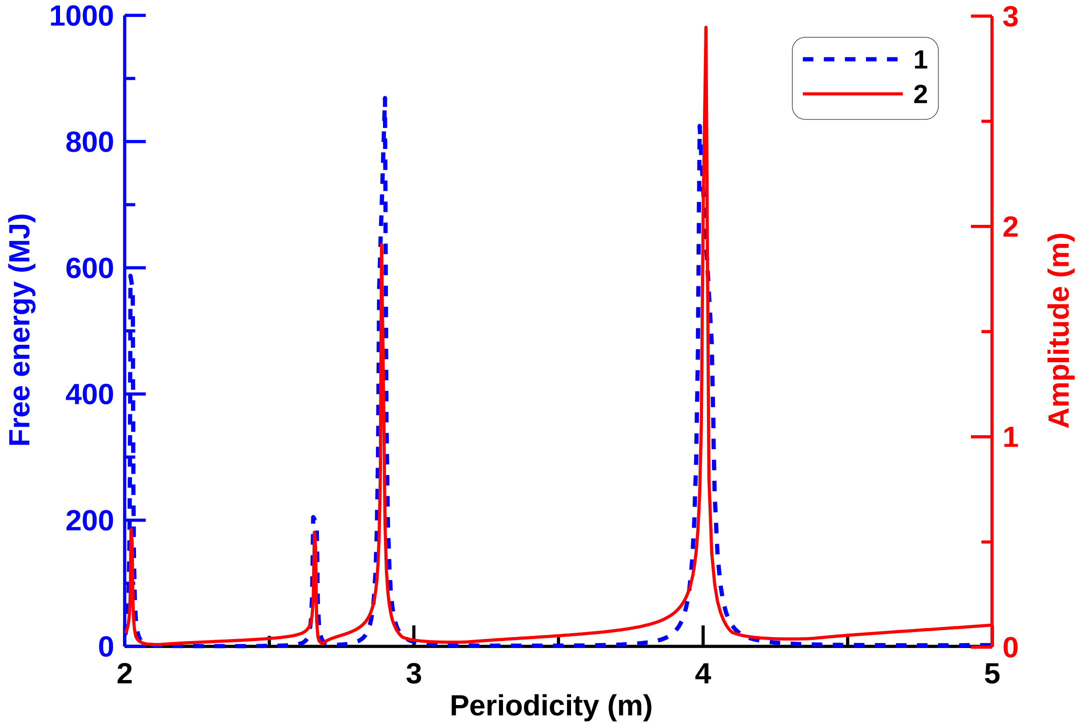

Figure B2. Free energy spectrum (**1**) and amplitude spectrum (**2**) obtained using **Model 1** for the ice thickness oscillation amplitude $\boldsymbol{A_H = 9\ m}$**.**

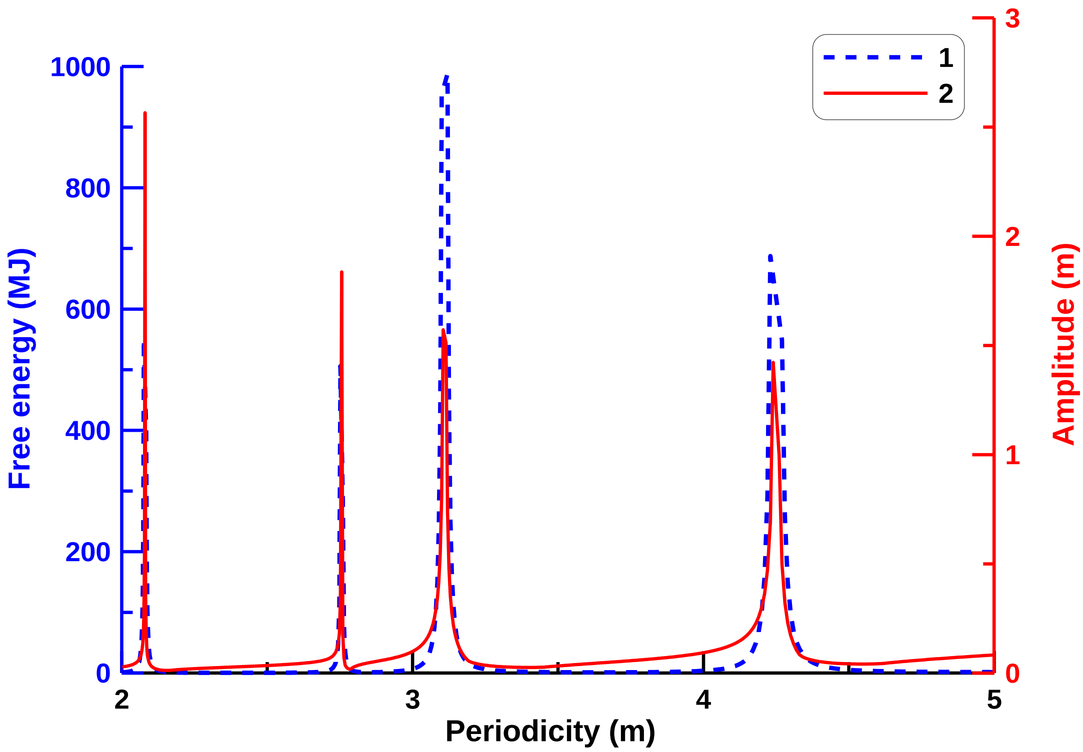

Figure B3. Free energy spectrum (**1**) and amplitude spectrum (**2**) obtained by **Model 1** for ice thickness oscillation amplitude $\boldsymbol{A_H = 11\ m}$

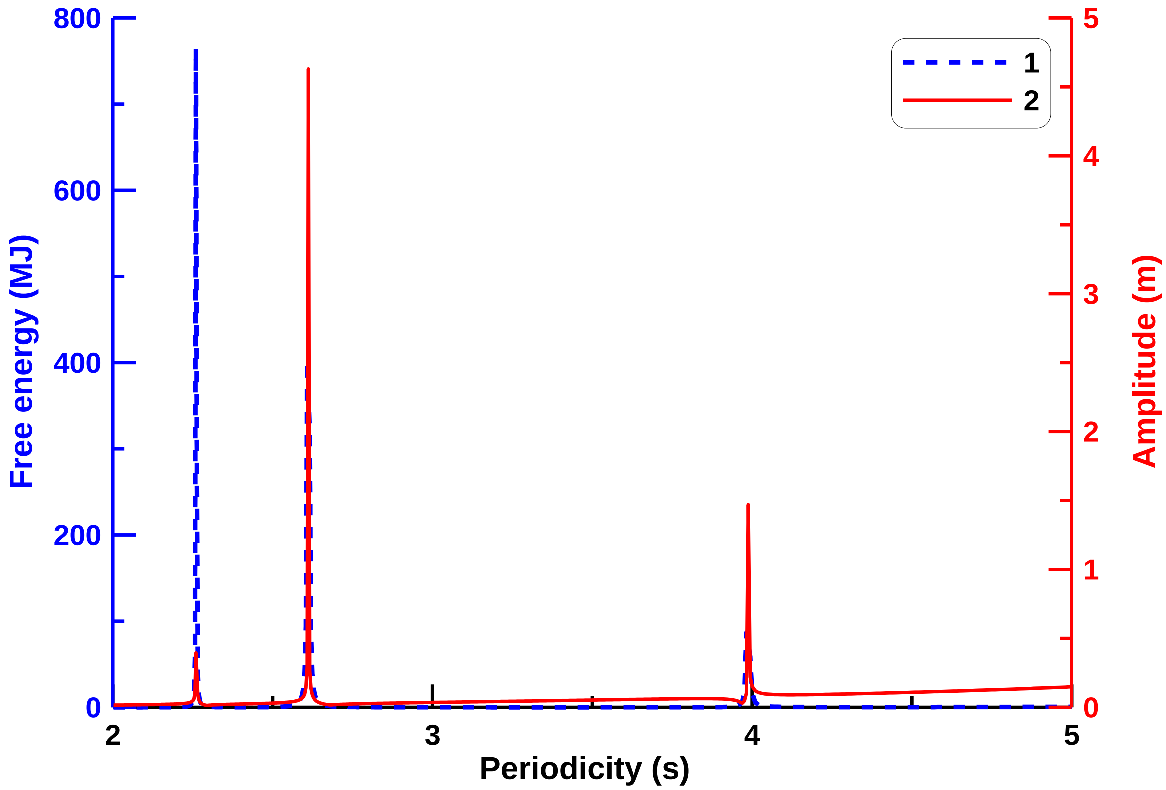

Figure B4. Free energy spectrum (**1**) and amplitude spectrum (**2**) obtained by **Model 1** for the ice thickness oscillation amplitude $\boldsymbol{A_H = 20\ m}$